DENSITY AND VISCOSITY OF HYDROCARBONS AT EXTREME CONDITIONS ASSOCIATED WITH ULTRA-DEEP RESERVOIRS-MEASUREMENTS AND MODELING

by

Hseen O. Baled

Dipl.-Ing., RWTH Aachen, 2003

Submitted to the Graduate Faculty of

Swanson School of Engineering in partial fulfillment

of the requirements for the degree of

Doctor of Philosophy

University of Pittsburgh

2012

UNIVERSITY OF PITTSBURGH

SWANSON SCHOOL OF ENGINEERING

This dissertation was presented

by

Hseen O. Baled

It was defended on

November 26th, 2012

and approved by

Badie I. Morsi, Ph.D., Professor, Department of Chemical and Petroleum Engineering

Sachin Velankar, Ph.D., Associate Professor, Department of Chemical and Petroleum Engineering

Yee Soong, Ph.D., Acting Division Director, National Energy Technology Laboratory

Dissertation Director: Robert M. Enick, Ph.D., Professor, Department of Chemical and Petroleum Engineering

DENSITY AND VISCOSITY OF HYDROCARBONS AT EXTREME CONDITIONS ASSOCIATED WITH ULTRA-DEEP RESERVOIRS-MEASUREMENTS AND MODELING

Hseen O. Baled, PhD

University of Pittsburgh, 2012

There is a lack of experimental density and viscosity data particularly at extremely high temperature, high pressure (HTHP) conditions associated with ultra-deep petroleum formations found at depths of approximately 20000 ft or more, where the pressure and temperature can reach as high as 35000 psia and 500^{o}F, respectively. In many applications, such as the simulation of oil reservoirs and the design of transport equipment, it is more convenient to use models to obtain such properties. However, development of reliable models requires sufficient experimental data that cover the entire temperature and pressure ranges of interest.

A HTHP density prediction model has been developed by utilizing the concept of volume- translation (VT) in the SRK and PR equations of state. The new proposed model provides very accurate density predictions over a wide range of temperature and pressure. The overall mean absolute percentage deviation (MAPD) of 1-2% obtained with the new model is substantially lower than those calculated with other models considered in this study.

A novel windowed, high temperature, high pressure rolling ball viscometer was designed and constructed specifically for this project. The viscometer has been calibrated with n-decane and used to measure the viscosity of n-octane for temperatures to 500^{o}F and pressures to 35000 psia. A literature review of different viscosity models has shown that the friction theory and free

volume theory models are superior to many other viscosity models. A correction term added to the friction theory model has been proposed to get more accurate predictions.

In the oil industry, there is a need to identify a viscosity standard that is representative of light oils produced from ultra-deep formations found beneath the deep waters of the Gulf of Mexico. Deepwater viscosity standard (DVS) is a liquid that would exhibit a viscosity of roughly 20 cP at 500^{o}F and 35000 psia. This work suggests Krytox® GPL 102 as a promising candidate for a HTHP DVS. The windowed rolling ball viscometer calibrated with dioctyl phthalate were used to determine the viscosity of Krytox® GPL 102, and all of the results were modeled with scaling theory and surface fitting.

TABLE OF CONTENTS

LIST OF TABLES

LIST OF FIGURES

LIST OF SYMBOLS

Latin letters

A	parameter for the new proposed equations of state
a	energy parameter of the cubic equations of state
B	parameter for the new proposed equations of state
b	co-volume parameter of the cubic equations of state
C	geometric constant
c	volume correction
D	tube diameter
d	ball diameter
DVS	deepwater viscosity standard
E	Young's modulus
EoS	equation of state
f	resistance factor
g	gravity acceleration
HTHP	high temperature, high pressure
I	constant
K	correlation factor used by Hubbard and Brown
k	viscometer constant
k_0-k_6	constants of the new proposed equations of state
k_{ij}	binary interaction parameter between molecules i and j
k,m,n	parameters of F-theory correction term
L,α,B	parameters of FV-theory
l	rolling distance
M	molecular weight
$MAPD$	mean absolute percentage deviation (%)
p	pressure
p_a	attraction pressure
p_r	repulsion pressure
PR	Peng-Robinson
R	gas constant
r	radius
Re	Reynolds number
SD	standard deviation
SRK	Soave-Redlich-Kwong
T	absolute temperature

t	time
T_b	boiling temperature
u	parameter for the general form of a two –parameter cubic EoS
u	speed of sound
v	velocity
v	molar volume
ν	Poisson's ratio
w	parameter for the general form of a two –parameter cubic EoS
x	mole fraction
Z	compressibility factor
Z_{RA}	Rackett compressibility factor

Greek letters

α	temperature-dependent function of the energy
α_b	thermal expansion of ball
α_t	thermal expansion of tube
β_T	isothermal compressibility
γ	thermodynamic interaction parameter related to intermolecular repulsive potential
$\bar{\dot{\gamma}}$	average shear rate
δ	relative deviation (%)
η	dynamic viscosity
η_0	dilute gas viscosity
η_f	friction viscosity
θ	tilting angle
κ_a	linear attractive viscous friction coefficient
κ_r	linear repulsive viscous friction coefficient
κ_{rr}	quadratic repulsive viscous friction coefficient
ρ	density
φ	dimensionless scaling parameter
ω	Pitzer's acentric factor

Subscripts

b	ball
c	critical
corr	corrected
exp	experimental
f	friction
fl	fluid
pred	predicted
r	reduced
ref	reference
rep	repulsive
t	translated

PREFACE

I would like to express my deepest gratitude to my advisor, Dr. Robert M. Enick for his support, encouragement, guidance and assistance throughout this research. I am very grateful to have such a great advisor. I would like to extend my gratitude to committee members, Dr. Badie Morsi, Dr. Sachin Velankar, and Dr. Yee Soong, for their time and thoughts.

I would like to thank Dr. Deepak Tapriyal, Dr. Ward Burgess, and Dr. Bryan Morreale for continual support and providing valuable remarks. I would like to express my special thanks to Dr. Mark McHugh and his graduate students Yue Wu and Babatunde Bamgbade, from Virginia Commonwealth University, for their support and invaluable research experience.

I would like to express my appreciation to Bob Maniet, Pat Park, Rita Leccia, Ron Bartlett, Robert Toplak and Adrian Starke for their assistance and cooperation. I would also like to thank my labmates, Dazun Xing, Matt Miller, Bing Wei, Kathy Barillas, James Mclendon, Lei Hong, Alex Stola, Sam McNulty, Peter Koronaios, Samantha Warman, and Craig Stevenson, for their helpful discussions and exchange of ideas.

I would like to acknowledge National Energy Technology Laboratory for the financial support.

This work is dedicated to the souls of my dear parents, and to the soul of my dear nephew, Jamal.

1.0 INTRODUCTION

Fluid properties such as density and viscosity are required in many petroleum applications from process and reservoir simulations to the production pipeline design. Despite the apparent significance of density and viscosity in the petroleum industry there is still a lack of experimental density and viscosity data in particular at extremely high temperature, high pressure (HTHP) conditions associated with ultra-deep petroleum formations that are found at depths of approximately 20000 ft or more, where the pressure and temperature can reach as high as 35000 psia and 500^{o}F, respectively. Taking measurements of density and viscosity at each pressure, temperature and composition may not possible due to limitation of time, cost, and equipment. Therefore, reliable and accurate models to predict density and viscosity of hydrocarbons at extreme temperature and pressure conditions are needed for the production of petroleum fluids from very deep reservoirs.

1.1 DENSITY PREDICTION OF HYDROCARBONS

Cubic equations of state (EoSs) are widely used to predict the phase behavior and volumetric properties of hydrocarbons. Two of the most common cubic equations of state in petroleum engineering industry are the Soave-Redlich-Kwong (SRK) EoS [1] and the Peng-Robinson (PR) EoS [2]. Equation 1 shows the general form of these two–parameter cubic equations of state [3] .

$$P = \frac{RT}{v-b} - \frac{a_c\,\alpha}{v^2 + ubv + wb^2} \tag{1}$$

where P is the pressure, T is the absolute temperature, and v is the molar volume. For the SRK EoS, u = 1 and w = 0, and for the PR EoS, u = 2 and w = -1. The function α in the attractive term is a correlation of temperature, critical temperature, and acentric factor. The parameter b represents the effective molecular volume in the hard sphere repulsive term. The parameters a_c and b depend only on the critical properties and the equations defining these two parameters are obtained by applying the constraints shown in Equation 2 at the critical point.

$$\left(\frac{\partial P}{\partial v}\right)_{T=T_c} = 0, \qquad \left(\frac{\partial^2 P}{\partial v^2}\right)_{T=T_c} = 0 \tag{2}$$

The SRK EoS predicts a critical compressibility, $Z_c = \frac{P_c\,v_c}{RT_c}$, of 0.3333 whereas the PR EoS predicts a value of 0.3074.

The experimental values of Z_c are generally smaller than those predicted by either cubic equation of state. As a result, the predicted liquid molar volumes in the near-critical region may differ considerably from experimental values. Nonetheless, satisfactory density calculation results can be obtained for sub-critical conditions associated with many chemical and petroleum engineering applications.

Other type of equations of state is the class of equations based on the statistical associating fluid theory (SAFT) proposed by Chapman et al. [4, 5]. One of the most successful modifications of SAFT EoS is the perturbed chain SAFT (PC-SAFT EoS) put forth by Gross and Sadowski [6]. The SAFT equations of state are generally more accurate than the cubic equations of state in estimating the liquid density. However, most SAFT models suffer from some major disadvantages. One of them, SAFT based models usually provide inaccurate

estimation of the pure compounds critical data. Another drawback is the multiple phase equilibria for pure compounds [7].

The Cubic-Plus-Association equations of state (CPA EoS) developed by Kontogeorgis et al.[8, 9] combines the SRK EoS with an association term from the Wertheim theory (the same as in SAFT models) accounting for hydrogen bonding effects. When dealing with non-associating fluids, the CPA EoS reduces to the SRK EoS. The three remaining CPA parameters a_0, c_1, and b are regressed than simultaneously from vapor pressure and saturated liquid density data instead of using the critical constants as is done for SRK EoS. Considerable improvements in the phase equilibria and density predictions of associating fluids can be achieved with the CPA EoS [10]. Recently, the CPA has been successfully used to predict the density of the non-associating ester mixtures at pressures up to 45 MPa when the regressed CPA pure compound parameters are used instead of the parameters computed from correlations [11]. However, the density predictions for n-alkanes (non-associating) obtained with the CPA EoS are not always reliable. For instance, the density predictions for n-pentane at 520.45 K obtained with the CPA EoS are even inferior to the results obtained with the classical SRK EoS, as can be seen in Figure 1.

Recently, Polishuk proposed a hybrid EoS model that combines a modified SAFT with the attractive term of cubic EoS (SAFT+Cubic) [7]. This model was developed based upon the idea of gathering the strengths of both SAFT and cubic equations of state. The performance of this model has been evaluated for several fluids including n-pentane, n-hexane, cyclohexane, and toluene at extremely high pressures. Its predictions of the density and some auxiliary properties such as speed of sound and bulk moduli are impressive [12].

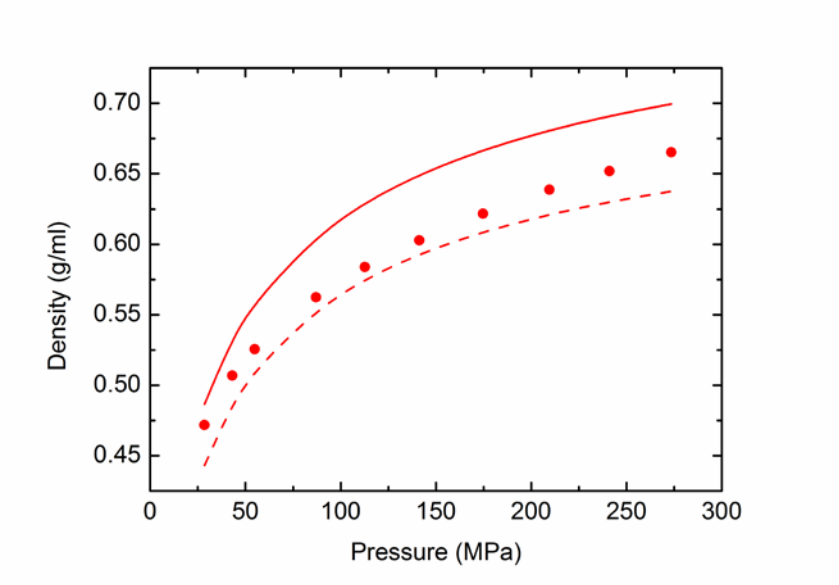

Figure 1: Density isotherm at 520.45 K for n-pentane. ● Experimental data [16], - - - - SRK EoS, —— CPA EoS (the three CPA parameters a_0, c_1, b were taken from [17])

Very high prediction accuracy for thermodynamic properties of fluids can be obtained with the empirical multiparameter equations of state [13-15]. These equations of state are fluid specific and commonly expressed in terms of the reduced Helmholtz energy.

RPSEA (Research Partnership for Securing Energy for America), a non-profit corporation formed by a consortium of premier U.S. energy research universities, industry and independent research organizations with a stated mission "to provide a stewardship role in ensuring the focused research, development and deployment of safe, environmentally sensitive technology that can effectively deliver hydrocarbons from domestic resources to the citizens of the United States" [18], recently affirmed the need for accurate thermodynamic models for hydrocarbon fluid density at extreme conditions associated with ultra-deep reservoirs. Citing the continued prevalence of cubic equations-of-state (specifically the Peng-Robinson and Soave-Redlich-Kwong EoSs) in modern reservoir simulation software packages and the simplicity of replacing cubic EoSs with volume-translated EoSs in a reservoir simulator, RPSEA stated its

desire for new volume-translated PR and SRK EoSs with enhanced predictive capabilities at temperatures to 500^{o}F (533 K) and pressures between 1000-35000 psi (7- 241 MPa). One objective of this study has been to develop a reliable volume-translated model for prediction of volumetric behavior of pure hydrocarbons and mixtures at temperatures to 500^{o}F (533 K) and pressures between 1000-35000 psi (7- 241 MPa).

1.2 VISCOSITY OF HYDROCARBONS

Modeling fluid flow in petroleum reservoirs and production wells requires reliable predictions of the viscosity of brine and hydrocarbon mixtures. Despite the significance of viscosity in the petroleum industry there is still a lack of experimental viscosity data in particular at extremely high temperature, high pressure (HTHP) conditions associated with ultra-deep petroleum formations. In many applications, such as the simulation of oil reservoirs and the design of transport equipment, it is more convenient to use models to obtain the viscosity because experimental data might not be available at specific conditions and carrying out viscosity measurements at all temperatures, pressures, and compositions is time and cost prohibitive. However, viscosity modeling requires a sufficient experimental viscosity data base that covers the entire temperature and pressure ranges of interest.

A windowed, volume-variable rolling ball viscometer has been constructed and put together to measure the viscosity of some hydrocarbons over the entire pressure and temperature ranges of interest. The new viscosity measurements at extreme conditions together with literature data will enable us to determine or develop an accurate viscosity model that can be used in conjunction with the new developed equations of state to predict accurately the viscosity of

hydrocarbon fluids at temperature and pressure conditions of interest. Accurate density and viscosity models will allow more confident predictions of the amount of petroleum that can be recovered from porous media at great depths.

In the oil industry, there is a need to identify a viscosity standard that is representative of light oils produced from ultra-deep formations found beneath the deep waters of the Gulf of Mexico. Deepwater viscosity standard is a liquid that would exhibit a viscosity of roughly 20 cP at 260^{o}C and 35000 psi. This work suggests a promising candidate for a high temperature, high pressure (HTHP) Deepwater viscosity standard (DVS).

2.0 PREDICTION OF HYDROCARBON VOLUMETRIC PROPERTIES

While cubic equations of state such as the SRK and PR EoS provide accurate predictions for vapor molar volumes, they fail to predict accurate liquid molar volumes over wide pressure ranges. One of the most straightforward ways to overcome this limitation has been to shift, or translate, the predicted liquid volume. In fact, a systematic deviation, *c*, is observed between the predicted liquid molar volume (v_{EoS}) and the corresponding experimental value ($v_{\exp}$).

$$c = v_{EoS} - v_{\exp} \tag{3}$$

The parameter *c* is also known as a volume translation which can be utilized to greatly improve the prediction of densities in the sub-critical region. The effect of the volume translation on the gas-phase density is insignificant due to the large value of the vapor volume compared to that of the liquid. The calculation of the pure component vapor pressure is not affected when *c* is a constant or is a function only of temperature.

Peneloux et al. [19] proposed a component-dependent volume correction constant, *c*, as the difference between the EoS-predicted and the corresponding experimental saturated liquid volume at $T_r = 0.7$

$$c = v_{EoS} - v_{\exp}\Big|_{T_r = 0.7} \tag{4}$$

Peneloux applied the volume translation to the SRK EoS and correlated c to T_c, P_c and the Rackett compressibility factor, Z_{RA}, for hydrocarbons up to n-decane. Equation 5, which only contains pure-component parameters, is the expression for c derived by Peneloux and coworkers.

$$c = 0.40768 \frac{RT_c}{P_c}(0.29441 - Z_{RA}) \tag{5}$$

Other authors have proposed enhanced volume translation correlations that account for the influence of temperature on c. For example, Ji and Lempe [20] , and Wang and Gmehling [21] defined a temperature-dependent volume correction expression applied to the SRK EoS as

$$c = c_c \; f(\omega, Z_c, T_r) \tag{6}$$

where c_c is the volume correction at the critical temperature. The parameters in the $f(\omega, Z_c, T_r)$ volume correction equation were optimized by fitting experimental saturated liquid densities.

Magoulas and Tassios [22] proposed a different temperature-dependent volume correction expression to improve the prediction of α modified PR EoS as shown in Equation 7.

$$c = c_0 + c_1 \exp\left(c_2 \left(\left|1 - T_r\right|\right)\right) \tag{7}$$

where c_0, c_1, and c_2 are component-dependent and are obtained by regressing saturated liquid density data.

Ungerer et al. [23-28] calibrated the volume translation correction for the PR EoS, generally at 50 MPa, and proposed the following correlation for hydrocarbons up to C_{13}

$$c = -34.5 + 0.46666\,M + (0.023 - 0.00056\,M)T \tag{8}$$

where M is the molecular weight (g/mol) and T the temperature (K).

For heavier hydrocarbons, these authors recommend the following correlation

$$c = v(T_{ref}, P_{ref}) - \frac{M}{\rho_{ref}} + (0.023 - 0.00056\,M)(T - T_{ref}) \tag{9}$$

where $v(T_{ref},P_{ref})$ is the liquid molar volume calculated by the untranslated EoS at the same conditions where a reference experimental density, ρ_{ref}, is available.

Several other investigators [29-32] incorporated a density dependency into the translation function in addition to the temperature dependency. Although this type of T-ρ volume translation expression, that is fit to saturated data, may substantially improve the predictive ability of a cubic EoS in the near-critical and low pressure regions, it has only a limited effect on the prediction accuracy at high temperatures and pressures. Recently, it has been demonstrated that a T-ρ-translated SRK EoS proposed by Frey et al. [32] provides only a modest improvement in the performance of the SRK EoS at HTHP conditions [16].

2.1 DEVELOPMENT OF A HIGH-TEMPERATURE-HIGH PRESSURE (HTHP) VOLUME-TRANSLATED (VT) EOS

In this work, as stated before, we are interested in the fluid density of hydrocarbon fluids at very high temperatures and extremely high pressures associated with the flow of petroleum in ultra-deep reservoirs and the production wells. Therefore, rather than correlating the volume correction to saturated liquid densities, as is done in most prior volume translation methods, the volume translation term in this study is correlated to pure component, single-phase density data [16, 33-40] for short- and long-chain alkanes, cycloalkanes and aromatics over a pressure range ~(7-276) MPa and a temperature range ~(278-533) K.

The difference between the predicted liquid molar volume, v_{EoS}, and the corresponding experimental value, $v_{exp,}$ has been averaged for each isotherm (i.e. each value of T_r indicated by data markers in Figure 2) for literature data within the HTHP range. Therefore, the density

dependency of the volume correction expression is neglected, hence a component-dependent, temperature-dependent volume translation was employed. After determining the optimal value of *c* for each isotherm associated with a specified component, the volume correction was plotted against reduced temperature and expressed as a linear function of T_r,

$$c = \Delta v = v_{EoS} - v_{\exp} = A + B \cdot T_r \tag{10}$$

Figure 2 shows these temperature dependent results for the SRK EoS for cyclohexane, toluene, n-heptane, and n-decane.

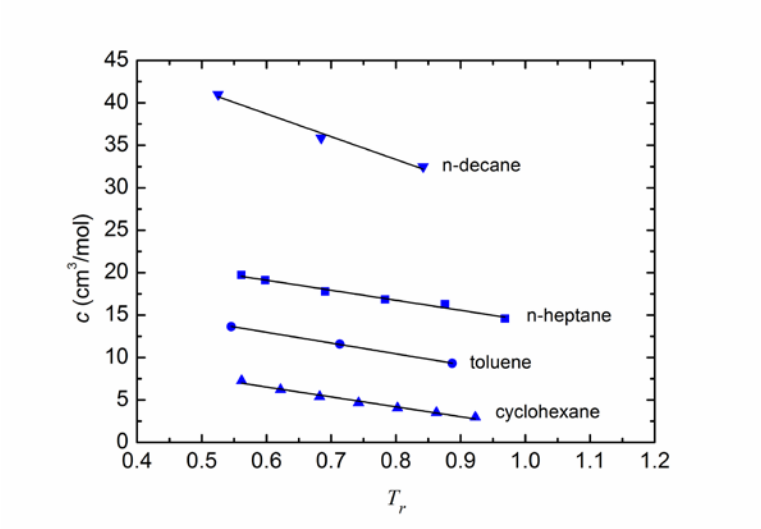

Figure 2: Volume correction, *c*, of the SRK EoS for cyclohexane [33] , toluene [16], n-heptane [34], and n-decane [16] as a linear function of the reduced temperature, T_r

Figure 3 shows an example of the results of utilizing this technique for the determination of *c* for n-decane at reduced temperatures of 0.53 and 0.84.

This approach was applied to the SRK EoS and PR EoS. The pure fluid parameters *A* and *B* in Equation 10 have been regressed for 17 pure components spanning the C_1 to C_{40} range and their values for both the SRK EoS and PR EoS are listed in Table 1.

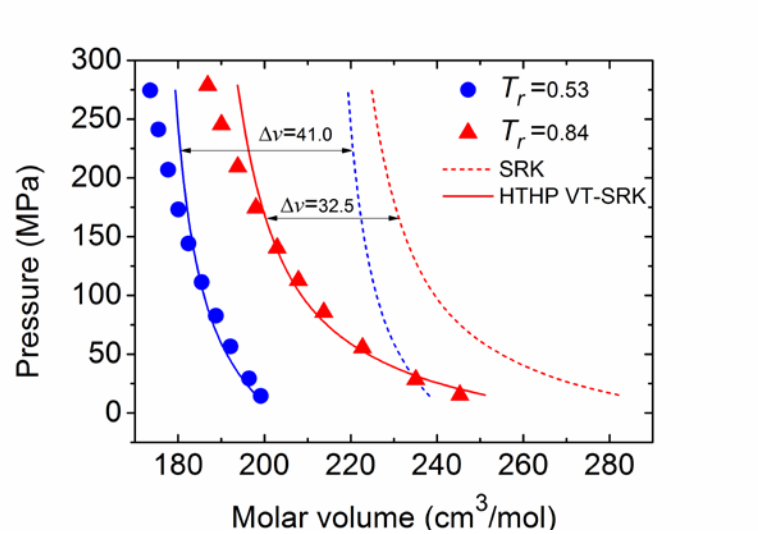

Figure 3: Volume translation results based on average volume differences between SRK EoS predicted molar volumes and their corresponding experimental values for n-decane at the isotherms T_r = 0.53 and 0.84

Table 1: Optimized values of the volume translation parameters *A* and *B* based on literature data in the ~(7-276) MPa and ~(278-533) K ranges

compound	Ref.	*M* (g/mol)	ω	T_c (K)	P_c (bar)	$(M\omega)^{-1}$ (mol/g)	HTHP VT-SRK EoS		HTHP VT-PR EoS	
							A (cm^3/mol)	*B* (cm^3/mol)	*A* (cm^3/mol)	*B* (cm^3/mol)
methane	[35, 36]	16.04	0.012	190.56	45.99	5.420	0.233	-0.420	-3.047	-0.610
propane	[37]	44.10	0.152	369.83	42.48	0.149	2.977	-1.225	-3.328	-3.189
n-pentane	[16]	72.15	0.251	469.70	33.70	0.055	17.95	-12.39	7.181	-13.89
cyclohexane	[33]	84.16	0.208	553.80	40.80	0.057	13.52	-11.65	3.864	-15.02
n-heptane	[34]	100.20	0.349	540.20	27.40	0.029	26.21	-11.82	11.24	-14.57
n-octane	[16]	114.23	0.399	568.70	24.90	0.022	36.80	-20.15	20.70	-23.73
isooctane	[16]	114.23	0.303	543.90	25.70	0.029	23.92	-17.46	7.824	-19.51
cyclooctane	[16]	112.21	0.236	647.20	35.60	0.038	23.48	-19.22	9.066	-20.72
n-decane	[16]	142.29	0.492	617.70	21.10	0.014	54.85	-26.90	33.71	-30.91
n-tridecane	[34]	184.36	0.617	675.00	16.80	0.009	90.21	-38.01	62.23	-45.39
n-hexadecane	[38]	226.45	0.717	723.00	14.00	0.006	127.5	-52.69	88.55	-55.34
n-octadecane	[38]	254.50	0.811	747.00	12.70	0.005	155.1	-73.00	109.0	-72.80
n-eicosane	[34, 38]	282.55	0.907	768.00	11.60	0.004	169.4	-62.91	116.5	-60.70
n-C_{30}	[34]	422.83	1.307	844.00	8.00	0.002	325.8	-146.7	250.3	-150.6
n-C_{40}	[34]	563.08	1.500	887.00	4.40	0.001	881.2	-201.1	750.5	-246.9
benzene	[39, 40]	78.11	0.210	562.05	48.95	0.061	11.51	-6.490	2.074	-8.227
toluene	[16]	92.14	0.264	591.75	41.08	0.041	20.57	-12.66	12.17	-15.37

In order to provide a generalized method for determining *A* and *B* for compounds not included in the database, correlations for *A* and *B* were developed as functions of molecular weight (*M*) and acentric factor (ω). Although correlations for *A* and *B* based on either *M* or ω were generated, but not shown here, the correlations in this study based on $(M\omega)^{-1}$ provided significantly better fits of the optimized *A* and *B* values. Figures 4-7 show the correlations developed in this study.

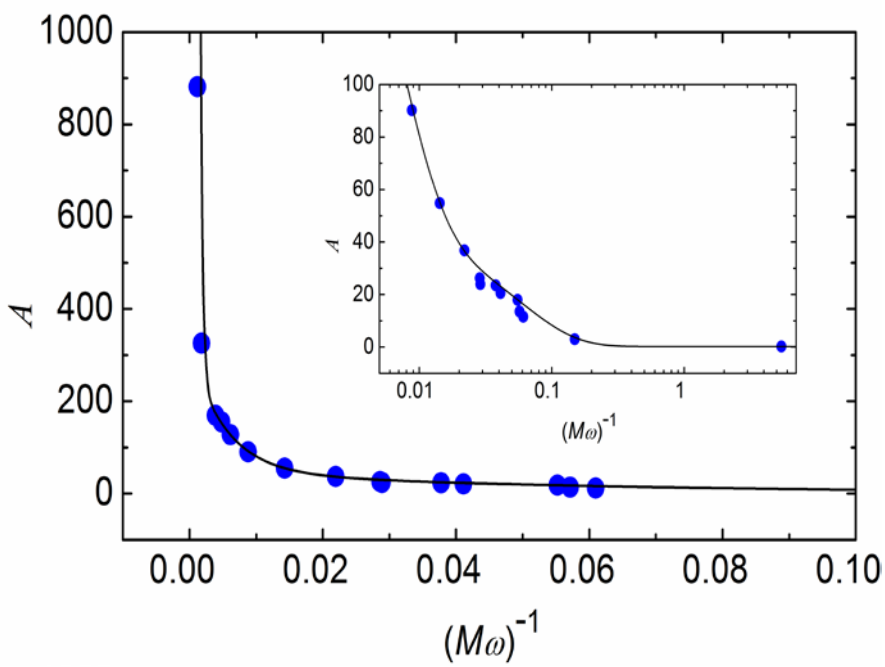

Figure 4: Parameter *A* of Equation 10 and its correlation, Equation 14, for HTHP VT-SRK EoS. Only the markers for components between and including n-C_{40} and n-pentane are shown; methane and propane values of $(M\omega)^{-1}$ are off-scale to the right. ● Optimized *A* values, —— Equation 14 for HTHP VT-SRK EoS.

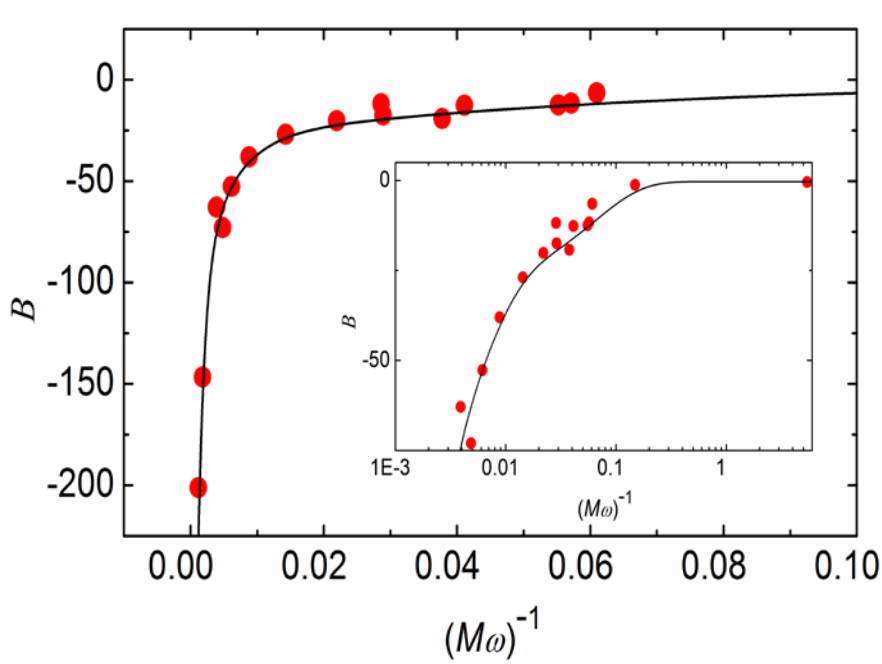

Figure 5: Parameter *B* of Equation 10 and its correlation, Equation 14, for HTHP VT-SRK EoS. Only the markers for components between and including n-C_{40} and n-pentane are shown; methane and propane values of $(M\omega)^{-1}$ are off-scale to the right. ● Optimized *B* values, —— Equation 14 for HTHP VT-SRK EoS.

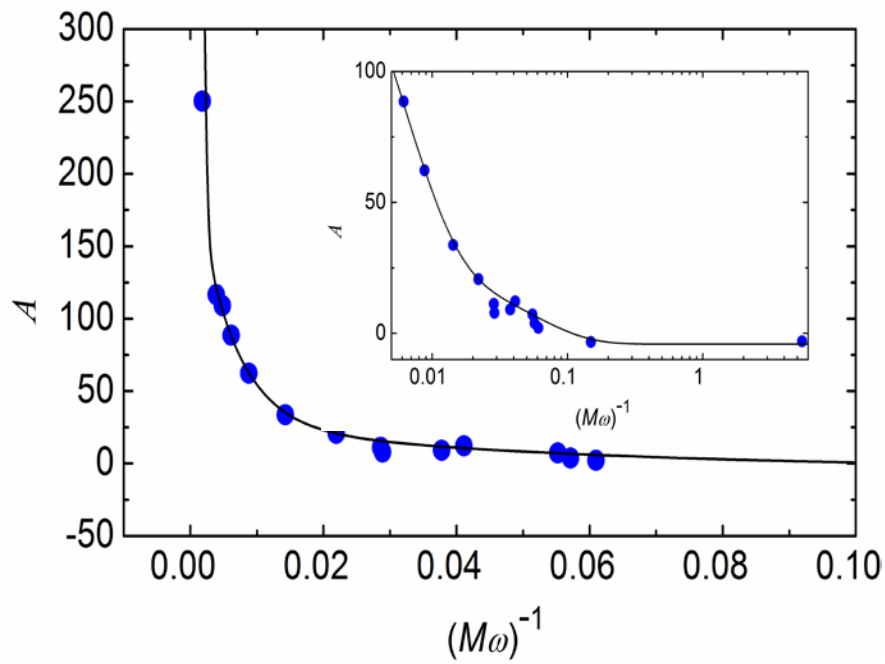

Figure 6: Parameter *A* of Equation 10 and its correlation, Equation 14, for HTHP VT-PR EoS. Only the markers for components between and including n-C_{40} and n-pentane are shown; methane and propane values of $(M\omega)^{-1}$ are off-scale to the right. ● Optimized *A* values, —— Equation 14 for HTHP VT-PR EoS.

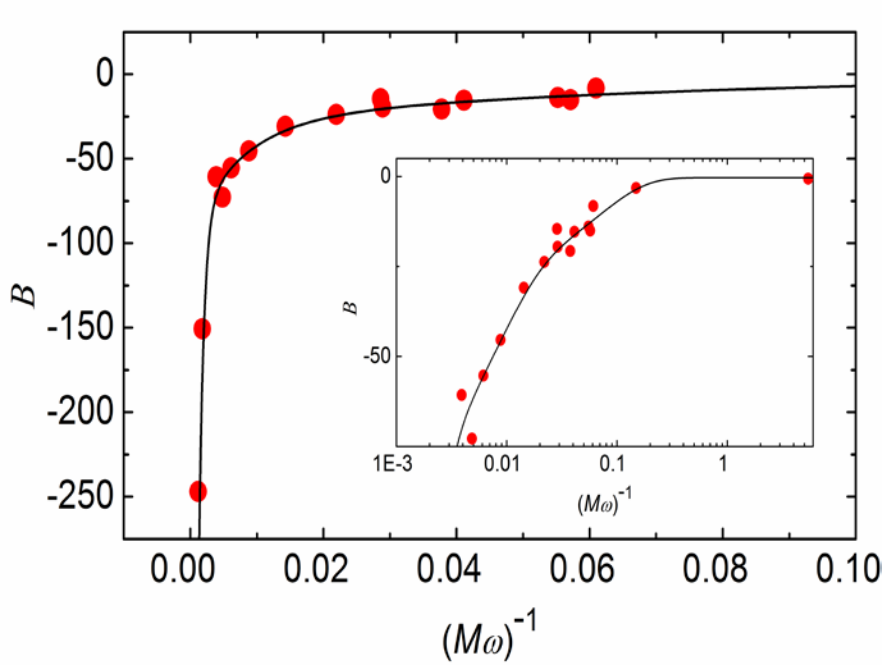

Figure 7: Parameter *B* of Equation 10 and its correlation, Equation 14, for HTHP VT-PR EoS. Only the markers for components between and including n-C_{40} and n-pentane are shown; methane and propane values of $(M\omega)^{-1}$ are off-scale to the right. ● Optimized *B* values, —— Equation 14 for HTHP VT-PR EoS.

The high temperature-high pressure volume translated forms of the SRK EoS and PR EoS, referred as HTHP VT-SRK and HTHP VT-PR EoS, are presented here.

HTHP VT-SRK EoS:

$$P = \frac{RT}{v+c-b} - \frac{a_c\,\alpha}{(v+c)(v+c+b)} \tag{11}$$

HTHP VT-PR EoS:

$$P = \frac{RT}{v+c-b} - \frac{a_c\,\alpha}{(v+c)(v+c+b)+b(v+c-b)} \tag{12}$$

where:

$$c = A + B\cdot T_r \tag{13}$$

$$A, B = f(M,\omega) = k_0 + k_1 \exp\left(\frac{-1}{k_2\,M\,\omega}\right) + k_3 \exp\left(\frac{-1}{k_4\,M\,\omega}\right) + k_5 \exp\left(\frac{-1}{k_6\,M\,\omega}\right) \tag{14}$$

Values for the parameters of Equation 14 are listed for both equations-of-state in Table 2. The correlations of parameters *A* and *B* (rather than the optimized values) have been used for subsequent density calculations reported in this study.

Table 2: Parameters of Equation 14

Constants		HTHP VT-SRK EoS	HTHP VT-PR EoS
A (cm^3/mol)	k_0	0.2300	-4.1034
	k_1	46.843	31.723
	k_2	0.0571	0.0531
	k_3	23161	188.68
	k_4	0.0003	0.0057
	k_5	267.40	20196
	k_6	0.0053	0.0003
B (cm^3/mol)	k_0	-0.3471	-0.3489
	k_1	-29.748	-28.547
	k_2	0.0644	0.0687
	k_3	-347.04	-817.73
	k_4	0.0010	0.0007
	k_5	-88.547	-65.067
	k_6	0.0048	0.0076

2.2 CALCULATION RESULTS FOR PURE COMPONENTS

The performance of the new volume translated equations of state, the HTHP VT-SRK EoS and the HTHP VT-PR EoS, is compared to the performance of seven other equations of state used to predict the density of 17 hydrocarbons in the range of temperatures from ~ 278 to 533 K and pressures from ~ 7 to 276 MPa, which are conditions relevant to the numerical simulation of ultra-deep reservoir processes. The equations of interest are classified into four groups: (1) standard Soave-Redlich-Kwong (SRK EoS) [1] and Peng-Robinson (PR EoS) [2]; (2) T-

dependent volume translated SRK EoS correlated to saturated liquid densities proposed by Ji & Lempe [20] and Wang & Gmehling [21]; (3) T-dependent volume translated PR EoS correlated to saturated liquid densities proposed by Magoulas and Tassios [22] and T-dependent volume translated PR EoS correlated to ~ 50 MPa density data proposed by Ungerer and Batut [23, 26]; and (4) perturbed chain statistical associating fluid theory (PC-SAFT) equation of state regressed to vapor pressure and saturated liquid density data [6, 41-44].

The performance of the different equations of state is based on data available in the literature [16, 33-40]. The accuracy of the predictions of each equation of state is represented by the mean absolute percentage deviation (MAPD) for the *n* data points

$$MAPD = \frac{1}{n}\sum_{1}^{n}\left|\frac{\rho_{i,experimental} - \rho_{i,calculated}}{\rho_{i,experimental}}\right| \times 100 \qquad (15)$$

and the standard deviation (SD) associated with the value of the MAPD.

Figures 8-12 show the calculated results of the different methods for n-pentane as an example. Figure 8a shows that the SRK EoS provides a reasonably small under-estimation of density at 520.45 K, but yields a more significant under-estimation of the n-pentane density at 325.85 K and 423.05 K over the entire pressure range of interest. Figure 8b shows that the PR EoS provides a reasonable fit of n-pentane density data at 325.85 K, a slight over-estimation at 423.05 K, and a significant over-estimation of density at 520.45 K. The MAPD for the PR EoS is 4.68%, while the MAPD for the SRK EoS is 5.63%. Given that the goal is to attain density values within ~1% of experimental values, both EoSs are considered unsatisfactory.

The results of the T-dependent volume translated SRK EoS designed to fit saturated liquid density data, shown in Figure 9, both exhibit reasonable fits of the 325.85 K isotherm, and significant over-estimations of the single-phase fluid density at high pressures for both higher

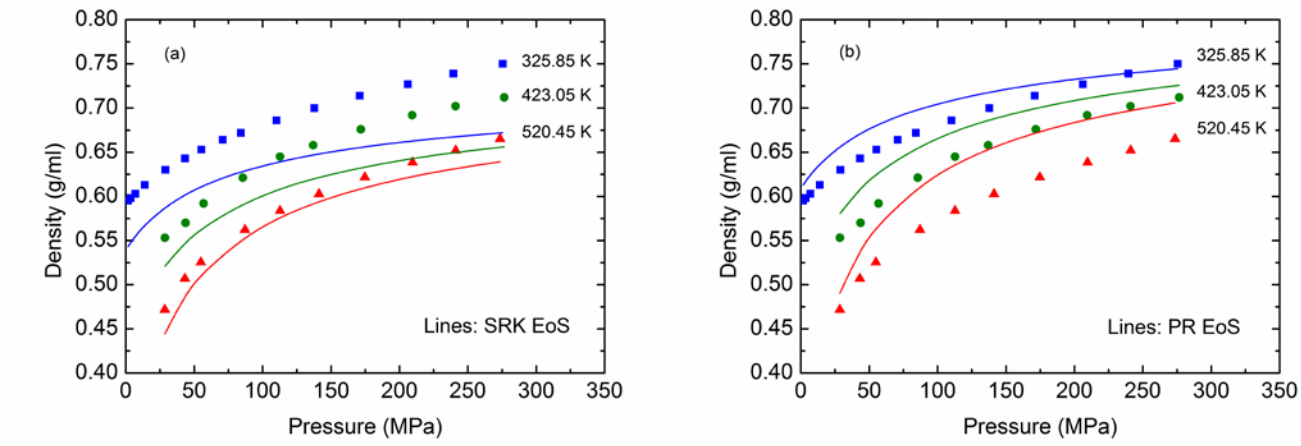

Figure 8: (a) Comparison of the SRK EoS with n-pentane density data [16], (b) Comparison of the PR EoS with n-pentane density data [16]

temperatures. Furthermore, these isotherms exhibit a thermodynamic inconsistency in that the 325.85 K isotherm crosses over both the 423.05 K and 520.45 K isotherms.

Figure 10a shows a comparison of experimental and calculated high pressure density values using the T-dependent volume translated PR EoS proposed by Magoulas and Tassios which was developed to fit vapor pressure and saturated liquid volume data. This model leads to crossing isotherms like the two previously mentioned volume translated SRK models.

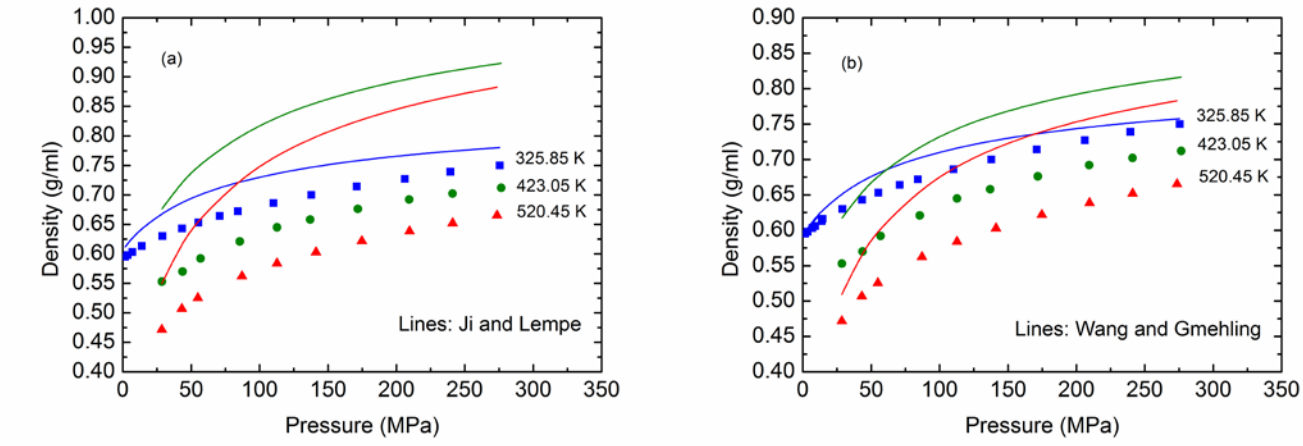

Figure 9: (a) Comparison of the T-dependent translated SRK EoS proposed by Ji and Lempe with n-pentane density data [16], (b) Comparison of the T-dependent translated SRK EoS proposed by Wang and Gmehling with n-pentane density data [16]

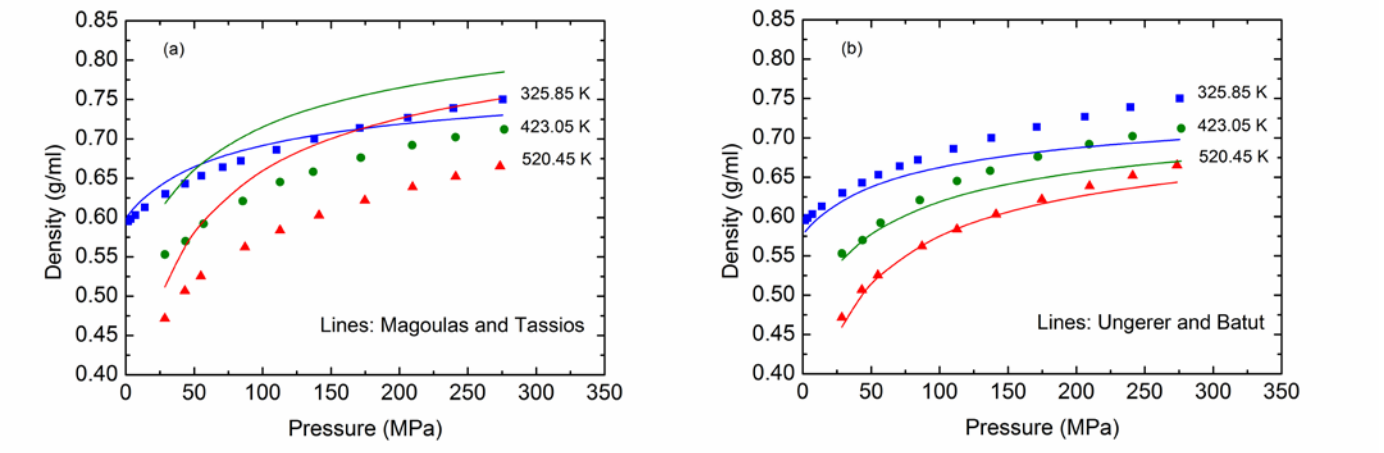

Figure 10: (a) Comparison of the T-dependent translated PR EoS proposed by Magoulas and Tassios with n-pentane density data [16], (b) Comparison of the T-dependent translated PR EoS proposed by Ungerer and Batut with n-pentane density data [16]

The prediction results obtained with the model of Ungerer and Batut are presented in Figure 10b. This method yields very good predictions at 520.45 K over the entire pressure range. However, this model provides good results at 325.85 K and 423.05 K only for pressures to 100 MPa. As the pressure increases above 100 MPa the model tends to under-estimate the density and the deviation from the experimental data becomes larger. The Ungerer and Batut model has an MAPD of 2.60%.

Figure 11 shows that the PC-SAFT EoS provides very good results at 325.85 K and 423.05 K over the entire pressure range. At 520.45 K, the PC-SAFT predictions are very good for pressures to 100 MPa, but PC-SAFT over-estimates the density as the pressure increases. For n-pentane, the PC-SAFT EoS has an MAPD of 1.72%, with most of the deviation occurring in the highest temperature and pressure ranges.

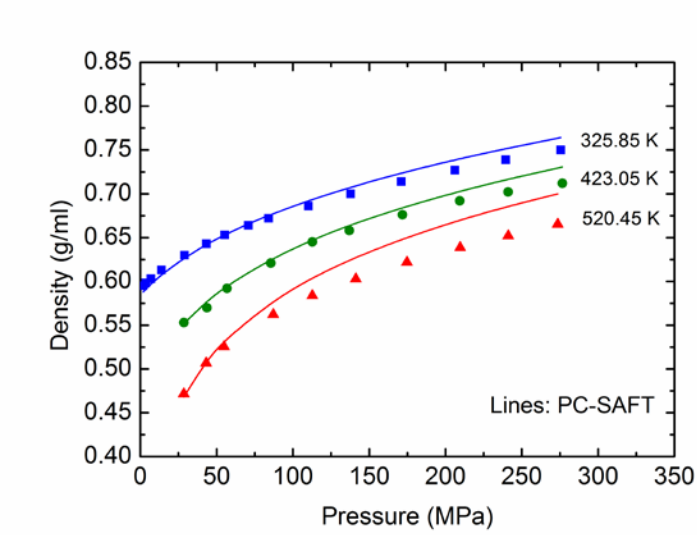

Figure 11: Comparison of the PC-SAFT EoS with n-pentane density data [16]

Figure 12 shows that the performance of the HTHP VT-SRK EoS and HTHP VT-PR EoS models developed in this study is superior to the performance of the other models. Both HTHP models provide very good results for pressures up to 200 MPa for all isotherms and then tend to under-estimate the density at 325.85 and 423.05 K as the pressure increases. The HTHP VT-SRK EoS has an MAPD of 1.11%, which is slightly better than the 1.54% calculated for the predictions of the HTHP VT-PR EoS.

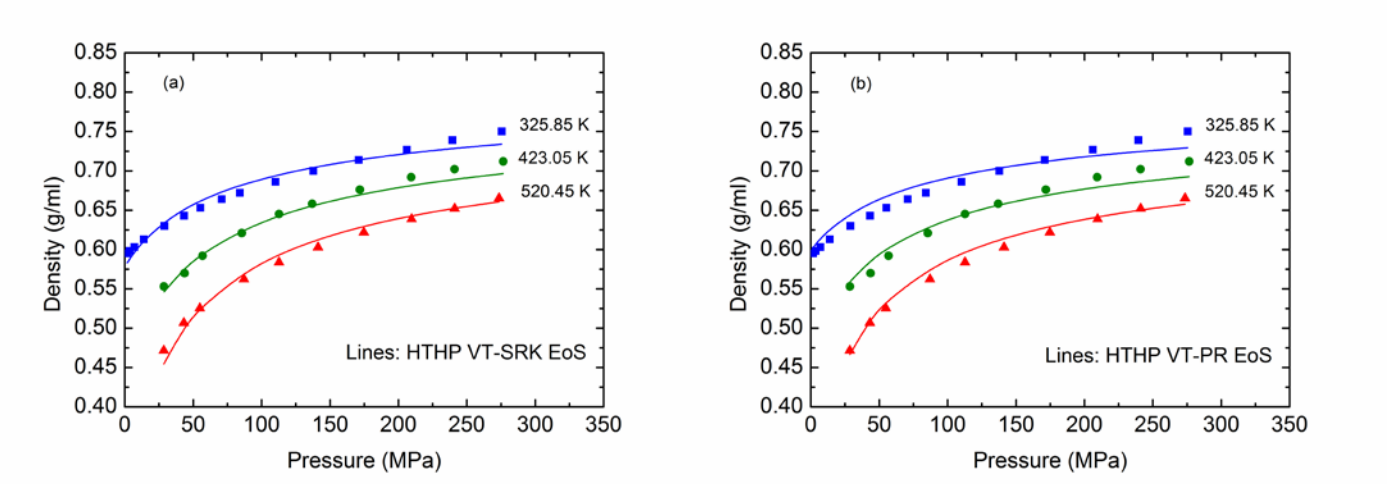

Figure 12: (a) Comparison of the new HTHP VT-SRK EoS with n-pentane density data [16], (b) Comparison of the new HTHP VT-PR EoS with n-pentane density data [16]

Table 3 presents the MAPD and SD values for the high pressure, high temperature densities for the 17 fluids considered in this study. The very low overall MAPD values of 1.47 % and 2.01 % for the HTHP VT-SRK and HTHP VT-PR EoS, respectively, in the HTHP region demonstrate the benefits of utilizing a volume translation approach for a cubic EoS. It should be noted that these values of the MAPD are obtained when utilizing an HTHP data base to determine the volume translation equation rather than using sub-critical saturated liquid phase density values. The volume translation correlations presented here provide a method for accurate EoS calculations for the ~(7 - 276) MPa pressure range and ~(278 - 533) K temperature range related to ultradeep reservoir and well conditions. The results presented here also demonstrate that PC-SAFT, with an overall MAPD value of 2.05%, also provides very good density predictions with an accuracy similar to that found with the HTHP VT-PR EoS. Given that the three pure component parameters for PC-SAFT are based on sub-critical liquid density and vapor pressure fits, its ability to provide such accurate density predictions at HTHP conditions indicates that PC-SAFT is a more powerful model for density predictions than cubic equations of state and conventional volume-translated cubic equations of state. Volume translated cubic equations of state can provide more accurate HTHP density predictions than PC-SAFT only when the volume correction is based on an HTHP data base (e.g. HTHP VT-SRK EoS and HTHP VT-PR EoS).

The performance of the equations of state along isotherms or isobars can also be assessed by means of the relative deviation δ, which is defined as

$$\delta = \frac{\rho_{i,experimental} - \rho_{i,calculated}}{\rho_{i,experimental}} \times 100 \quad \% \tag{16}$$

Figure 13 compares the relative deviations as a function of pressure using nine different models for calculating the density of n-decane at 520.15 K-isotherm.

Table 3: Mean absolute percentage deviation (MAPD) and standard deviation (SD) for all compounds and equations of state studied in this work

compound	SRK		PR		Ji and Lempe		Wang and Gmehling		Magoulas and Tassios		Ungerer et al.		PC-SAFT		HTHP VT-SRK		HTHP VT-PR	
	MAPD	SD	MAPD	SD	MAPD	SD	MAPD	SD	MAPD	SD	MAPD	SD	MAPD	SD	MAPD	SD	MAPD	SD
methane	1.27	0.64	8.62	3.28	2.32	1.40	1.30	1.02	0.83	0.85	22.57	8.30	1.79	0.63	0.81	0.80	0.66	0.35
propane	2.00	1.29	8.79	1.36	48.67	18.78	21.42	7.47	20.95	8.34	9.02	1.19	1.91	0.77	1.54	1.30	1.16	0.63
n-pentane	5.63	2.45	4.68	2.44	19.71	11.75	10.67	6.55	8.45	5.67	2.60	1.89	1.72	1.52	1.11	0.74	1.54	0.81
cyclohexane	5.47	1.35	5.95	1.29	8.15	7.73	4.90	3.83	4.73	3.91	1.77	0.71	0.48	0.37	2.15	1.17	3.60	1.15
n-heptane	10.22	1.81	1.58	1.18	13.87	19.51	9.13	9.83	8.32	12.91	1.11	0.96	1.07	0.84	1.30	1.52	1.33	0.73
n-octane	11.89	2.60	2.75	2.13	13.40	12.87	10.09	8.83	6.17	6.00	1.66	1.32	2.80	1.47	1.36	1.31	1.56	1.07
isooctane	6.27	2.43	4.77	2.13	19.95	23.88	14.57	13.26	12.48	13.75	5.74	2.05	3.35	1.92	2.63	1.39	4.34	2.01
cyclooctane	6.77	2.05	3.88	2.19	7.16	4.47	5.75	3.49	3.04	1.54	3.85	1.54	1.91	0.93	1.91	1.07	3.65	1.36
n-decane	15.67	2.59	6.13	2.93	8.33	6.16	7.27	5.57	2.67	1.93	2.37	1.94	2.46	1.39	1.19	0.95	1.59	1.02
n-tridecane	20.95	2.49	11.87	2.87	6.87	3.78	4.16	5.07	3.03	2.18	5.53	1.75	1.23	0.73	1.14	0.61	1.55	0.76
n-hexadecane	31.79	4.30	18.40	3.91	8.76	5.62	5.67	4.60	3.55	2.37	1.81	1.99	1.93	1.24	1.24	1.05	1.62	1.23
n-octadecane	33.31	4.70	19.75	4.25	13.32	4.89	7.59	6.16	2.69	1.82	1.80	2.04	2.68	1.76	1.55	1.03	1.90	1.20
n-eicosane	35.88	4.69	22.05	4.27	6.02	4.17	N/A	N/A	2.59	1.64	2.24	2.46	2.11	1.39	1.60	1.65	2.02	1.66
n-C30	30.69	2.53	22.88	2.84	8.40	6.57	N/A	N/A	18.32	3.04	2.26	2.32	2.59	1.53	1.98	0.81	2.45	1.11
n-C40	50.63	2.05	45.10	2.26	15.31	8.10	N/A	N/A	3.61	2.23	1.55	1.63	5.11	1.45	1.27	1.00	1.58	0.96
benzene	7.33	1.38	4.00	1.42	7.37	9.51	3.80	4.89	3.34	4.76	2.95	1.34	0.80	0.50	1.57	1.20	1.53	0.85
toluene	9.73	2.11	2.12	1.51	9.69	8.84	6.54	5.85	4.69	2.12	4.33	1.33	0.94	0.71	0.70	0.52	2.07	1.28
Overall	16.79	2.44	11.37	2.49	12.78	9.30	8.06	6.17	6.44	4.42	4.30	2.04	2.05	1.13	1.47	1.07	2.01	1.07

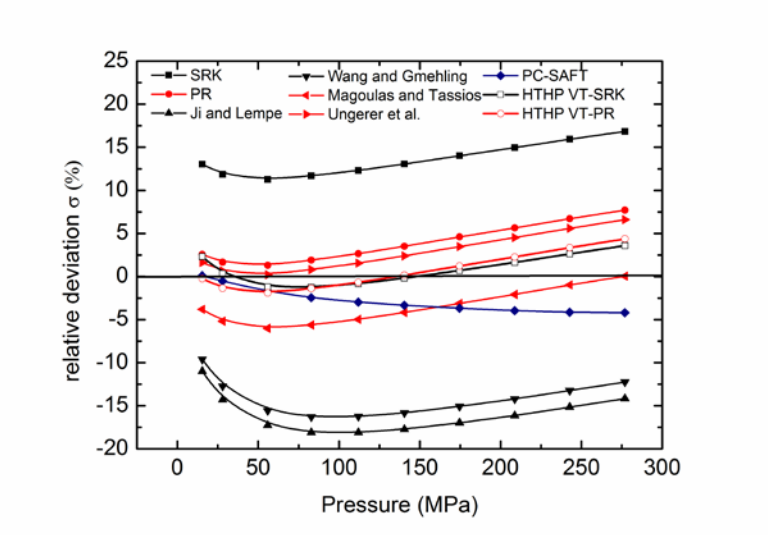

Figure 13: Relative deviation of the calculated density associated with all in this study investigated models for n-decane at 520.15 K [16]

The SRK and the volume translated SRK equations of state fit to the saturated liquid densities show large deviations from the experimental data over the entire range of pressure. The PR EoS provides a modest fit for n-decane densities at pressures to ~ 100 MPa, but as the pressure increases the deviation becomes larger. The model of Magoulas and Tassios improves the density predictions of n-decane at this temperature only for pressures higher than ~ 150 MPa. The volume translated PR model of Ungerer and Batut shows good results for pressures to ~ 100 MPa and then exhibits behavior similar to the PR EoS. The PC-SAFT EoS provides very good results for pressures up to 75 MPa, but the deviation becomes larger as the pressure increases. Both the HTHP VT-SRK EoS and the HTHP VT-PR EoS provide very good predictions for pressures up to 200 MPa, but as the pressure increases the equations tend to under-estimate the density of n-decane. The performance of the HTHP VT-SRK EoS is slightly better than that of the HTHP VT-PR EoS.

2.3 EXTENSION TO MIXTURES

The HTHP VT-SRK EoS and HTHP VT-PR EoS can be extended to mixtures using the following mixing rule proposed in other volume-translated cubic EoS models [20, 21, 26]:

$$c_m = \sum_i x_i \, c_i \tag{17}$$

where x_i and c_i are the mole fraction and the volume translation term of pure component i in the mixture, respectively.

Both new models have been tested on binary mixtures using the conventional van der Waals mixing rules for the parameters of the original cubic equations of state:

$$a_m = \sum_i \sum_j x_i \, x_j \left(a_i a_j\right)^{0.5} \left(1 - k_{ij}\right) \tag{18}$$

$$b_m = \sum_i x_i b_i \tag{19}$$

where k_{ij} is the binary interaction parameter between molecules i and j. The use of one interaction parameter is sufficient, even at high pressures, but near the critical region, the use of two parameters (k_{ij} , l_{ij}) provides more accurate predictions [45] . k_{ij} values are typically obtained by fitting sub-critical VLE data. For alkane-alkane pairs, k_{ij} can be approximately set to zero if experimental VLE data are unavailable. For other pairs, especially those including non-hydrocarbons, k_{ij} should be different from zero and must be determined [46].

Figure 14 shows the density predictions for the binary system methane / n-decane ($x_{methane}$= 0.3124) at 293.15, 333.15, and 373.15 K obtained with the HTHP VT-SRK EoS (k_{ij} = 0.062) , Figure 14a, and the HTHP VT-PR EoS (k_{ij} = 0.065), Figure 14b. The binary interaction parameters, which were determined by fitting to experimental VLE data taken from [47], were used in both the translated and untranslated estimates. The prediction results of both HTHP VT

equations of state are in good agreement with the experimental data throughout the entire pressure range. The total MAPD values obtained with the HTHP VT-SRK EoS and the HTHP VT-PR EoS for these density isotherms are 0.70 % and 0.42 %, respectively.

Figure 15 shows the calculated density isotherms for the binary system n-hexane/n-hexadecane ($x_{n\text{-}hexane}$= 0.4) at 298.15, 323.15, and 373.15 K obtained with the HTHP VT-SRK EoS (k_{ij} = 0.0056), Figure 15a, and the HTHP VT-PR EoS (k_{ij} = 0.0042), Figure 15b. The binary interaction parameters, which were determined by fitting to experimental VLE data taken from [48], were used in both the translated and untranslated equations of state. The predictions of both translated HTHP equations of state are in good agreement with the experimental data for pressures to ~ 100 MPa, but as the pressure increases the equations tend to under-estimate the density of this mixture. The total MAPD values obtained with the HTHP VT-SRK EoS and the HTHP VT-PR EoS for these density isotherms are 0.98 % and 1.06 %, respectively.

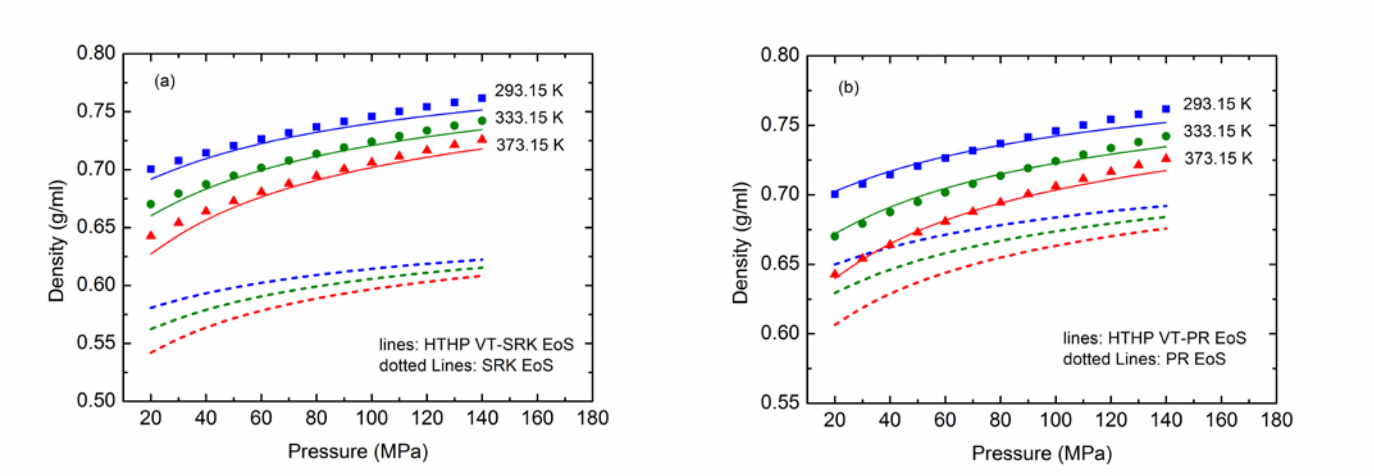

Figure 14: Comparison of density experimental data [49] (symbols) of the binary mixture methane/n-decane ($x_{methane}$= 0.3124) at 293.15, 393.15, and 373.15 K with (a) predicted densities using SRK EoS (dashed lines) and HTHP VT-SRK EoS (lines) with k_{ij} = 0.062. (b) predicted densities using PR EoS (dashed lines) and HTHP VT-PR EoS (lines) with k_{ij} = 0.065

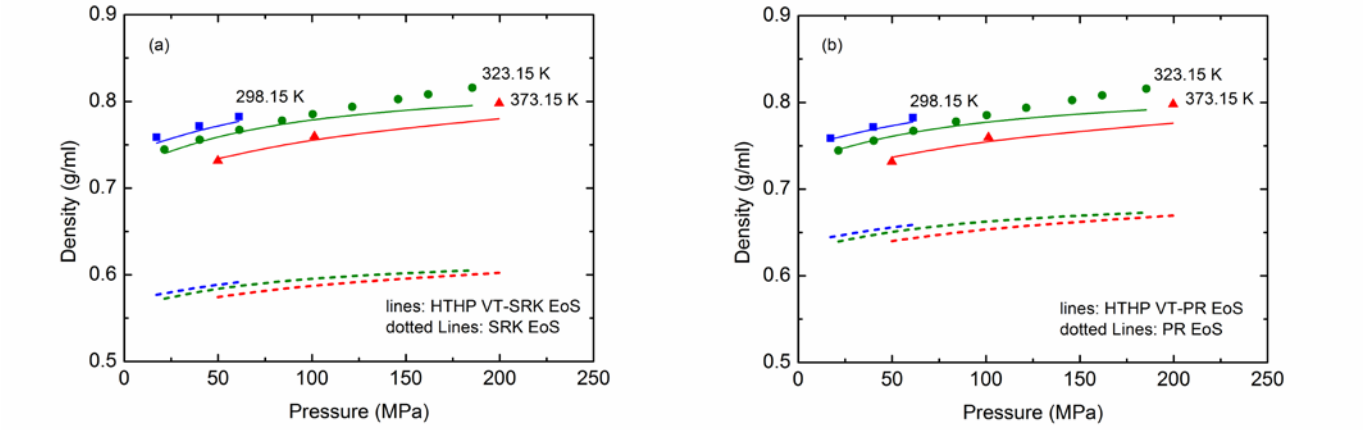

Figure 15: Comparison of density experimental data [50] (symbols) of the binary mixture n-hexane/n-hexadecane ($x_{n\text{-}hexane}$= 0.4) at 298.15, 323.15, and 373.15 K with (a) predicted densities using SRK EoS (dashed lines) and HTHP VT-SRK EoS (lines) with k_{ij} = 0.0056. (b) predicted densities using PR EoS (dashed lines) and HTHP VT-PR EoS (lines) with k_{ij} = 0.0042

2.4 EXTENSION TO LOW PRESSURE CONDITIONS

This study was based on a need to provide the petroleum industry with simple-to-implement thermodynamic models that provide accurate predictions of fluid density at extremely high temperatures and pressures. Because cubic equations of state, especially the SRK and PR EoS, are so prevalent in compositional simulators, the relatively straightforward volume-translation modification of these particular models was deemed a desirable solution for pressures from ~(7 - 276) MPa and a temperature range of ~(278-533) K. In order to provide the user with a measure of the accuracy of the HTHP VT-SRK and HTHP VT-PR models if employed for low pressure calculations, the saturated densities of several hydrocarbons were determined for each of the thermodynamic models employed in this study.

Figure 16 compares the ability of some of these models to predict the saturated density for n-pentane. All of the models fit the saturated vapor density curve. It is evident that the Ji &

Lempe and Magoulas & Tassios models that are fit to saturated data provide the best results for the saturated liquid density. The HTHP models improve the saturated liquid density only in the region away from the critical point at relatively low reduced temperatures.

Figure 17a-f shows *PVT* predictions using (a) SRK EoS, (b) Ji and Lempe's VT-SRK EoS, (c) Magoulas and Tassios's VT-PR EoS, (d) PC-SAFT EoS, (e) HTHP VT-SRK EoS, and (f) HTHP VT-PR EoS. All of the models provide reliable vapor phase molar volume predictions. Figure 17a shows that the SRK EoS exhibits good results at 520.45 and 600.15 K, but fails to provide a good fit for the saturated liquid molar volume and consistently over-estimates the n-pentane molar volume for the other isotherms over the entire pressure range.

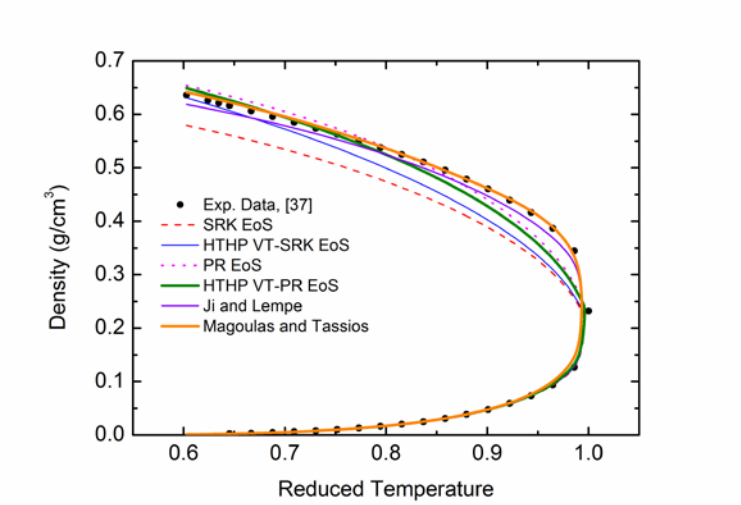

Figure 16: Prediction results of saturated density for n-pentane using some thermodynamic models studied in this work

Figure 17b shows that the VT-SRK EoS of Ji and Lempe yields a good fit for the saturated liquid molar volume and provides reasonable results at 325.85 K over the entire pressure range. However, for the other isotherms the model gives reasonable molar volume predictions only at low pressures since the isotherms cross in the high pressure region. The volume translated PR model of Magoulas and Tassios, presented in Figure 17c, shows behavior similar to the model of Ji and Lempe. The *PVT* calculation results obtained with the PC-SAFT model, shown in Figure

17d, demonstrate that the performance of this model for n-pentane is very good over the entire temperature and pressure ranges of interest. Figure 17e and 17f show the calculation results of n-pentane obtained with the HTHP VT-SRK EoS and the HTHP VT-PR EoS. The prediction results of these equations of state in the low pressure region are still inferior to those of the Magoulas and Tassios VT-PR and PC-SAFT models. Note, however, that the deviation between the predicted molar volume and the corresponding experimental value becomes smaller for isotherms in the liquid region at high pressures. This behavior shows that, as expected, the HTHP models perform best in the higher pressure range achieving even slightly better performance than the PC-SAFT model in the high pressure range of interest.

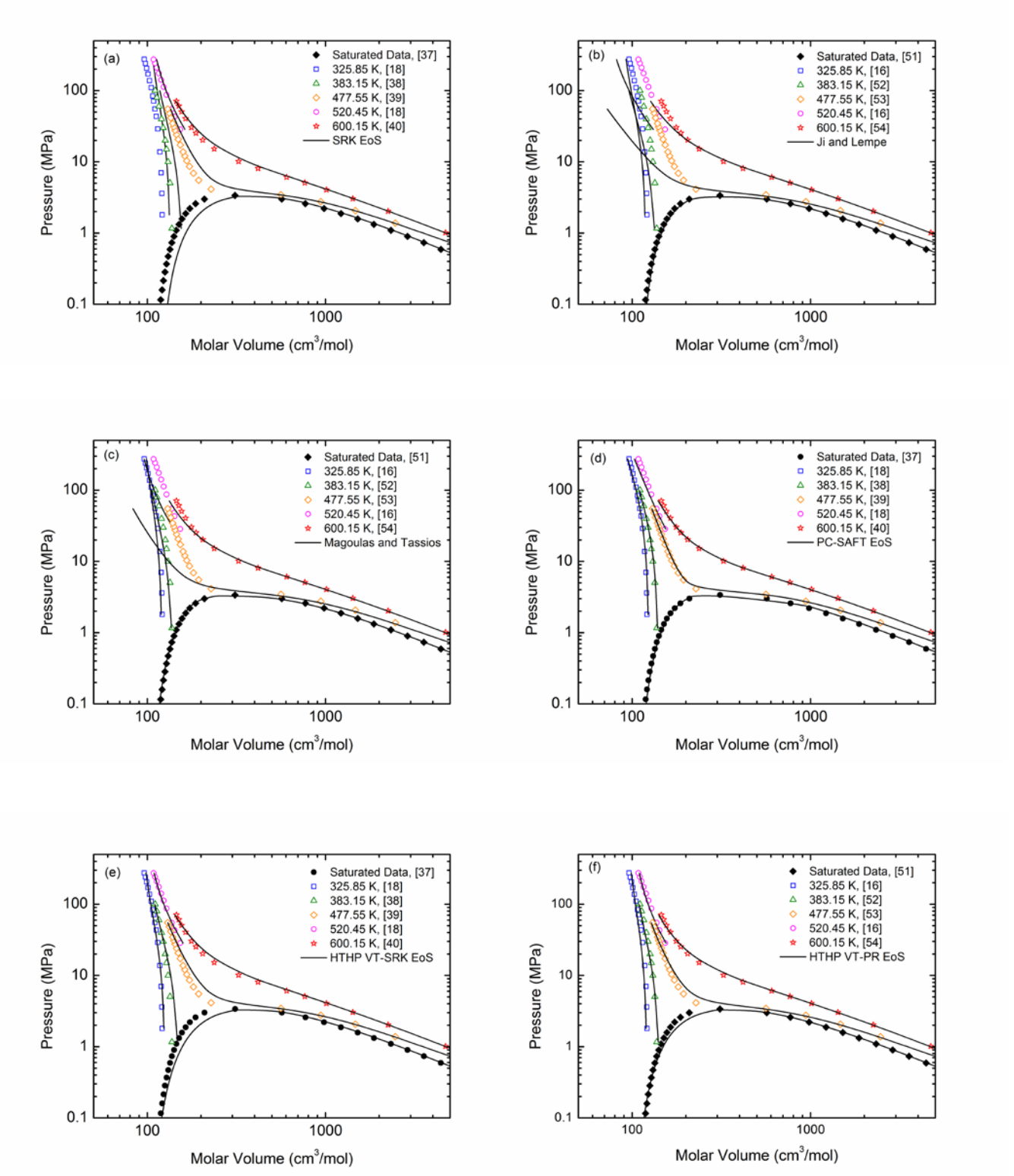

Figure 17: Comparison of the calculated PVT data for n-pentane with the experimental data [16, 51-54]. (a) Predicted PVT data with SRK EoS. (b) Predicted PVT data with Ji and Lempe's VT-SRK EoS. (c) Predicted PVT data with Magoulas and Tassios's VT-PR EoS. (d) Predicted PVT data with PC-SAFT EoS. (e) Predicted PVT data with HTHP VT-SRK EoS. (f) Predicted PVT data with HTHP VT-PR EoS

2.5 EXTENSION TO DERIVATIVE PROPERTIES

The HTHP volume translation affects the equilibrium phase molar volumes without changing the equilibrium temperature, pressure and phase compositions, because the volume translation effects on the fluid fugacities in the different phases cancel each other out in the phase equilibrium calculations[20, 55]. Therefore, both the volume translated and untranslated model predict the same saturation pressure and as a result of this the enthalpy of vaporization, which is related to the slope of the saturation pressure curve by the Clausius-Clapeyron equation, remains unchanged upon volume translation. The enthalpy of vaporization is usually the derivative property that is most accurately predicted by cubic equations of state [56].

To verify if there are any thermodynamic inconsistencies associated with the HTHP volume translated equations of state, other derivative properties, such as the isothermal compressibility and speed of sound (its calculation involves first and second-order derivatives), were also studied. Figure 18 shows the calculations of the isothermal compressibility of n-pentadecane with the PR EoS and HTHP VT-PR EoS. Predictions of the speed of sound of n-hexane with the PR EoS and HTHP VT-PR EoS are compared with experimental data in Figure 19. The HTHP VT- EoSs fail to accurately reproduce these properties. However, they do not exhibit any unphysical results within the studied conditions.

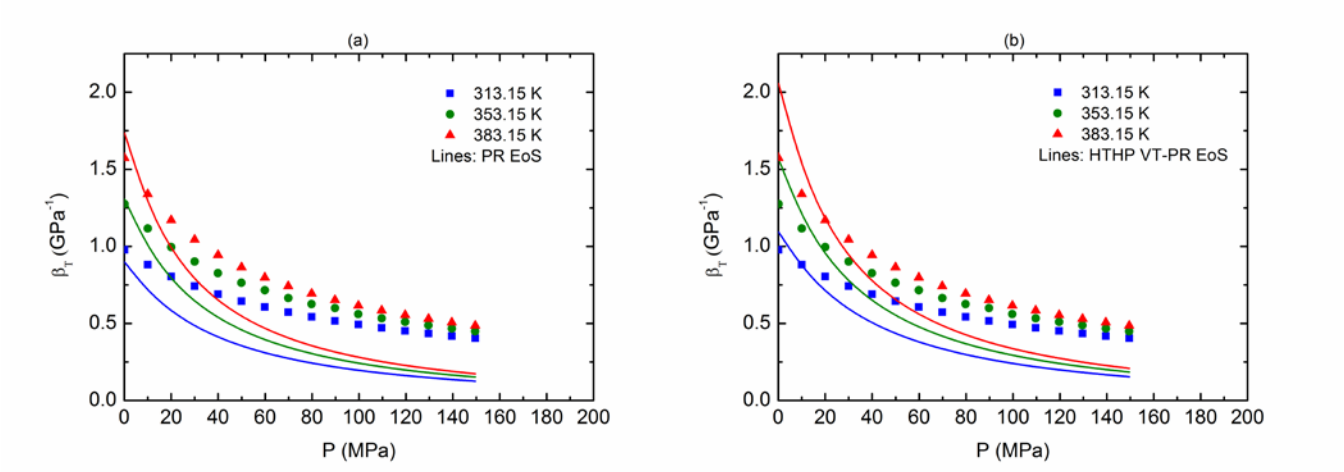

Figure 18: Isothermal compressibility (β_T) of n-pentadecane. Comparison of literature data [57] (symbols) with the predictions (lines) of (a) PR EoS, and (b) HTHP VT-PR EoS

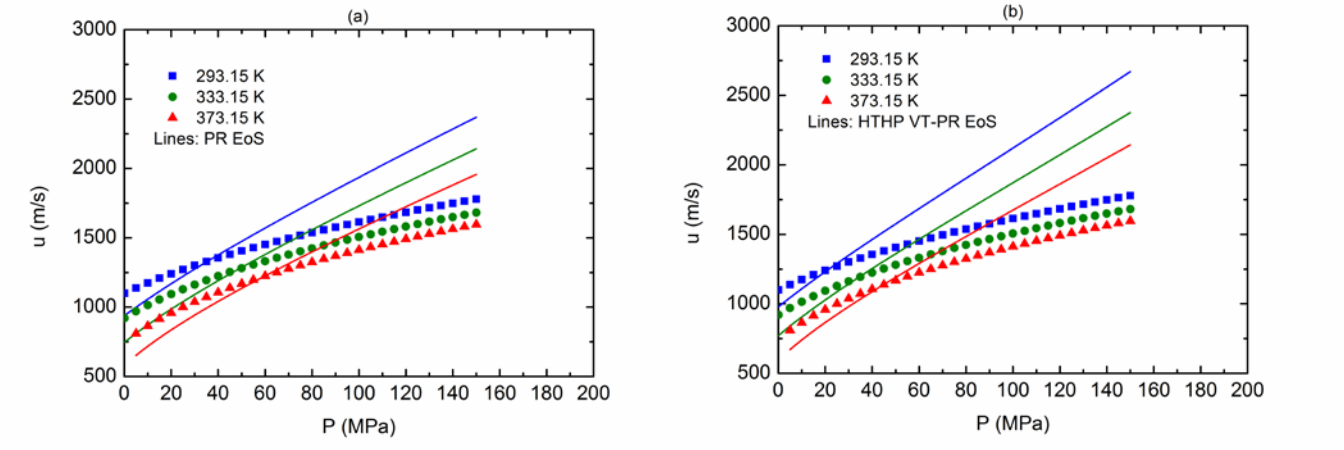

Figure 19: Speed of sound (u) of n-hexane. Comparison of literature data [58] (symbols) with the predictions (lines) of (a) PR EoS, and (b) HTHP VT-PR EoS

2.6 VALIDATION OF THE HTHP VT EQUATIONS OF STATE

The HTHP VT equations of state have been tested on several hydrocarbons not included in the model development database. Figure 20 shows improved density predictions obtained with the HTHP VT-PR EoS for n-dodecane and p-xylene.

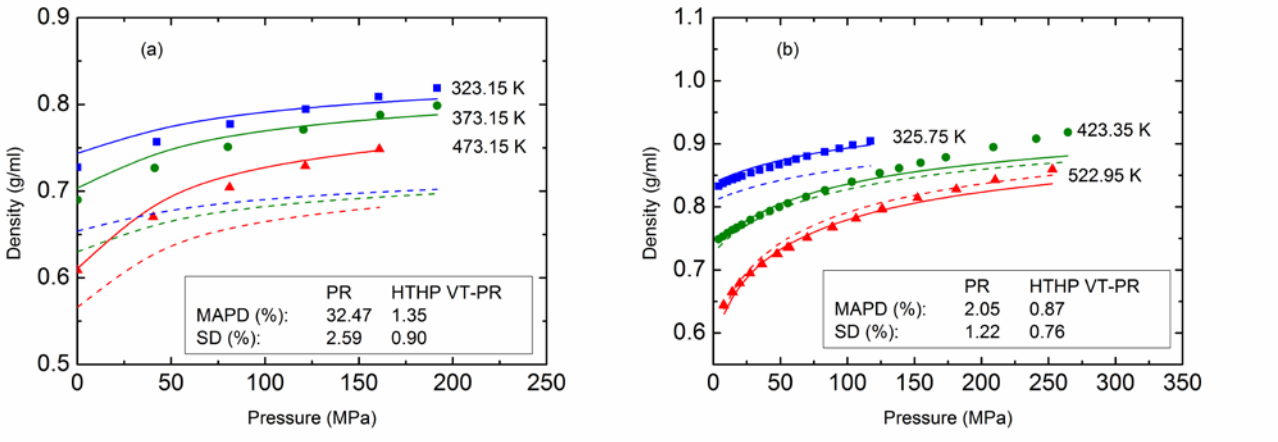

Figure 20: (a) Comparison of the new HTHP VT-PR EoS with n-dodecane density data [59], (b) Comparison of the new HTHP VT-PR EoS with p-xylene density data [60]

The performance of the HTHP VT-PR EoS has also been tested on dioctyl phthalate (DOP), a fluid that has a major role in viscosity section of this work. Experimental density data measured by [61] were used for evaluation and the properties needed for the volume correction were estimated with group contribution method proposed by Marrero and Gani [62] (T_c=868.70 K, P_c=1.220 MPa, ω=0.439). Figure 21 shows a comparison for three isotherms. The MAPD obtained with the HTHP VT-PR EoS of 2.22% is substantially smaller than the value calculated for PR EoS predictions of 14.3%.

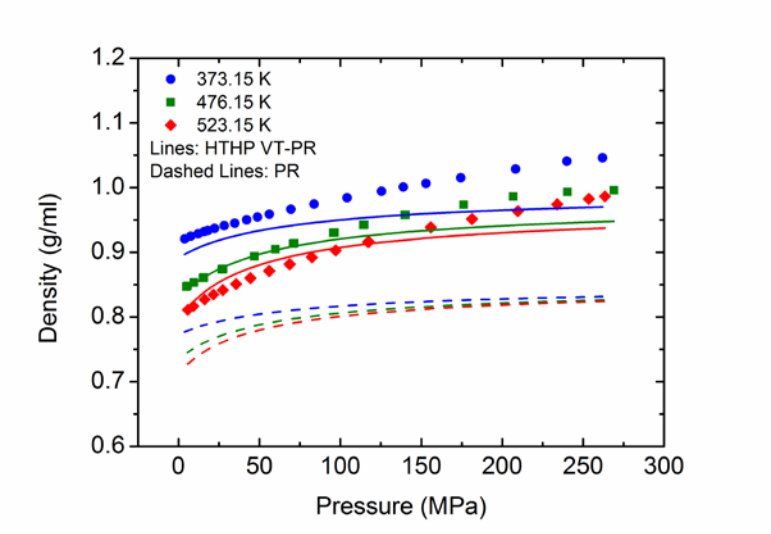

Figure 21: Comparison of density experimental data [61] (symbols) of dioctyl phthalate with predicted densities using PR EoS (dashed lines) and HTHP VT-PR EoS (lines)

2.7 CONCLUSIONS

Temperature dependent volume translation expressions have been proposed for the SRK and PR equations of state for predicting molar volumes at extreme temperature and pressure conditions associated with ultra-deep reservoirs. Rather than correlating the volume correction to saturated liquid densities, as is done in most prior volume translation methods, the volume translation term in the HTHP VT-SRK EoS and HTHP VT-PR EoS is correlated to pure component, single-phase density data for short- and long-chain alkanes, cycloalkanes and aromatics over a pressure range up to 276 MPa and a temperature range up to 533 K. Density predictions of the new proposed volume translated equations of state have been compared to the predictions of the standard SRK and PR, temperature dependent volume translated SRK and PR , and PC-SAFT equations of state.

All original and volume translated SRK and PR models fit to saturated liquid density data were found to be inappropriate for predicting the molar volumes at the temperature and pressure ranges of interest. The correlations of Ungerer and Batut provide moderate to good density predictions for most components studied in this work with an overall MAPD of 4.30%, although this model has two drawbacks. Not only it fails to accurately predict the density of some light alkanes like methane and propane, but a reference experimental density value is also required for the correlation of heavy hydrocarbons. Such information is not always at hand. Although the PC-SAFT EoS was fit to vapor pressure and saturated liquid density data, its results are very good for most fluids with an overall MAPD of 2.05%.

The new proposed HTHP VT-SRK and HTHP VT-PR equations of state provide very good results with an overall MAPD of 1.47% and 2.01%, respectively. The proposed models have been successfully extended to mixtures. Good results have been obtained for density calculations of several binary mixtures. Within the temperature and pressure ranges of interest, the new HTHP VT-EoSs do not exhibit any thermodynamic inconsistency that other volume translated models (fit to saturated liquid density data) might have. The new models were tested on various hydrocarbons not included in the database used in the model development. In all cases, improved density predictions have been obtained. Because of the good performance at the temperature and pressure conditions of interest and the relative simplicity of the new proposed equations of state compared to SAFT based models, these correlations are recommended for ultra-deep reservoir fluid applications.

3.0 VISCOSITY OF HYDROCARBONS AT ULTRA-DEEP RESERVOIR CONDTIONS

Viscosity is an important fluid property required in the development and production of petroleum reservoirs. Despite the significance of viscosity in the petroleum industry there is still a lack of experimental viscosity data in particular at extremely high temperature, high pressure (HTHP) conditions associated with ultra-deep petroleum formations that are approximately 4,600 meters or more underground, where the pressure and temperature can reach as high as 241 MPa and 533K, respectively. Figure 22 shows literature viscosity data for n-pentane [52, 53, 63, 64] and n-hexadecane [65, 66] as examples for literature experimental viscosity data gap at HTHP conditions. These plots show clearly the need for obtaining viscosity data at elevated temperatures and pressures. Viscosity data that cover the entire temperature and pressure ranges of interest are required for the assessment of literature viscosity correlations and the development of reliable models. For this purpose, a windowed, volume-variable rolling ball viscometer has been designed and constructed to carry out viscosity measurements for various hydrocarbons. The viscosity measurement technique using a rolling ball viscometer can be used in the measurement of both low and high pressure viscosity of pure hydrocarbons and mixtures [67].

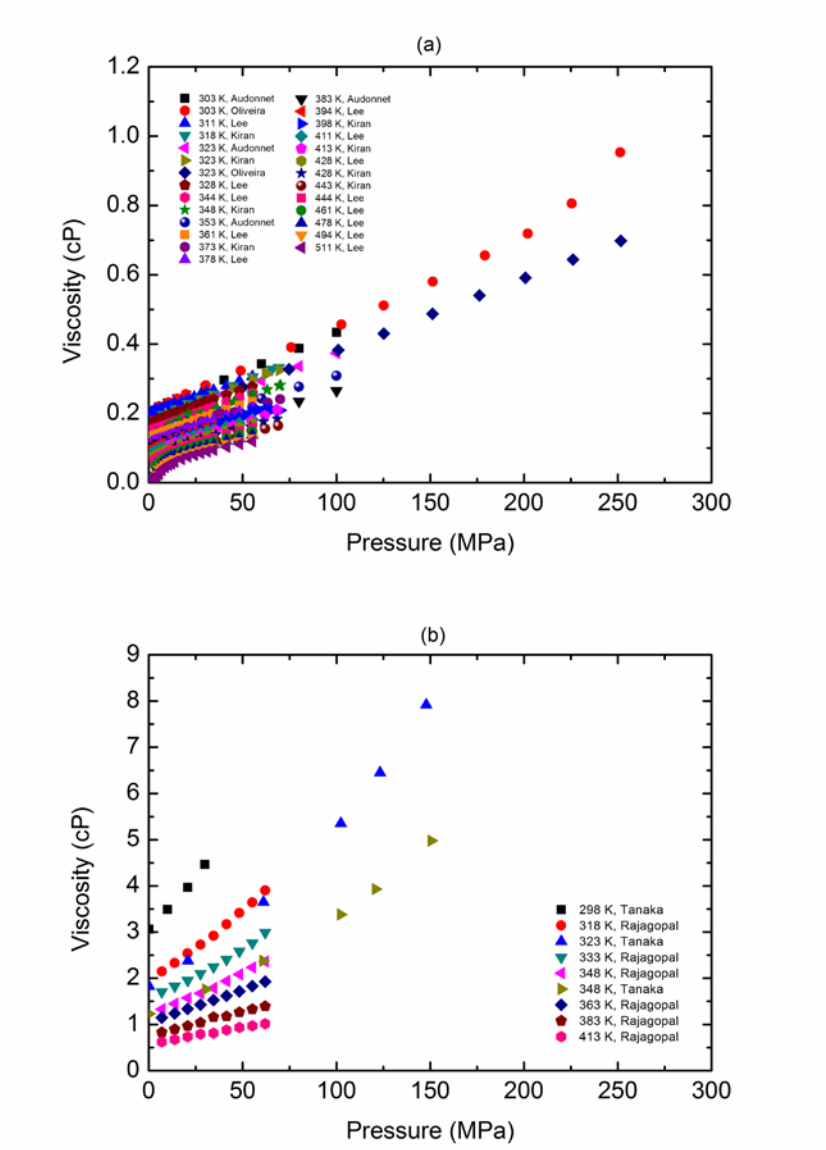

Figure 22: Experimental viscosity data available in the literature for (a) n-pentane, and (b) n-hexadecane

3.1 THE ROLLING BALL VISCOMETER

The rolling ball viscometer was first suggested by Flowers [68] in 1914. Two years later, Hersy [69] developed a correlation of the variables involved in the measurement. In 1933, Sage [70] used the rolling ball technique to measure the viscosity of hydrocarbons. In the same year, Hoeppler [71] developed a commercial instrument which is known as Hoeppler viscometer. He

used an inclined tube at an angle of 80^o for his measurements. In 1943, Hubbard and Brown [72] used dimensional analysis to derive relations between the variables involved in the system. Table 4 lists some of the references in which the rolling ball viscometer has been used for viscosity measurements.

Table 4: Some references for rolling ball viscometer

Reference	Year	Tube	Ball	D, mm	d, mm	θ, ^{o}	max.T, K	max.P, psi	Detection technique
Sage [73]	1937	steel	steel	12.705	12.591	15	380	3,000	recording of electrical contact
Hubard [72]	1943	glass	aluminum, …	6.0-10.0	85-99.28 % D	4-25	298	14.7	using photoelectric device
Carmichael [74]	1952	steel	steel	12.7	12.59	15	378	6,000	using sensing coils
Stanley [75]	1968	steel	steel	6.502	6.2992	0-90	323	20000	using sensing coils (magnet)
Voorst [76]	1976	glass	steel	3.5	3.17	10-70	310	14.7	using photodiodes
Geils [77]	1977	silica	alumina,…	10	6.35	0-70	1273	14.7	generating of sound pulses
Nishibata [78]	1986	steel	steel	12	11.82	10-70	333	145,000	using differential transformers
Sawamura [79]	2004	pyrex	pyrex	8.23	8	10	298	50,000	sensing of light beam
Tomida [80]	2006	glass	steel	7.15	7	NA	353	3,000	NA
Sato [81]	2008	titanium	steel	10.34	10.32	10	350	1,700	sensing of electromotive force

Measuring principle and defining equation:

The rolling ball viscometer composed of a closed cylindrical tube filled with the fluid sample. The tube can be heated and pressurized to the desired conditions. When the tube is tilted to a certain angle, and the ball starts rolling down. After an initial acceleration, the ball reachs a constant terminal velocity that can be measured and used to determine the viscosity.

If the flow around the ball is laminar, the viscosity η is proportional to the roll time in the expression [82]

$$\eta = C\left(\rho_b - \rho_{fl}\right) t \tag{20}$$

where

$$t = \frac{l}{\mathrm{v}} \tag{21}$$

$\left(\rho_b - \rho_{fl}\right)$ is the difference in the density between the ball and the fluid, and *t* is the time taken by the ball to roll at its terminal velocity, v, through a certain distance, *l*. *C* is a geometric constant that incorporates different parameters including the diameters of the ball and the tube, and the angle of inclination of the tube. It can be determined by calibration with a fluid of known viscosity. Unlike the falling cylinder viscometer, because of the complex geometry of this system, it is not possible to accurately predict the viscometer constant.

Since the parameter *C* is a function of the angle of inclination, there exist different values of *C* for each angle [78]. By the use of dimensional analysis, Hubbard and Brown [72] obtained a correlation that gives a first estimation of the viscometer constant from the dimensions of the instrument.

$$C = \frac{5\pi}{42} K\, g\ sin\theta \frac{d\left(D+d\right)}{l} \tag{22}$$

where *g* is the gravity acceleration (9.8 *m/sec*^{2}), θ is the angle of inclination of the tube to the horizontal, *d* is the diameter of the ball (*cm*), *D* is the diameter of the tube (*cm*), *l* (*cm*) is the rolling distance of the ball, and *K* is a dimensionless correlation factor determined from experimental data for different viscometer geometries and fluids obtained by Hubbard and Brown [72], Hoeppler [71], Benning and Markwood [83], and Spée [84]. Figure 23 shows this correlation factor as a function of the diameter ratio *d/D*.

Sage and Lacey [85] extended Equation (20) to the turbulent region by relating a fluid specific viscosity-ratio correction factor to a Reynolds number dependent function.

Lewis [86] treated the rolling ball viscometer theoretically and developed an equation for the viscometer constant as

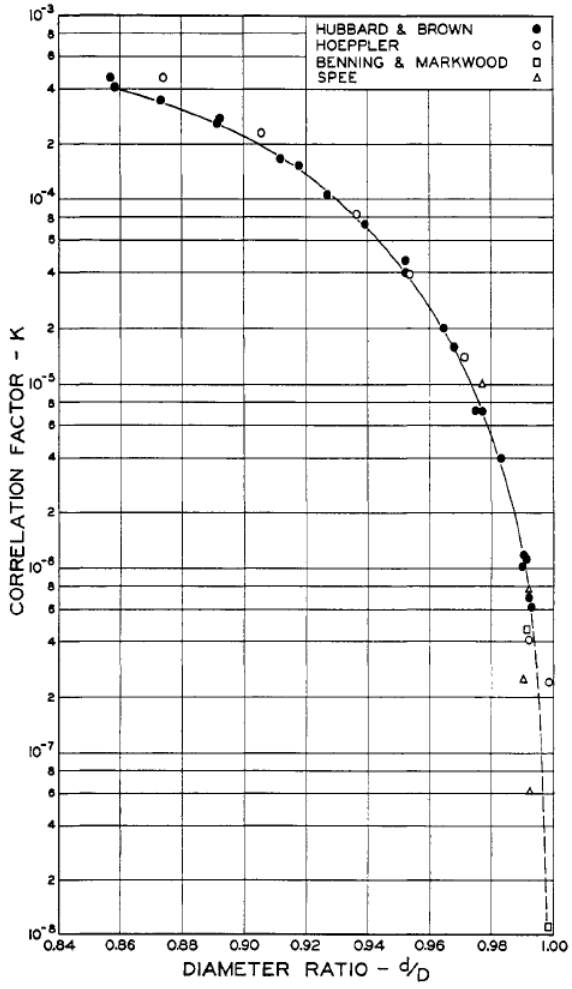

Figure 23: Correlation factor K for rolling ball viscometers, after Hubbard and Brown [56]

$$C = \frac{1}{12\pi I} g \sin\theta \frac{D^2}{l}\left(\frac{D-d}{D}\right)^{5/2} \tag{23}$$

where I = 0.398. His results agree with the dimensional analysis and experimental tabulation of Hubbard and Brown[72].

Tilting angle:

By inclination of tube, care must be taken that no sliding of the ball and no turbulent flow around the ball occur. Increasing the tilting of the viscometer to the horizontal reduces the roll time, while decreasing the inclination increases the roll times. By very steep tilting sliding the ball may occur. Depending on the viscosity range, the tilting angle can be adjusted.

Critical Reynolds number:

The best viscosity results can be obtained when the viscometer is operated in the laminar region of fluid flow, because the sensitivity to viscosity in this region is greater than in turbulent flow region. Hubbard and Brown [72] found upon studying rolling ball viscometers of different tube and ball diameters, inclination, and sixteen fluids that for laminar flow, if we plot a resistance factor, *f*, vs. Reynolds number, *Re*, on logarithmic coordinate diagram, we get a straight line. The resistance factor and Reynolds number are defined as:

$$f = \frac{5\pi}{42} g \cdot t^2 \frac{(D+d)^2}{l^2 \cdot d} \frac{(\rho_b - \rho_{fl})}{\rho_{fl}} \sin\theta \tag{24}$$

$$Re = \frac{l \cdot d^2}{(D+d) \cdot t} \frac{\rho_{fl}}{\eta} \tag{25}$$

Effect of temperature and pressure changes:

The effect of temperature and pressure changes on the rolling ball viscometer may be appreciable when materials with high coefficients of thermal expansion and compressibility are used. The effect is greater if the ball and tube are of different materials. In our newly designed rolling ball viscometer, both the tube and the spheres are made of Inconel 718 which has low thermal expansion and compressibility coefficients of (7.40±0.20) x 10^{-8} $^{o}F^{-1}$ and (4.60±0.40) x 10^{-8} psi^{-1}, respectively [87]. This choice minimizes the thermal and mechanical effects associated with the high temperatures and pressures. However, under extreme pressure, the ball becomes slightly

smaller, whereas the cell expands. To illustrate this effect, Figure 24 shows the change of a diameter ratio (d/D) of 0.99816 with pressure and temperature. The calculation steps of these results can be found in Appendix A.

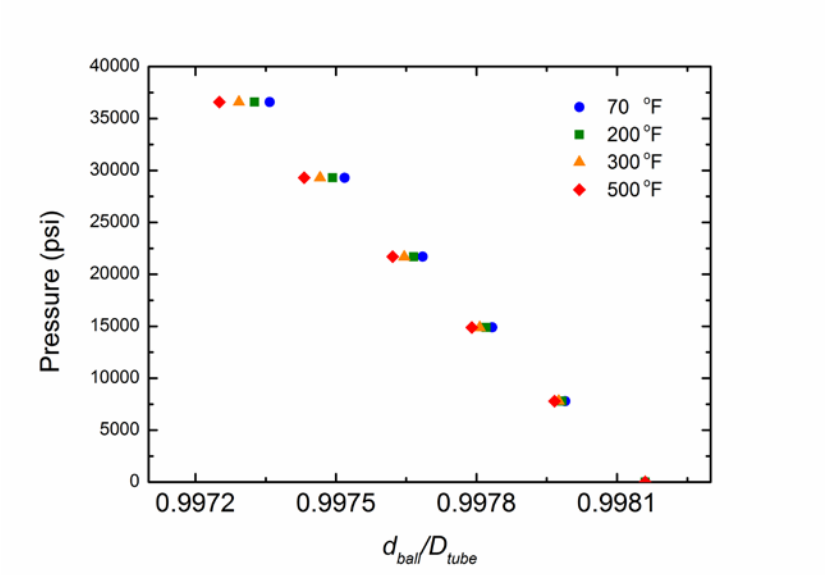

Figure 24: Pressure and temperature effects on diameter ratio

Based on the Hubbard and Brown [72] and Lewis [86] equations, Izuchi and Nishibata [88] proposed the following relationships to describe the deformation of materials with temperature and pressure:

$$\frac{C}{C_0} = 1 + \left\{ \alpha_b + \alpha_t + \left(\frac{r_0}{1+r_0} - \frac{5}{2}\frac{r_0}{1-r_0} \right) (\alpha_b - \alpha_t) \right\} (T - T_0) + \left\{ \beta - \beta_{tb} + \left(\frac{5}{2}\frac{r_0}{1-r_0} - \frac{r_0}{1+r_0} \right) (\beta + \beta_{tb}) \right\} (P - P_0) \tag{26}$$

$$\beta = \frac{1}{E_t} \left(\frac{r_1^2 + r_2^2 - \nu_t r_1^2}{r_2^2 - r_1^2} + \nu_t \right) \tag{27}$$

where C_0 is the viscometer constant at a given inclination angle, reference temperature, T_0, and reference pressure, P_0; r_0 is the diameter ratio (d_0/D_0) of the ball to the tube at the reference condition; r_1 and r_2 are the inner and outer radii of the viscometer; α and β_t are the thermal

expansion and isothermal compressibility of the materials, respectively; and ν and E are the Poisson's ratio and the Young's modulus, respectively, of the tube and ball materials. Subscripts t and b denote the tube (viscometer) and ball, respectively.

Shear rate:

The shear rate at the surface of the ball is a function of the spatial variables z and ϑ, see Figure 25. Šesták and Ambros [89] proposed an expression for the mean shear rate by assuming a parabolic flow velocity distribution in the clearance between the ball and the tube. The mean shear rate for a Newtonian fluid was defined as

$$\bar{\dot{\gamma}} = 2.4\ \mathrm{v}\frac{D}{(D-d)^2} \tag{28}$$

where v is the terminal velocity of the rolling ball.

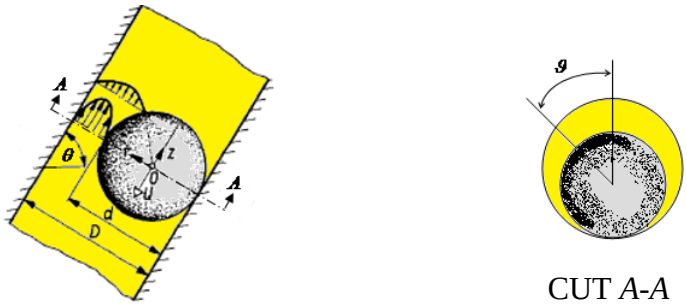

Figure 25: Shear rate in the rolling ball viscometer

According to equation 28, the average shear rate increases with the increase of the ball velocity v and the ratio of diameter of ball to diameter of tube d/D, Figure 26.

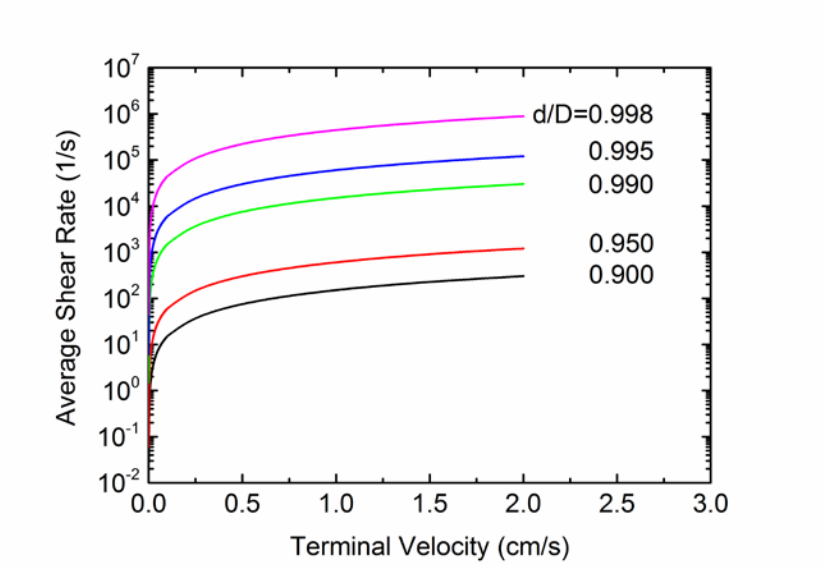

Figure 26: Average shear rate as a function of the terminal ball velocity and the diameter ratio

Advantages of rolling ball viscometers:

Rolling ball viscometers offer several advantages, including

- The apparatus is very simple.
- The apparatus can be based on the design of a densimeter with a cylindrical sample volume
- Only a small amount of sample is required.
- Visual observation through sapphire windows is possible even with opaque liquids, since the ball will be visible at the point where it contacts the glass tube making it possible for use of optical sensing system.
- A number of parameters such as ball diameter, tube diameter, tilting angle, ball and tube materials, and rolling distance can be varied.
- It is easier to get a uniform path for a rolling ball than for a cylinder falling co-axially through a cylinder.
- The rolling ball viscometer can be used in the measurement of both low and high pressure viscosity of pure hydrocarbons and mixtures [67, 90].

Rolling ball viscometers can be used to measure the viscosity of both liquids and gases. However, most of studies using rolling ball viscometers are for liquids, and very few are actually for gases. Liquid viscosity measurements are easier since liquids have higher dynamic viscosities as compared to gases. High viscous fluids have larger roll times which make the detecting of the rolling ball easier. Pyrex glass spheres and tubes can be used, if it is desired to measure the viscosity of low viscous fluids.

3.2 WINDOWED VOLUME-VARIABLE HTHP ROLLING BALL VISCOMETER

The rolling ball technique has been selected for our viscosity measurements because of the numerous advantages that the rolling ball viscometer offers and also because it is virtually identical to the densimeter used by McHugh and NETL in the PVT research project [16]. This densimeter has already been used to collect data to 260^{o}C and 40000 psi.

Figure 27 shows an expanded view of the design of the rolling ball viscometer used for viscosity measurements performed in this study. The body of the cell is constructed from Inconel 718, has an outside diameter of 3 inch, an inside diameter of 0.625 inch, and a maximum working volume of 50 ml. The spheres are also made of Inconel 718 in order to match any thermal expansion that might occur when operating over a broad range of temperature and pressure. Pyrex 7740 tubes and balls can be inserted into this viscometer for the measurement of extremely low-viscosity fluids, such as methane and propane. Pyrex is significantly less dense than Inconel, therefore the Pyrex ball will roll more slowly within the Pyrex tube, enabling more accurate velocity (and hence viscosity) values to be obtained.

Figure 27: Expanded view of the HTHP rolling ball viscometer used in this study. The front window and rolling ball are shown on the left-hand side of the viscometer body. The floating piston that separates the test fluid from the overburden fluid (water) is shown on the right-hand side of the viscometer body

Detailed drawings of the viscometer can be found in Appendix B. The experimental setup is shown in Figure 28. Two tilting tables are used to tilt the viscometer. The top one allows the cell to be tilted to the desired angle, after which the magnetic pin is lifted and the ball is allowed to roll down past the small sets of opposing sapphire windows. The bottom tilting table allows the ball to roll back to the starting position at the front sapphire window. Once the ball gets there the magnetic pin is lowered and the ball is held in place.

A borescope (Gradient Lens Corp.) is positioned against the window at the front end of the cell to view the fluid sample inside the cell and to watch the motion of the rolling ball. This study is concerned with measuring the single-phase viscosity of single- and multi-component hydrocarbons over wide ranges of temperature and pressure. As upon changing the conditions phase change may occur, the large sapphire front window allows direct visual verification that only a single-phase exists in the cell and the ball is rolling continuously during the course of the

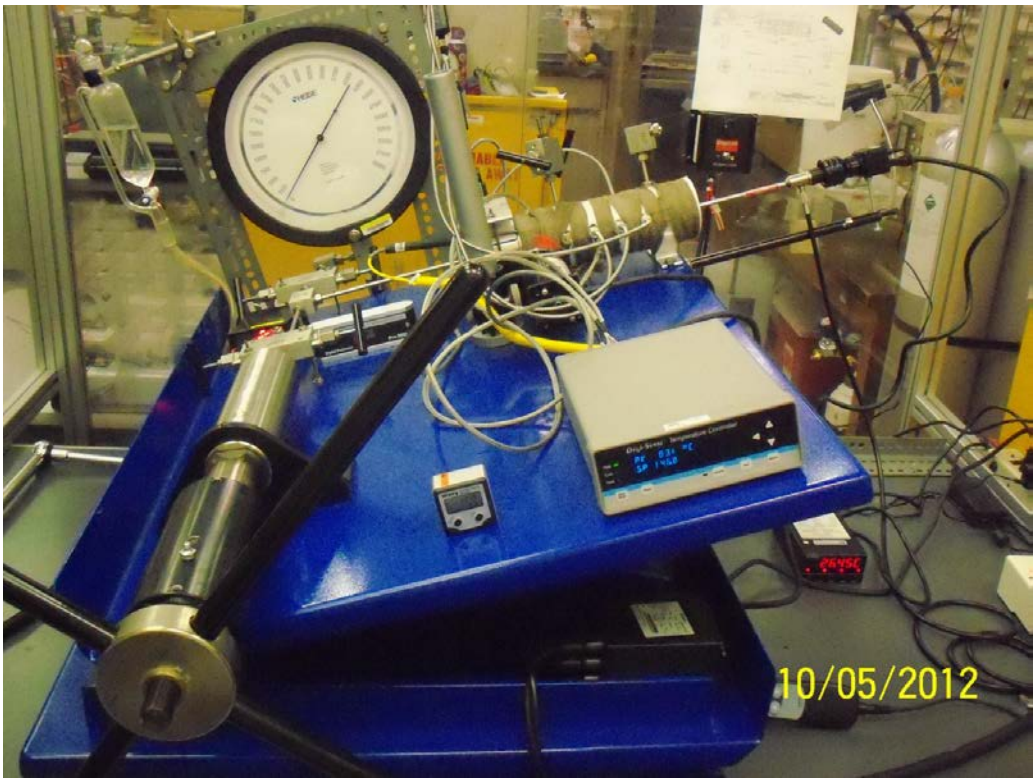

Figure 28: HTHP rolling ball viscometer cell

experiment. The cell has also three sets of opposing sapphire windows arranged a fixed distance of 1.5 inch apart along the viscometer tube. These three sets of small windows on the sides of the viscometer allow the position of the ball and hence its velocity to be determined without exposing any electronic devices to high temperatures and pressures. The cell contents is compressed to the desired operating pressure by displacing a piston in the cell using water pressurized with a high pressure generator (HIP Inc. model 37-5.75-60). The system pressure is measured on the water side of the piston using a pressure transducer (Viatran Corporation, model 245-BZS).

The velocity of the rolling ball through the inclined tube is determined by recording the time the ball needs to pass the three sets of opposing sapphire windows arranged radially along the length of the viscometer. The detection system is composed of a light source and three pairs

of glass fiber optic attached to the small sapphire windows. This arrangement allows for five independent ball velocity measurements since the velocity can be determined from the time it takes for a ball of specified diameter to roll past each set of three opposed windows, or the time it takes the ball to roll between two windows that are separated by a known distance, or the time it takes to roll past the first and last set of opposing windows. The three glass fiber optic sensors are interfaced with a computer through a LabVIEW program, Appendix C.

3.3 CALIBRATION OF THE ROLLING BALL VISCOMETER

The rolling ball viscometer has been calibrated with n-decane (Sigma Aldrich, Lot# SHBB3348 V, anhydrous, purity ≥ 99%), since reliable viscosity data have been reported in the literature for this alkane [63, 91]. In addition to the geometry, the calibration constant depends on the temperature and pressure too. Therefore, the viscometer was calibrated for temperatures to 500^{o}F and pressures to 35000 psia. Before running each experiment, care must be taken to clean all parts of the measurement system. In order to avoid any air bubbles to be trapped inside the cell, after assembling the viscometer, the cell has to be either evacuated using a vacuum pump or purged with low a molecular weight hydrocarbon such as methane or ethane. Upon this, the test sample fluid is loaded to the cell. Before starting the measurement, the viscometer is pressure-tested to about 20000 psi at room temperature. If the system holds this pressure for about 10 minutes, the pressure is taken back to the atmospheric pressure and the viscometer can be jacketed with band heaters (Rama Corporation) and insulation tape and the cell is heated up to the set temperature. The type-k thermocouple (Omega Corporation) used to measure the temperature of the fluid in the view cell is calibrated (20-260^{o}C) against a high precision

thermometer (Medicus Health, 0.01^{o}C resolution). The temperature of the viscometer is controlled with NIST certified temperature controller (Oakton Digi-Sense, 0.1^{o}C resolution). Once the system reaches the thermal equilibrium, which takes usually about two hours, the viscometer is tilted to the desired angle and the magnetic pin is lifted to allow the ball to roll down the tube and rolling times at different distances are acquired through a LabVIEW program. The ball stops at the immersed thermocouple and is brought back to the starting position by tilting the bottom tilting table. Once the ball gets to its initial position, the magnetic pin is lowered and the ball is held in place and a new pressure is set and the system is allowed about 30 minutes to get stabilized before taking a new measurement. Viscosity is very sensitive to any temperature change; therefore, the temperature of the fluid sample must be kept constant during the experiment. A summary of the calibration conditions and references used for calibration is given in Table 5. The calibration results are presented in Figure 29a for 30 and 50^{o}C, and Figure 29b for 146 and 247^{o}C.

Table 5: Summary of calibration conditions and references used for the calibration

Temperature ^{o}C	Ball Diameter inch	Diameter Ratio	Tilt Angle, θ	Density Reference	Viscosity Reference
30	0.621875	0.995	10^{o}	[63]	[63]
50	0.621875	0.995	10^{o}	[63]	[63]
146	0.623850	0.998	10^{o}	Tait Equation fit to density data from [16]	[91]
247	0.623850	0.998	10^{o}	Tait Equation fit to density data from [16]	[91]

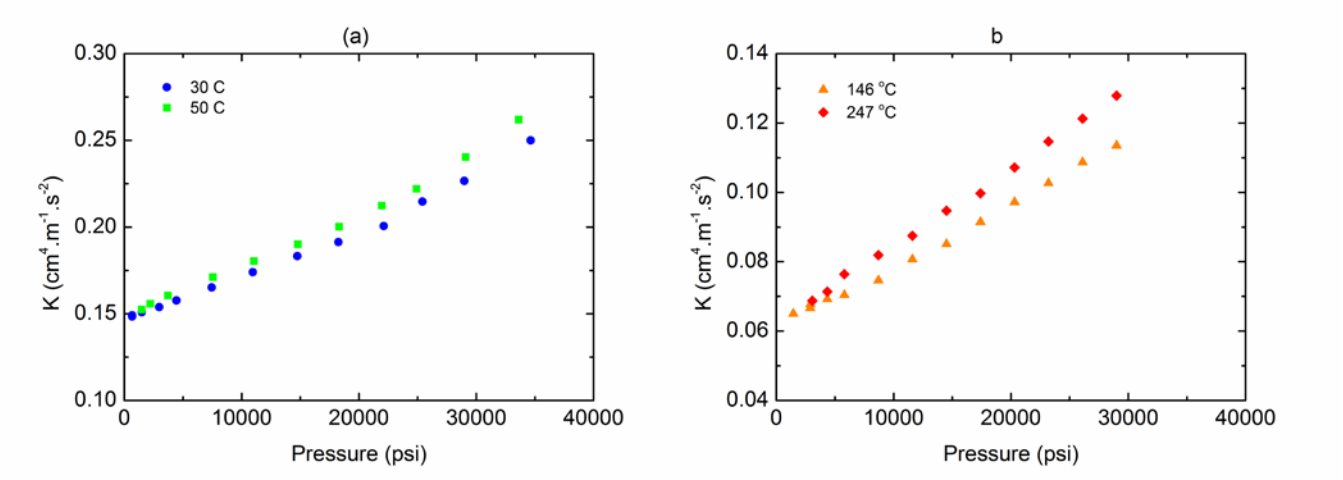

Figure 29: Calibration results with n-decane

The calibration constant, *k*, is calculated by

$$k = \frac{\eta \cdot \mathrm{v}}{(\rho_b - \rho_{fl})\sin\theta} \tag{29}$$

In Equation 29, *k* is in units of ($cm^4.m^{-1}.s^2$), η is viscosity in in *cP*, v is the terminal velocity in $cm.s^{-1}$, ρ_b and ρ_{fl} are densities of ball and fluid, respectively, in $g.cm^{-3}$. The terminal velocity, v, at the third window has been used for all the calibration data points where the rolling distance is taken as the same as the diameter of the ball. The calibration results are correlated linearly with the pressure for all isotherms. Table 6 lists the slope, *a*, and intercept, *b*, values for the correlations of the calibration constant for the four isotherms.

$$k = a \cdot P + b \tag{30}$$

where *P* is the pressure in psi.

Table 6: Linear correlations of the calibration results with n-decane

Temperature ^{o}C	*a*	*b*
30	2.80592E-06	1.44646E-01
50	3.29281E-06	1.45246E-01
146	1.89023E-06	5.75235E-02
247	2.12978E-06	5.67523E-02

Figure30a and b show the linear relationship between the resistance factor, *f*, and the Reynolds number, *Re*, for all isotherms which indicates that the flow around the ball is laminar.

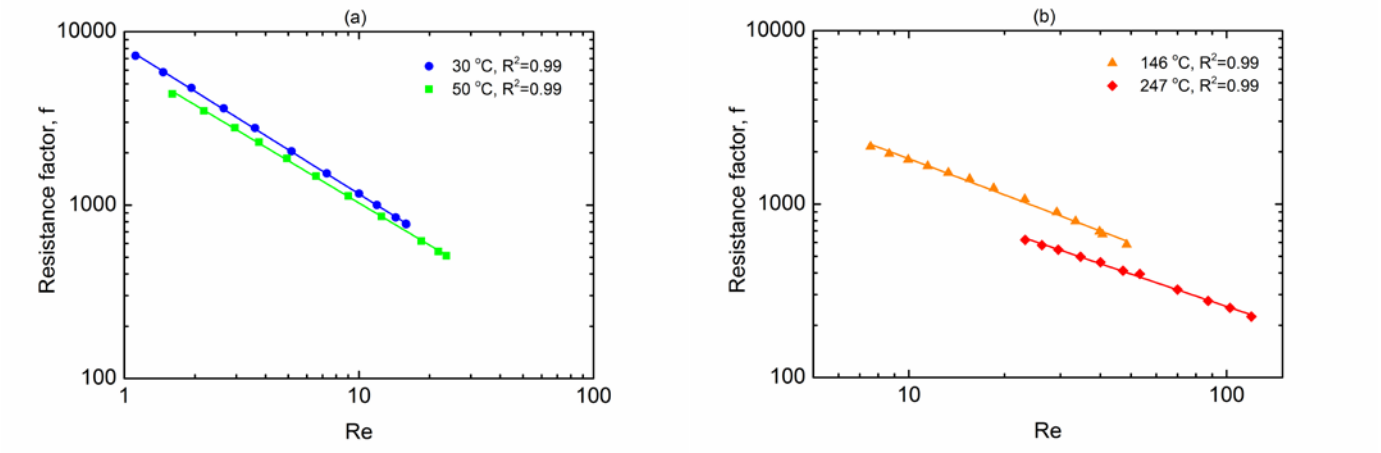

Figure 30: The straight lines show that the flow around the spheres is laminar

3.4 VISCOSITY RESULTS OF N-OCTANE

Viscosity of n-octane (Sigma Aldrich, Lot# 07696APV, anhydrous, purity ≥ 99%) has been measured at the same conditions listed in table 5 using the calibration results presented in Figure 29 and Table 6. Figure 31a and b confirm that the flow for all measured data is laminar. Table 7 lists the measured viscosity of n-octane for the four isotherms at different pressures.

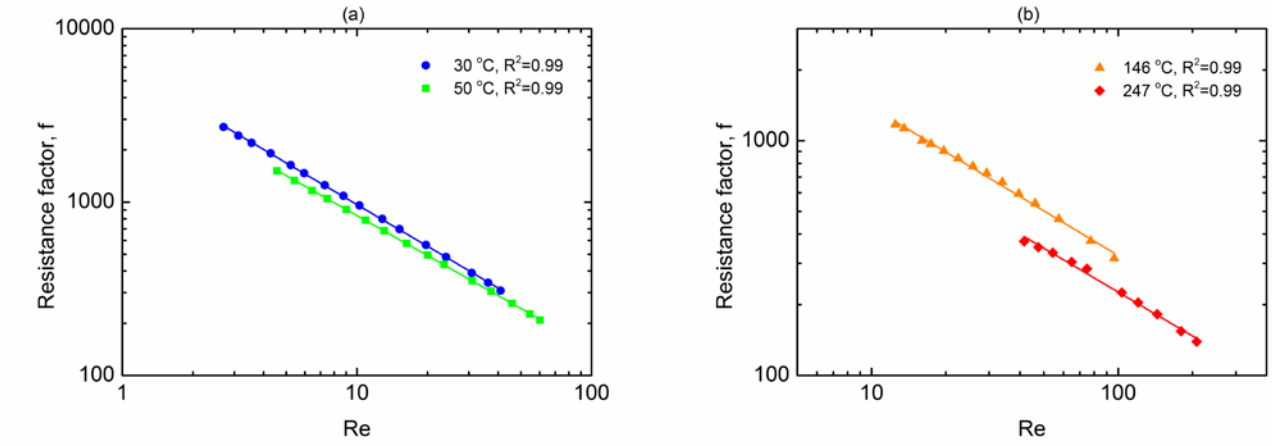

Figure 31: The straight lines indicate that the flow around the spheres is laminar

Table 7: Viscosity of n-octane

30 °C		50 °C		146 °C		247 °C	
P (psi)	*η (cP)*	*P (psi)*	*η (cP)*	*P (psi)*	*η (cP)*	*P (psi)*	*η (cP)*
235	0.4981	253	0.4082	1620	0.1999	3170	0.1352
1076	0.5364	1163	0.4355	3170	0.2296	4470	0.1501
2679	0.5953	2672	0.4818	6150	0.2810	6234	0.1731
5055	0.6924	4807	0.5519	8649	0.3314	8444	0.1979
7155	0.7802	7070	0.6302	11000	0.3707	10420	0.2214
10207	0.9222	10157	0.7435	12711	0.4040	13945	0.2625
12275	1.0226	12235	0.8246	15256	0.4533	17172	0.3098
15176	1.1777	15185	0.9469	18156	0.5020	21124	0.3542
17229	1.2923	18310	1.0904	21233	0.5586	25112	0.4024
20115	1.4599	21076	1.2259	24274	0.6181	29142	0.4498
23130	1.6500	24125	1.3835	27305	0.6788		
25089	1.7964	27217	1.5585	30240	0.7343		
28137	2.0262	30215	1.7237	33300	0.8136		
31090	2.2945	33170	1.9288	36107	0.8721		
33140	2.4880	36640	2.1610				
35300	2.7262						

The measured data were compared to literature data. For the isotherms 30 and 50°C, viscosity data published by Oliveira and Wakeham [63] were used for comparison with our data for the entire pressure range. An accurate correlation (± 0.5 %) for the viscosity as a function of pressure given by Oliveira and Wakeham [63] was used for these two viscosity isotherms. The isotherms 146 and 247°C were compared to NIST data [35] which are available for pressures to approximately 14500 psi. The MAPD values obtained for the measured isotherms 30, 50, 146, and 247°C, are 1.88, 1.25, 1.51, and 1.54 %, respectively. Figure 32 shows the relative deviations of the present data from the literature data.

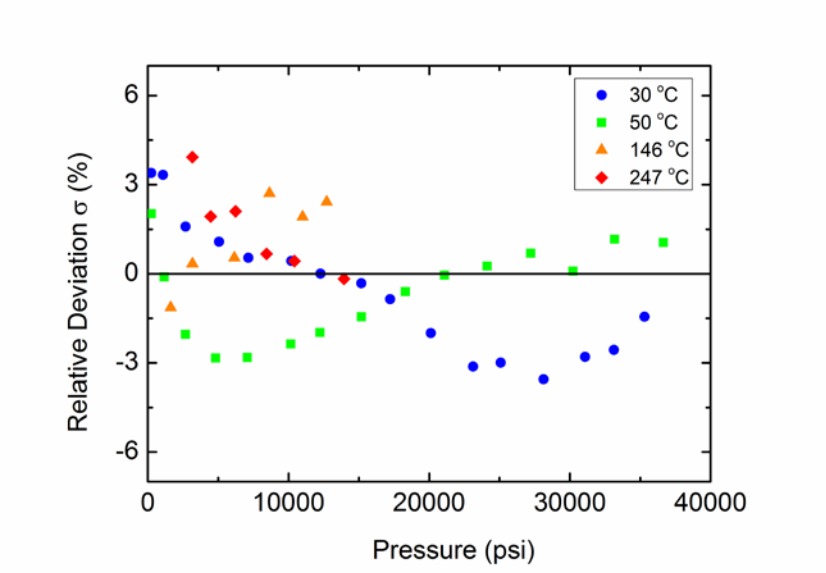

Figure 32: Deviations of viscosity data for n-octane from literature data

The viscosity of n-octane along each isotherm has been correlated as a function of pressure by means of a cubic polynomial

$$\eta = a_0 + a_1 \cdot P + a_2 \cdot P^2 + a_3 \cdot P^3 \tag{31}$$

The viscosity η is in units of *cP* and the pressure *P* is in *MPa*. Table 8 lists the coefficients of the polynomial approximation (Equation 31) together with the mean absolute percentage deviations (MAPD) between the experimental data and the calculated curves. Figure 33 presents the measured viscosity of n-octane together with the smoothed values obtained with Eq. 31. The pressure and temperature dependence of viscosity will be discussed with more details in the next chapter.

Table 8: Coefficients of polynomial fit Equation 46 and MAPD values

T (^{o}C)	a_0	a_1	a_2	a_3	MAPD (%)
30	0.48610	0.00602	-9.93081E-07	5.72160E-08	0.42
50	0.40043	0.00429	7.88502E-06	1.07194E-08	0.15
146	0.16734	0.00287	-2.96609E-06	1.14339E-08	0.42
247	0.10044	0.00156	2.33534E-06	-7.26475E-09	0.48

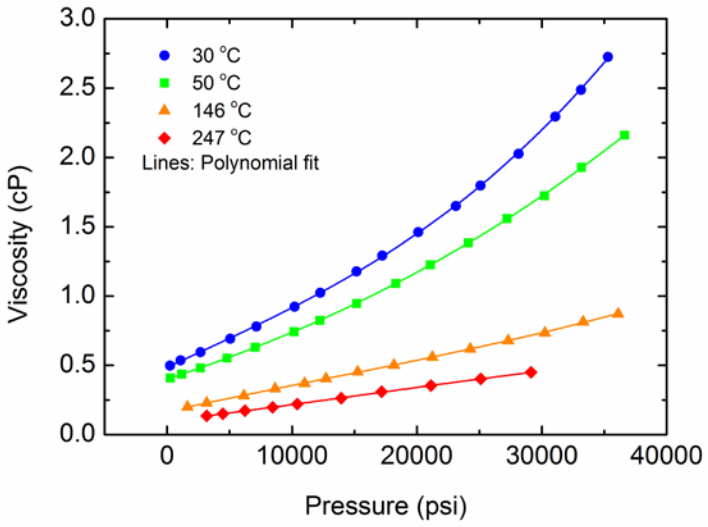

Figure 33: Comparison of the experimental viscosity data of n-octane with the polynomial fit of Equation 31

3.5 CONCLUSIONS

A high temperature-high pressure, windowed, volume-variable rolling ball viscometer rated to about 40000 psi and 260^{o}C has been designed and constructed from Inconel 718. This novel viscometer has been calibrated with n-decane at different temperatures and pressures to 36000 psi. Viscosity of n-octane was measured at 30, 50, 146, and 247^{o}C for pressures up to 36000 psi. The measured viscosity data are in good agreement with the literature data.

4.0 VISCOSITY MODELING

Viscosity is an important fluid property required in the development and production of petroleum reservoirs. In many applications such as the simulation of oil reservoirs and the design of transport equipment, it is more convenient to use models to obtain the viscosity because experimental data might not be available at specific conditions and carrying out viscosity measurements at all temperatures, pressures and compositions is time and money consuming. Hence, there is a need in the oil industry for reliable prediction models for viscosity. There are many different viscosity models in the literature ranging from highly theoretical to simple empirical correlations. A critical literature review of different viscosity models has shown that the friction theory model [92, 93], and free volume theory model [94, 95] are superior to many other viscosity models.

4.1 FRICTION THEORY VISCOSITY MODEL (F-THEORY)

The friction theory (F-theory) has been described in detail in [93]. An underlying assumption central to many viscosity models including the F-theory model is that fluid viscosity η can be expressed as the summation of two terms

$$\eta = \eta_0 + \Delta\eta \tag{32}$$

η_0 is defined as the viscosity of the fluid in the dilute gas limit, while the $\Delta\eta$ term dominates for liquid viscosities. The dilute gas term η_0 is derived from the kinetic gas theory at very low pressures [96], whereas the second term $\Delta\eta$ is based on the friction concepts of classical mechanics. The dilute gas model proposed by Chung et al. [97] is used. It is given by:

$$\eta_0 = 40.785 \frac{\sqrt{M\,T}}{v_c^{2/3}\Omega^*} F_c \qquad (\text{in } \mu P) \tag{33}$$

where the following empirical equation is used for the reduced collision integral Ω^*:

$$\Omega^* = \frac{1.16145}{T^{*0.14874}} + \frac{0.52487}{\exp(0.77320\,T^*)} + \frac{2.16178}{\exp(2.43787\,T^*)} - 6.435\times10^{-4} T^{*0.14874} \sin(18.0323\,T^{*-0.76830} - 7.27371) \tag{34}$$

with

$$T^* = \frac{1.2593}{T_c} \tag{35}$$

where M is the molecular weight in g/mol; T is the temperature in K; v_c is the critical volume in cm^3/mol; and the F_c factor for non-polar gases, such as n-alkanes, is given as a function of the acentric factor, ω,

$$F_c = 1 - 0.275\,\omega \tag{36}$$

As previously mentioned, the $\Delta\eta$ term is based on the friction concepts of classical mechanics. In analogy with the Amontons-Coulomb friction law, this term can be expressed by quadratic functions in the van der Waals attractive pressure P_a and the repulsive pressure P_{rep} as follows:

$$\Delta\eta = \kappa_a P_a + \kappa_{aa} P_a^2 + \kappa_r P_{rep} + \kappa_{rr} P_{rep}^2 \tag{37}$$

The parameters κ_a, κ_{aa}, κ_r, and κ_{rr} are determined by fitting experimental viscosity data. In this work, the F-theory viscosity model has been tested for several alkanes. The equations of state used to calculate the attractive and repulsive contributions to the thermodynamic pressure are the SRK and PR equations of state. The HTHP volume translated equations of state have exactly the same attractive and repulsive pressures as the ones of the corresponding untranslated equations of state. Therefore, the viscosity predictions obtained with the F-theory model coupled with the untranslated SRK and PR equations are identical to the results when the F-theory model is used in conjunction with the corresponding translated equations of state. The performance of the F-theory model in conjunction with the PR EoS or HTHP VT-PR EoS has been studied for some hydrocarbons, including n-hexane, n-octane, n-decane, n-dodecane, n-hexadecane, and n-octadecane. The F-theory constants reported in [93] have been used in this evaluation. Figure 34 shows the viscosity predictions for n-octane obtained with the F-theory model in combination with the PR EoS or HTHP VT-PR EoS.

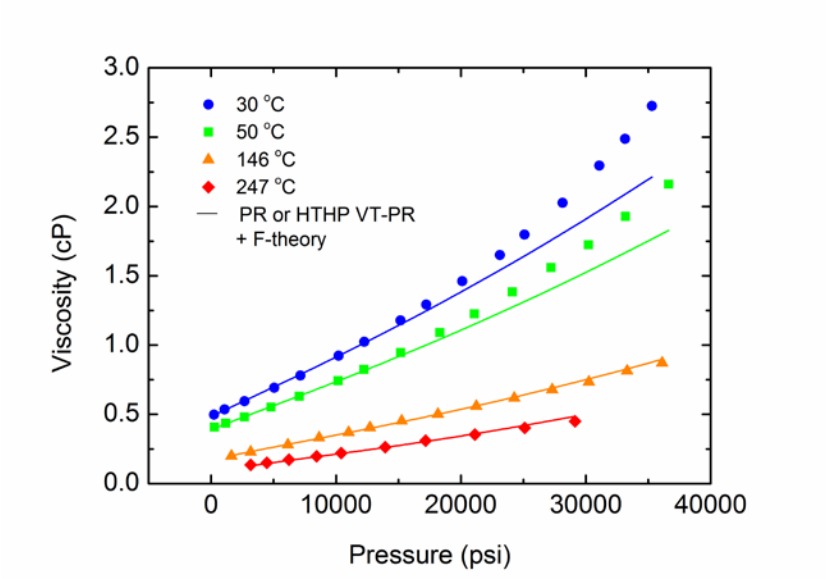

Figure 34: Comparison of experimental viscosity data (symbols) of n-octane with the prediction of the F-theory model coupled with the PR EoS or HTHP VT-PR EoS

The predictions are in good agreement with the experimental viscosity data for all isotherms for pressures up to approximately 15000 psi but as the pressure increases the calculated viscosities for the lower isotherms 30 and 50^{o}C tend to deviate from the corresponding experimental ones. Similar trend has been observed for the other alkanes studied in this work. The F-theory model predicts the viscosity within ~ ± 2 to 5% of experimental values for pressures up to ~ 15000 psi over the full temperature range of interest. However, at elevated pressures, the viscosity can often be under-predicted by more than 10% and even as high as 20 %. The performance of the F-theory model can be improved by adding a translation term, η_t, to the viscosity predicted by the F-theory model.

$$\eta_{corr} = \eta_{pred} + \eta_t \tag{38}$$

where the correction term η_t is given as

$$\eta_t = k\left[\frac{1}{1+m\left(\frac{T-T_b}{T_c}\right)}-1\right]\cdot\left(\frac{P_{rep}}{P_c}\right)^n \tag{39}$$

where T_b is the boiling temperature in K, T_c is the critical temperature in K, P_c is the critical pressure in bar, and P_{rep} is the repulsive pressure in bar. The parameters *k, m,* and *n* are determined by fitting the corrected viscosity in Equation 38 to experimental viscosity data. Equation 39 was derived based on two observations: (1) the largest deviations from the experimental data occur at temperatures away from the boiling temperature of n-octane (125.65^{o}C). In the vicinity of this temperature, the predictions of the f-theory model for n-octane are in very good agreement with the experimental data, therefore a distance factor (that is the expression in the square brackets in Equation 39) has been incorporated into the viscosity translation term. This term vanishes at the boiling temperature. (2) the repulsive pressure term

P_{rep} strongly dominates at high pressures where most of the deviations occur. This is when a fluid is put under high pressure, the distance between fluid molecules decreases; as a result of this the repulsive forces outweigh the attractive forces. For this reason only the repulsive pressure has been considered in the Equation 39.

Figure 35 shows the viscosity predictions for n-octane obtained with the corrected F-theory model coupled with the HTHP-VT-PR EoS. The results are in very good agreement with the experimental data over the entire temperature and pressure ranges. The mean absolute percentage deviation, MAPD, 1.86% is less than the value of 3.97% obtained with the untranslated F-theory model. The three parameters *k*, *m*, and *n* are listed together with the MAPD and SD values in Table 9 for some hydrocarbons studied in this work.

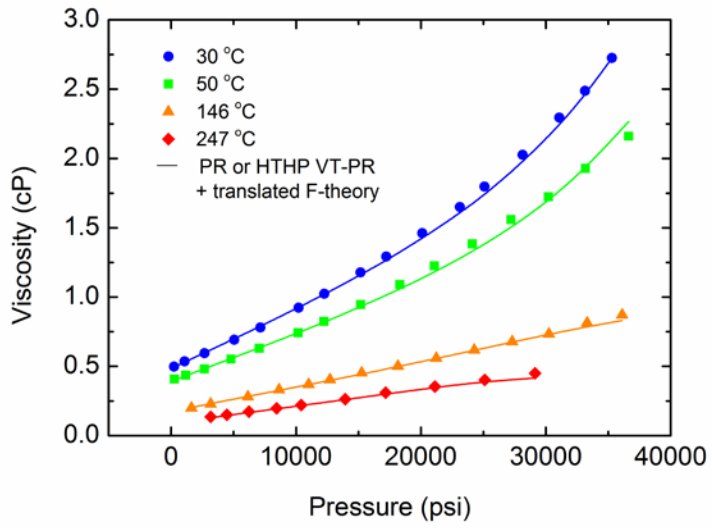

Figure 35: Comparison of experimental viscosity data of n-octane with the prediction of the F-theory model coupled with the HTHP-VT-PR EoS

Table 9: Values for the F-theory correction parameters *k*, *m*, and *n* for selected compounds; comparison of MAPD and SD values for predictions with the original and corrected F-theory

Compound	*k*	*m*	*n*	**Original**		**Corrected**		
				MAPD	SD	MAPD	SD	Reference
n-hexane	-5.275E-08	-4.908E-10	7.74331	3.36	1.97	2.71	1.90	[98]
n-octane	-5.275E-08	-4.908E-10	7.77642	3.97	4.67	1.86	1.52	[Our data]
n-decane	-5.275E-08	-4.908E-10	7.70067	4.91	4.77	3.21	1.77	[63, 91]
n-dodecane	-5.275E-08	-4.908E-10	7.45018	2.21	2.64	1.75	1.83	[99]
n-hexadecane	-5.275E-08	-4.908E-10	6.91066	3.31	4.97	1.87	1.96	[98]
n-octadecane	-5.275E-08	-4.908E-10	6.89509	4.98	3.22	3.06	2.18	[100]

4.2 FREE VOLUME THEORY VISCOSITY MODEL (FV-THEORY)

In this viscosity model, the second term in Equation 32, $\Delta\eta$, is given as an exponential function in the free volume which is the space within a system not occupied by molecules. Allal et al. [94] assumed that the free volume is ultimately dependent on PM/ρ, the energy required to form a vacuum site required for diffusion, and $\alpha\rho$, a barrier energy that a molecule must cross to diffuse. Their relatively simple final equation, Equation 40, requires as inputs only the molecular weight M, $P\rho T$ values, and the three pure-component parameters L, α, and B. Unlike the case with F-theory, an equation of state is not necessary if experimental $P\rho T$ data points are available.

$$\Delta\eta = \frac{\rho L\left(\alpha\rho + \frac{PM}{\rho}\right)}{\sqrt{3RTM}} \exp\left[B\left(\frac{\alpha\rho + \frac{PM}{\rho}}{RT}\right)^{1.5}\right] \tag{40}$$

where $\Delta\eta$ is in units of cP, M is the molecular weight in kg/mol, ρ is density in kg/m^3, T is in Kelvin, R = 8.3145 J/mol*K, P is pressure in MPa, the length parameter L is in Å, α is in units of m^5/mol*s^2, and B is unitless.

The coupling of FV theory with density predictions obtained using the HTHP VT-PR equation of state was investigated. Figure 36 shows the calculated results of the viscosities of n-octane as an example. The results are in very good agreement with the experimental data over the entire temperature and pressure ranges. The mean absolute percentage deviation, MAPD, 1.38% is slightly better than the value of 1.86 % obtained with the translated F-theory model.

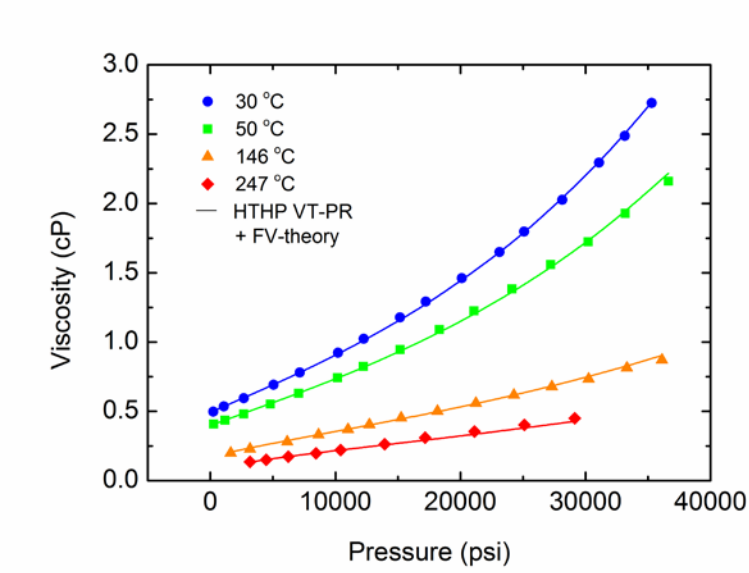

Figure 36: Comparison of experimental viscosity data of n-octane with the prediction of the FV-theory model coupled with the HTHP-VT-PR EoS

The three parameters L, α, and B are listed together with the MAPD and SD values in Table 10 for some hydrocarbons studied in this work. Both, corrected F-theory and free volume theory

model coupled with the HTHP VT-PR EoS, provide reliable predictions over the entire pressure and temperature ranges of interest.

Table 10: Values for the FV-theory parameters *L, α, and B* for selected compounds; MAPD and SD values for predictions with the FV-theory

Compound	*L* Å	*α* $m^5/mol.s^2$	*B* $x10^{-3}$	MAPD	SD	Reference
n-hexane	1.0497	78.796	7.2709	1.16	0.86	[98]
n-octane	0.9594	100.88	7.3428	1.38	1.42	[Our data]
n-decane	0.7333	131.92	6.6535	0.76	1.16	[63, 91]
n-dodecane	0.7457	160.41	5.5529	2.54	2.20	[99]
n-hexadecane	0.4096	269.45	3.8055	2.27	1.97	[98]
n-octadecane	0.4224	310.78	3.3067	2.69	2.11	[100]

4.3 CONCLUSIONS

The friction theory of viscosity (F-theory) and the free volume theory of viscosity (FV-theory) provide good viscosity predictions of hydrocarbons. However, F-theory under-predicts the viscosity by as much as 20% at pressures near 40000 psi, but this problem is greatly diminished by including a correction term which is a function of system temperature, boiling temperature, critical temperature, critical pressure, and repulsive pressure. For n-alkanes, viscosity predictions from the corrected F-theory are comparable with those obtained from FV-theory. When coupled to density predictions made using an accurate equation of state (EoS) such as the HTHP VT-PR EoS, FV-theory typically gives mean absolute percentage deviations (MAPDs) from experimental viscosity values of less than 3%.

5.0 DEEPWATER VISCOSITY STANDARD (DVS)

On June 19, 2009, the International Association of Transport Properties (IATP) held its 9th meeting in Boulder Colorado [101] and decided to identify a short term and long term high temperature, high pressure viscosity standard (HTHP VS). The short term target was to identify a fluid that would have a dynamic viscosity of 200 mPa s at 473.15 K (200°C) and 173 MPa (25000 psi) with an uncertainty of ± 2%. The long term standard of 200 mPa s at 573.15 K (300°C) and 241 MPa (35000 psi) with an uncertainty of ± 1% was more demanding with respect to temperature, pressure and uncertainty. Subsequently, during the HTHP Workshop initiated by Schlumberger and Cambridge Viscosity on January 22, 2010 [102], these specifications were changed to reflect interest in two types of petroleum targets, both of which have increasing importance as the search for domestic energy sources in increasingly harsh conditions escalates. These include light oils found in ultra-deep formations that are typically accessed via offshore platforms in the deep waters of the Gulf of Mexico (the Deepwater Viscosity Standard or DVS), and heavy oils produced from bitumen reserves found in shallower oil sands (the Heavy Oil Viscosity Standard or HOVS) [103]. The targeted DVS has a dynamic viscosity of roughly 20 mPa s at 533.2 K (260°C, 500°F) and 241 MPa (35000 psi), while the HOVS is to have a dynamic viscosity of 1000 mPa s at 473.2 K (200°C, 392°F) and 10.34 MPa (1500 psi). The desired uncertainty for both standards was set at 5-10% [104]. One of the conclusions of this meeting was that candidates for these standards should be assessed at multiple labs using

multiple experimental techniques. For example, it was anticipated [105,106] that oscillating piston, rolling ball, falling object, torsional crystal, vibrating cylinder, oscillating disk, vibrating crystal, and capillary viscometers could be used to evaluate the DVS and HOVS. A review of current viscometry laboratories [106] indicated, however, that these Deepwater Standard conditions of 533.2 K (260^{o}C, 500^{o}F) and 241 MPa would be particularly challenging and would require modifications to existing viscometry equipment.

The objective of this section is to suggest a candidate for the DVS, to assess the candidate's viscosity at 533.2 K and 241 MPa using our newly developed rolling ball viscometer, and to model the viscosity of the DVS candidate using scaling theory. With respect to our selection of the DVS, the desirable attributes [103, 106] include thermal stability, inertness, insensitivity to UV radiation, and ready availability throughout the world at a specified purity. Further the candidate should be safe to use in the laboratory and environmentally benign.

This study proposes that DuPont's Krytox® perfluoropolyether oils were excellent candidates for the DVS. There are eight polydisperse Krytox® oils (100 – 107). It is unlikely that any of these would exhibit the targeted value of 20 mPa s at 533.2 K and 241 MPa. It was anticipated, however, that two of the oils would "straddle" this targeted value (one being slightly greater than 20 mPa s while the other exhibited a value slightly less than 20 mPa s), and either of these oils could serve as the DVS. If one desires to attain the value of 20 mPa s more precisely, two alternate strategies are available. One could simply blend the two oils that exhibit viscosity values that straddle the 20 mPa s target in order to attain a polydisperse DVS, or one could fractionate either of the Krytox® oils using supercritical CO_2 as our research group have done in prior studies [107, 108] in an attempt to realize a more monodisperse Krytox® oil DVS with the desired viscosity value of 20 mPa s.

Viscosity data collected with our novel windowed, variable-volume, rolling ball viscometer will be compared to results obtained with a HTHP Couette viscometer [109] rated to 316°C and 276.0 MPa (40000 psia) and calibrated with silicone oil. This apparatus, located at the Morgantown campus of NETL, was designed to measure the viscosity of drilling fluids with viscosity values of 3–300 mPa s employed for ultra-deep drilling. Modeling of the Krytox® GPL 102 viscosity results over a broad range of temperature and pressure was accomplished using scaling theory [111-113], which has previously been shown to accurately model the viscosity of Krytox® GPL 107 (143AD) at temperatures to 473.2 K and pressures to 172 MPa [114]. Krytox® GPL 102 viscosity results have also been correlated as a simultaneous function of temperature and pressure for the purpose of interpolation.

5.1 MATERIALS

The full Krytox® GPL 100 series of fluorinated lubricating oils was obtained from DuPont. Molecular weight estimates of these perfluoropolyethers, Figure 37, are given below in Table 11. These oils have a "fairly broad" molecular weight distribution [115]. Krytox® GPL 100-107 oils are additive-free, non-reactive, non-flammable, thermally stable materials that are resistant to oxidation. Thus, they are typically used in general purpose applications, such as lubricating bearings that come into contact with chemicals and oxygen.

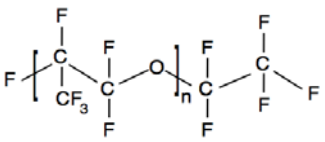

Figure 37: Chemical structure of the Krytox® GPL 100 series of fluorinated oils

Table 11: Number average molecular weight estimates and average number of repeat units based on ^{19}F NMR provided by DuPont Performance Lubricants for the Krytox® 100 series of perfluoropolyethers [115]

Krytox® GPL	Number Average Molecular Weight (g/mol)	n_{avg}
100	960	4.95
101	1180	6.28
102	1720	9.53
103	2275	12.8
104	3150	18.1
105	4730	27.7
106	5940	35.0
107 (formerly 143AD)	7475	44.2

Krytox® GPL 102 (99.9%, lot K1537) was obtained from Miller Stephenson and used without further purification. Although the lots of these oils are fairly large, they can sell out within several months. Therefore, should Krytox® GPL 102 oil be considered as a viable HTHP DVS, a significant portion of a single lot could be set aside by a distributor such that numerous research groups could receive the Krytox® GPL 102 from the same lot.

Di(2-ethylhexyl) phthalate, DEHP, also known as Dioctyl phthalate, DOP, [99%, Sigma Aldrich], was used for the calibration of the rolling ball viscometer because the viscosity of DEHP is in the same order of magnitude of the targeted DVS at elevated temperature and pressure (e.g. 10.93 mPa s at 491.5 K and 390 MPa; 23.57 mPa s at 491.5 K and 555 MPa) and there is an old yet reliable source of DEHP viscosity data at temperatures to 491 K and pressures

to 1000 MPa [116]. More recent DEHP viscosity data at temperatures between 273 and 348 K and pressures to 371 MPa is also available [117].

5.2 EXPERIMENTAL RESULTS

Our novel windowed, high temperature, high pressure rolling ball viscometer, previously described in section 3.2, has been calibrated with DEHP over the entire pressure and temperature ranges of interest and used then to measure the viscosity of Krytox® GPL 102.

5.2.1 Rolling ball viscometer calibration with DEHPFirst subsection

Equation (29) has been used for determining the calibration constant of the rolling ball viscometer.

$$k = \frac{\eta \cdot \mathrm{v}}{(\rho_b - \rho_{fl})\sin\theta} \tag{29}$$

The viscosity and density of DEHP 77, 100, 210 and 425°F were taken from an ASME viscosity report [116]. Although the DEHP density values were inexplicably not listed in the tabular results, the values were determined by solving the equation for ρ_{fl} at 425°F, and the results were in good agreement with DEHP density data recently taken in Dr. McHugh's laboratory at Virginia Commonwealth University [117]. An Inconel 718 ball (d/D = 0.990) was used for the calibration of the viscometer at all temperatures from reference [116] because high temperature results were of primary importance to this study; the terminal velocities of the same ball (d/D = 0.990) at lower temperatures from reference [118] were too slow for practical use of the

instrument. The tilt angle was set at 40°, 40°, 15°, and 10° for the isotherms 77, 100, 210 and 425°F, respectively.

The terminal velocity of the rolling ball was determined at the third window from the large sapphire end window, and the terminal velocity of the rolling ball was the same whether the viscometer was tilted $+\theta$ or $-\theta$. In all cases, the ball rolled at its terminal velocity and no sliding was observed. The pre-rolling distances are 3.88 and 0.88 inch for $+\theta$ and $-\theta$ tilting, respectively.

The calibration results are shown in Figure 38, which presents the calibration constant values, *k*, as a function of pressure for each isotherm. This dependency is consistent with the changes in the geometry of the viscometer with changes in temperature and pressure because the ball diameter decreases slightly and the cell internal diameter increases slightly with increasing pressure, with the effect enhanced with increasing temperature [118].

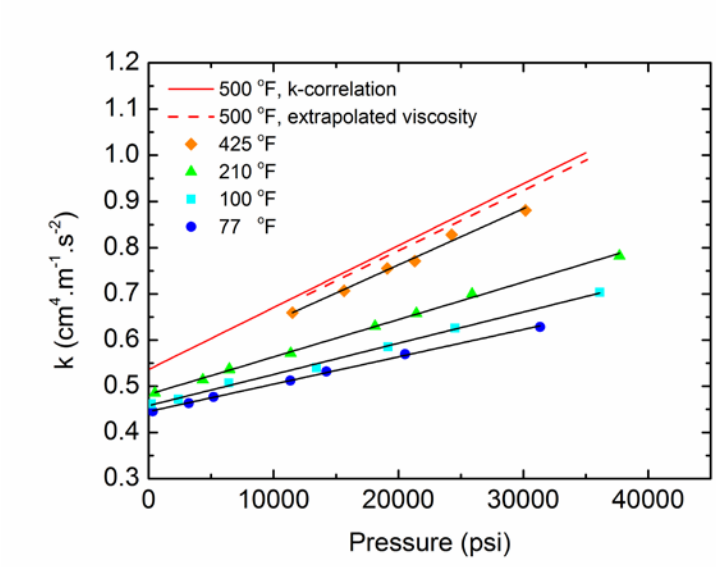

Figure 38: Rolling ball viscometer calibration results based on terminal velocity of the Inconel ball (d/D = 0.990) rolling past the third set of side-mounted window from the large sapphire end window; 77- 425°F data point results based on ASME data for the viscosity of DEHP [116]; 500°F results based on either a k-correlation, or extrapolated data for DEHP viscosity based on surface fitting of lower temperature data

Because the temperature associated with the DVS is 500°F and the DEHP calibration extended from 77–425°F, a means of extrapolating the calibration to 500°F was required. Two alternatives were considered. In the first method, linear temperature-dependent expressions for the intercept, *a*, (Figure 39) and slope, *b*, (Figure 40) of the four linear isotherms in Figure 38 were used to estimate the intercept and slope of a 500°F calibration constant isotherm.

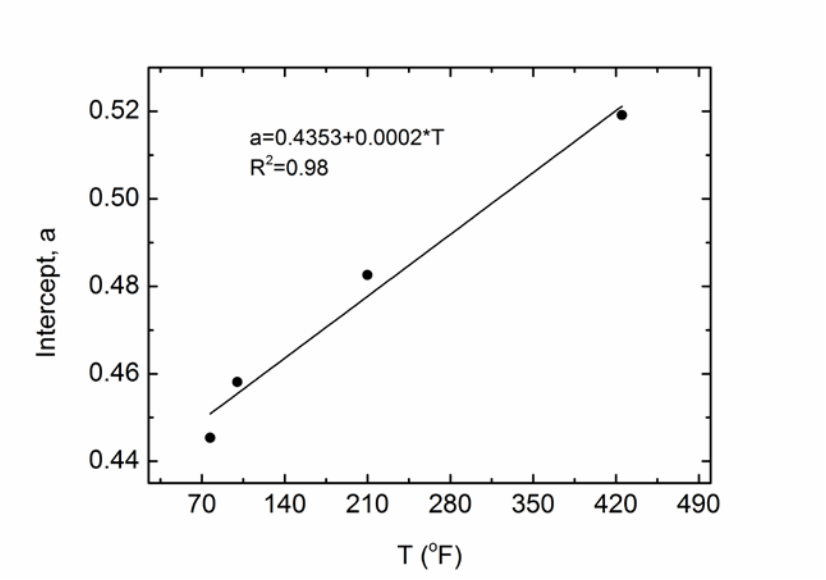

Figure 39: A linear fit of the intercept, *a*, values of the 77-425°F linear isotherms in Figure 38. When extrapolated to 500°F, $a = 0.5353$

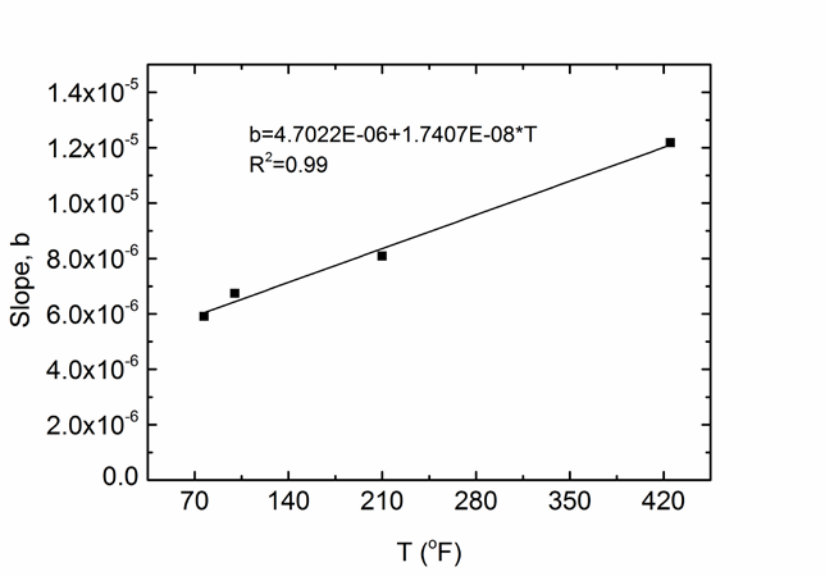

Figure 40: A linear fit of the slope, b, values of the linear isotherms in Figure 38. When extrapolated to 500°F, $b = 1.3406 \times 10^{-5}$

The results (a = 5.36350E-01 at 500°F, b = 1.34057E-05 at 500°F) were used to generate the solid red line in Figure 38.

In the second method, k was determined using DEHP viscosity data at 500°F as estimated by extrapolating a surface-fitting correlation [118] of the lower temperature $TP\eta$ data [116] to 500°F, Figure 41.

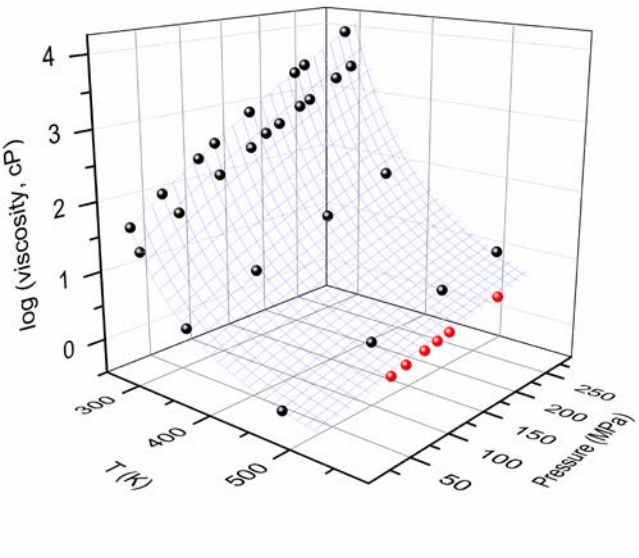

Figure 41: Surface fitting of the DEHP viscosity data at 77 (298K), 100 (311 K), 210 (372 K) and 425°F (491K) [116] (black data markers) and extrapolated DEHP viscosity values at 500°F (533K) (red data markers)

The nonlinear surface fitting given in Equation 41 was performed with OriginPro 8.6.

$$\log\eta = \frac{a_0 + a_1T + b_1P + b_2P^2 + b_3P^3}{1 + a_2T + a_3T^2 + a_4T^3 + b_4P + b_5P^2} \tag{41}$$

where the viscosity, η, is in cP, temperature, T, is in K, and pressure, P, is in MPa. The coefficients of the surface fitting are given in Table 12. The mean absolute percentage deviation obtained with the surface fitting of the DEHP viscosity is 0.91 %.

Table 12: Coefficients of Equation 41 for DEHP

a_0	-1.08080E+09
a_1	2.22234E+06
b_1	-2.57823E+06
b_2	1.61412E+03
b_3	-1.11182E+00
a_2	1.12821E+06
a_3	-8.07788E+03
a_4	5.46553E+00
b_4	-1.25513E+05
b_5	1.39797E+02

DEHP density values at 500°F were obtained with the modified Tait equation [110, 119],

$$\frac{\rho - \rho_0}{\rho} = C \log_{10} \frac{P + B}{P_0 + B} \tag{42}$$

The parameters ρ_0, B, and C are determined by fitting Equation 42 to new HTHP DEHP density data recently produced by Dr. McHugh's research group at Virginia Commonwealth University [117]. Table 13 lists the extrapolated parameter values at 500°F.

Table 13: Parameters used in Equation 57 to predict the DEHP density at 500°F

P_0 (MPa)	ρ_0 (g.cm^{-3})	C	B (MPa)
0.1	0.805	0.220	42.078

The results for the calibration constant k based on the surface fitting are represented by the dashed red line in Figure 38. The solid and dashed red lines are in good agreement, therefore for Krytox® GPL 102 viscosity calculations, the calibration constant based on the extrapolated viscosity values (the dashed red line in Figure 38) was used.

5.2.2 Rolling ball viscometer measurements of the viscosity of Krytox® GPL 102

Having calibrated the viscometer, and with the modified Tait correlation, Equation 42, for the density of Krytox® GPL 102, the viscosity of Krytox® GPL 102 was determined over a wide range of pressure at 100, 210 and 500°F. The required parameters for the Tait equation are based on Krytox® GPL 102 density data recently produced by Dr. McHugh's research group at Virginia Commonwealth University [110]. The parameter values for each density isotherm are presented in Table 14. In all cases the ball was observed to roll and attain its terminal velocity. The viscosity results are presented in Table 15 and illustrated in Figure 42.

Table 14: Parameters used in Equation 43 to predict the Krytox® GPL 102

T (^oF)	P_0 (MPa)	ρ_0 (g.cm^{-3})	C	B (MPa)
100	0.1	1.826	0.156	32.893
210	0.1	1.733	0.156	23.080
500	0.1	1.430	0.195	9.423

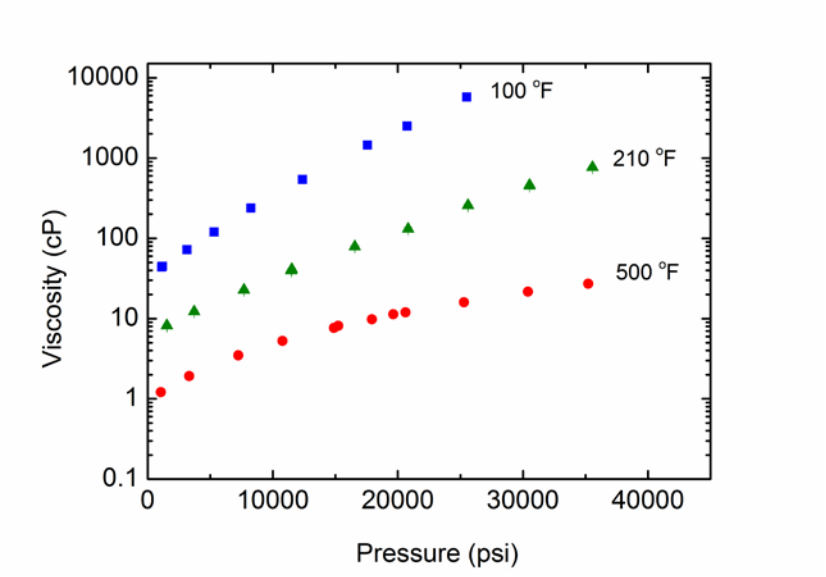

Figure 42: Rolling ball viscometer results for the viscosity of Krytox® GPL 102 (Lot-K1537) over a wide range of pressure at 100, 210 and 500°F

Table 15: Krytox GPL®102 rolling ball viscosity data. Viscosity values are based on the 260°C calibration constant derived from the surface fitting extrapolation of the lower temperature DEHP viscosity data. The bold entry is closest to the DVS conditions

T °F	P psi	θ^o	ρ g/cm^3	η mPa s	Re	f	$\bar{\dot{\gamma}}$ 1/s	φ
100	1160	30	1.853	44.814	0.10787	36334	498	1.0530
	1175	30	1.854	44.929	0.10736	36500	497	1.0519
	3145	30	1.891	72.417	0.04310	88390	315	0.9377
	5314	30	1.924	120.28	0.01629	226892	195	0.8493
	8247	30	1.959	237.20	0.00441	805378	102	0.7637
	12376	30	1.999	541.63	0.00090	3726410	47	0.6794
	17575	30	2.039	1445.9	0.00014	23111975	19	0.6058
	20740	30	2.060	2498.7	0.00005	63751068	11	0.5715
	25500	30	2.087	5777.4	0.00001	304289207	5	0.5296
210	1530	30	1.778	8.208	3.3154	1113	2923	1.6565
	3717	30	1.825	12.221	1.5785	2257	2019	1.4234
	7685	30	1.885	22.820	0.49218	6811	1138	1.1438
	11470	30	1.927	39.649	0.17487	18149	687	1.0073
	16555	30	1.970	79.014	0.04792	61811	367	0.8846
	20822	30	2.000	131.59	0.01843	152151	232	0.8107
	25607	30	2.029	256.37	0.00519	509607	125	0.7467
	30530	30	2.055	452.18	0.00178	1405136	75	0.6945
	35550	30	2.078	770.13	0.00065	3630199	46	0.6511
500	1053	11	1.501	1.2081	56.957	60	8813	5.8751
	3327	11	1.595	1.9252	25.150	125	5845	4.1452
	7247	11	1.692	3.4845	8.7999	328	3495	2.9520
	10776	11	1.753	5.2856	4.1342	649	2408	2.4138
	14880	20	1.807	7.6556	3.8255	649	3133	2.0234
	15227	11	1.811	8.1256	1.9263	1280	1671	1.9972
	17920	20	1.841	9.8048	2.4903	944	2566	1.8189
	19635	20	1.858	11.309	1.9387	1178	2284	1.7238
	20620	20	1.868	11.967	1.7653	1273	2190	1.6744
	25280	20	1.908	16.035	1.0728	1945	1747	1.4797
	30390	20	1.947	21.611	0.64459	3002	1388	1.3188
	35225	**20**	**1.979**	**27.255**	**0.43736**	**4140**	**1169**	**1.1995**

At the conditions closest to those associated with the HTHP DVS, the viscosity of Krytox® GPL 102 is 27.25 cP at 500°F and 35225 psi. In order to verify that the flow was laminar in each of these experiments, a log-log plot of the resistance factor, *f*, vs. the Reynolds number, *Re*, was generated for each isotherm [72] where Equations 24 and 25 were used to

calculate *f* and *Re*, respectively. Turbulent flow is typically indicated by a gradual flattening of the log *f* vs. log *Re* data at higher values of *Re* of any isotherm. If the data are linear for each isotherm, however, as shown in Figure 43, then the nature of the fluid flow around the rolling ball was laminar in all experiments. (note that all of the isotherms do not have to be coincident). Unlike falling cylinder viscometers that are characterized by a single shear rate at the surface of the falling cylinder as the fluid flows through the well-defined gap of fixed dimensions, the fluid flow around a close-clearance ball rolling through a tube experiences a range of shear rates.

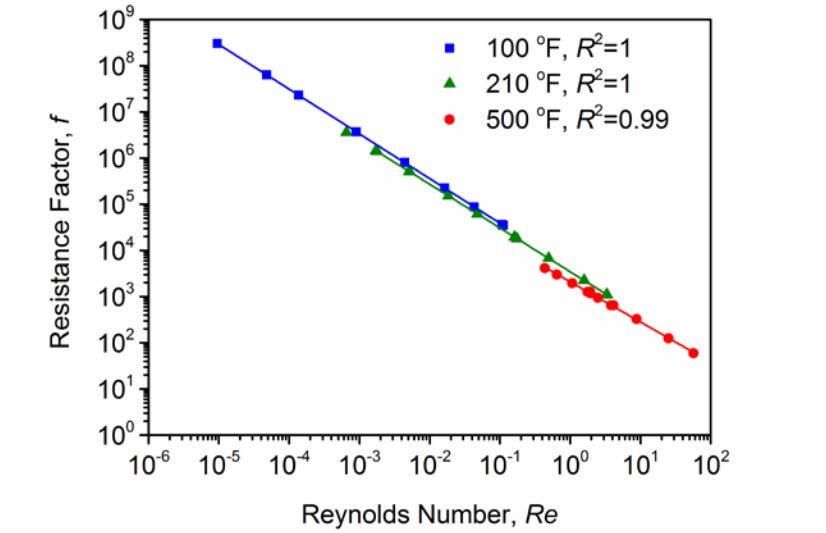

Figure 43: Log-log plot of *f* vs. *Re*. A linear correlation for each isotherm such as those shown in the figure is indicative of laminar flow. There is no flattening of the correlated data at higher values of *Re*, which would indicate turbulent flow

Therefore, an average shear rate was estimated for each experiment, using the expression given in Equation 28

$$\bar{\dot{\gamma}} = 2.4 \text{ v} \frac{D}{(D-d)^2} \tag{28}$$

The average shear rates are provided in Table 15.

The accuracy of the measurements has been studied and the estimated accumulated error in the reported Krytox® GPL 102 viscosity found to be ±2.35%, ±2.38%, and ±4.68%, for 100, 210, 500 ^{o}F isotherms, respectively, at 95% confidence limits. The calculation steps of the expanded uncertainty in viscosity measurements are given in Appendix D.

The Krytox® GPL 102 rolling ball viscometer results have been compared to viscosity values obtained with a high temperature, high pressure Chandler Couette viscometer (calibrated with a silicone oil viscosity standard) located at the Morgantown campus of NETL and operated at 1021 s^{-1}. The comparison is presented in Figure 44, along with the DVS target. At DVS conditions, the viscosity of Krytox® GPL 102 is **27.2 cP** based on the rolling ball viscometer, and **26.3 cP** based on the Couette viscometer; a 3.3% difference relative to the rolling ball viscometer value. As shown in Figure 44, these values are in good agreement given the extent of the error bars for the 35000 psi data points.

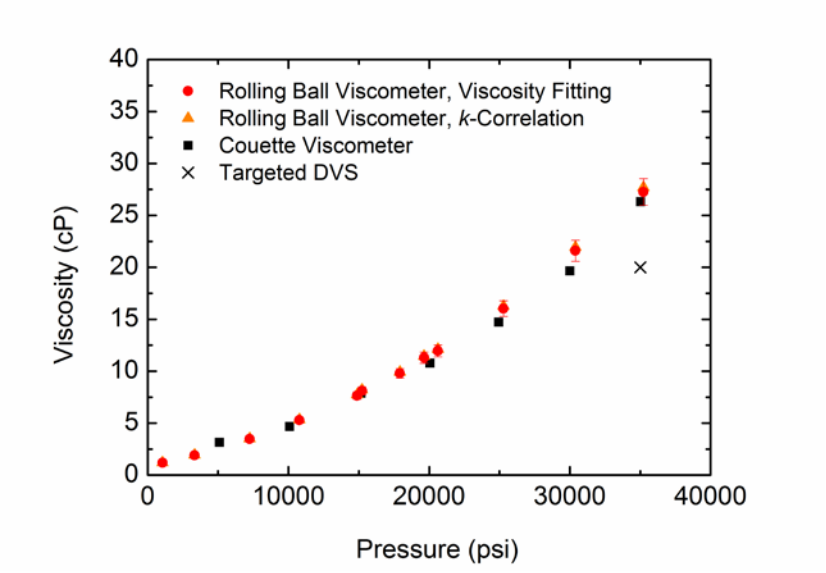

Figure 44: A comparison of the 500^{o}F viscosity values of Krytox® GPL 102 based on the rolling ball viscometer and the Couette viscometer at 1021s^{-1}. The error bars for the rolling ball viscometer results based on the calibration constant derived from the surface fitting of the DEHP viscosity data are also shown. The targeted DVS viscosity value is also indicatedEquation (29)

5.3 ALTERNATIVE KRYTOX-BASED DVS CANDIDATES

Two methods are available for formulating a Krytox-based DVS that exhibits a viscosity closer to 20 cP at 500°F and 35000 psi than Krytox® GPL 101 (~17 cP) or 102 (~27 cP). The first is to simply combine Krytox® GPL 101 and 102. For example, because Krytox® GPL 101 has a viscosity that is 3 cP too low, and Krytox® GPL 102 has a viscosity that is 7 cP too high, then a 1:2 mixture of Krytox® GPL 101:Krytox® GPL 102 would probably yield a polydisperse Krytox-based DVS with a viscosity close to 20 cP.

Alternately, because each Krytox® oil is a polydisperse mixture or perfluoropolyethers, it is possible to fractionate them into a series of more monodisperse fractions that will exhibit viscosity values greater than and less than the parent oil. For example, perfluoropolyether oils can be fractionated using supercritical CO_2 at varying pressures as the solvent [107, 108], and in one case Krukonis and co-workers [108] demonstrated that the resulting fractions exhibited viscosity values greater than and less than the viscosity of the parent oil. The challenge of employing supercritical fluid fractionation is that it is not possible *a priori* to know how to conduct the supercritical CO_2 extraction process (e.g. temperature, sequence of pressures (i.e. number of fractions) to obtain a fraction with a viscosity of 20 cP at 500°F and 35000 psi. Krytox® GPL 102 was successfully fractionated into 6 fractions using CO_2 at 60°C using the standard procedures described elsewhere [107, 108]. The fraction (1) extracted with the lowest pressure/density CO_2 is the lower molecular weight constituents of the parent oil, while the last fraction recovered (6) with the highest pressure/density CO_2 corresponds to the highest molecular weight fraction of the parent oil. 96.2% of the Krytox® GPL 102 charged to the fractionation vessel was recovered in the six fractions, Table 16.

Table 16: The amount of parent oil (Krytox® GPL 102) and each fraction obtained via supercritical CO_2 fractionation at incremental pressures

Fraction	Amount collected g	Pressure psi	CO_2 density[35] gm/cm^3
Parent K 102	105.22	--	--
1	10.05	1400	0.269
2	15.04	1500	0.311
3	16.03	1550	0.335
4	26.02	1600	0.360
5	17.26	1650	0.386
6	16.75	2000	0.550
Sum of 1-6	101.15		

A benchtop Brookfield cone-and-plate viscometer (model LVDV-II+Pro) with a small sample size adapter was used to demonstrate that at ambient pressure and temperatures between 25 and 150°C, fractions 2, 3 and 4 exhibited viscosity values intermediate to those of Krytox® GPL 101 and 102, Figure 45. Because the mass of each fraction was so small, it was not possible to evaluate the fractions with either high pressure apparatus. Nonetheless this result conceptually demonstrates that supercritical fluid fractionation of Krytox® GPL 102 can produce multiple lower molecular weight, more monodisperse fractions that exhibit viscosity values that may be closer to the DVS target of 20 cP than either Krytox® 101 or 102.

When these results were recent presented at the 12th Meeting of the International Association for Transport Properties [120, 121], the unanimous consensus of the attendants was that addition processing of a purchased DVS candidate, whether blending or fractionating, was highly undesirable. Further, it was agreed that the targeted 20 cP value was a very approximate

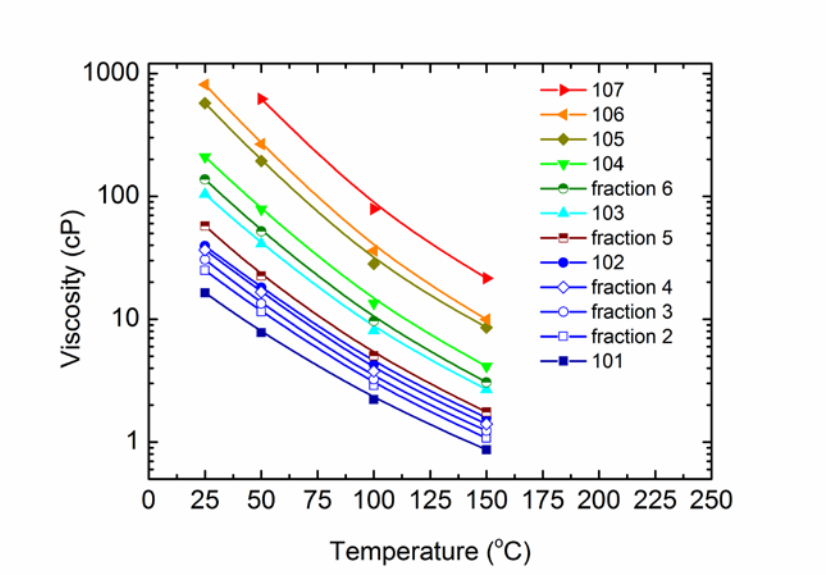

Figure 45: Fractions 2, 3, and 4 fall between Krytox® GPL 101 and 102 based on 25-150°C viscosity data at 1 ambient pressure

target. Therefore, fluids exhibiting viscosity values reasonably close to this value (e.g. 10 – 30 cP) would be considered as viable candidates without the need for further processing. Therefore, either Krytox® GPL 101 or 102 are reasonable candidates for the DVS; we favor Krytox® GPL 102 only because extensive HTHP density data have been recently published by Dr. McHugh's research group [110].

5.4 VISCOSITY MODELING RESULTS

The scaling theory was used to model the rolling ball viscometer results listed in Table 15. In the scaling theory, viscosity can be written as a function of a dimensionless scaling parameter, φ, which is based on the repulsive intermolecular potential [112] and given by

$$\varphi = \left(\frac{T}{T_{ref}} \right) \left(\frac{V}{V_{ref}} \right)^{\gamma} \tag{43}$$

where T_{ref} is a reference temperature, V_{ref} is a reference volume defined at $T=T_{ref}$ and in the limit of $P=0$, and γ is a thermodynamic interaction parameter related to the intermolecular repulsive potential.

Scott Bair [114] investigated Krytox® GPL 107 for temperatures to 170°C and pressures to 21200 psi. He found that a Vogel-Tammann-Fulcher (VTF)-like function would let all viscosity values obtained at different temperatures and pressures collapse onto a single curve

$$\eta = a \exp\left(\frac{b}{\varphi - c} \right) \tag{44}$$

Equation 44 was used to model our viscosity data of Krytox® GPL 102 too. The optimized parameters are presented in Table 17. The scaling factor, φ, for each datum is listed in Table 15.

Table 17: Optimized parameters of the scaling theory model

T_{ref} °C	V_{ref} cm^3/g	γ	a cP	b	c
20	0.5402	5.7816	0.7965	3.6904	0.1136

The results are illustrated in the semi-log plot of viscosity vs. scaling factor Figure 46. Although not used in the optimization of the scaling theory parameters, the HTHP Couette viscometer results at 1021 s^{-1} and the ambient pressure viscosity reported by DuPont [122] are also shown on the plot. The mean absolute percentage deviation (MAPD) obtained with the scaling model for the viscosity data measured with the rolling ball viscometer is 13%. Figure 47 shows the curve corresponding to the experimental viscosity versus calculated viscosity with the scaling function.

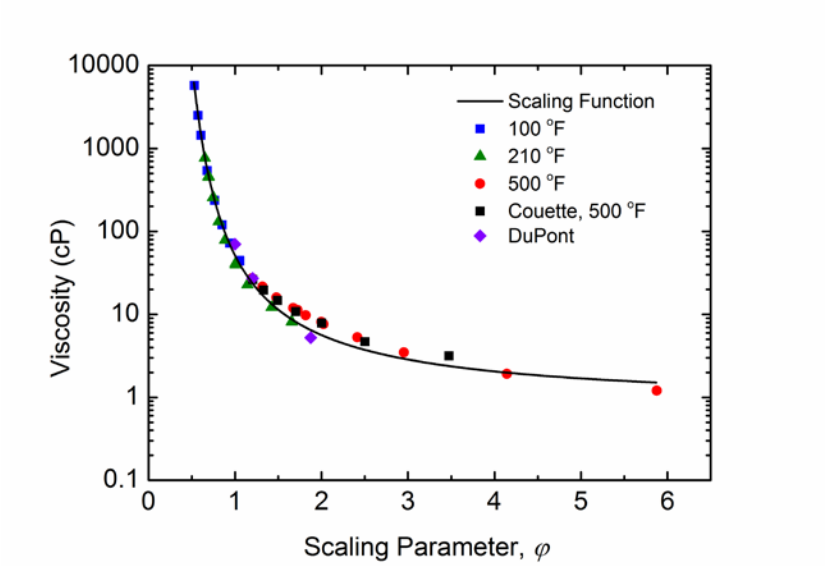

Figure 46: Semi-log plot of viscosity vs. scaling factor. The curve and the parameters were derived solely from the rolling ball viscometer data. The Couette viscometer data at 1021 s^{-1} and DuPont Technical Bulletin data are presented for comparison only

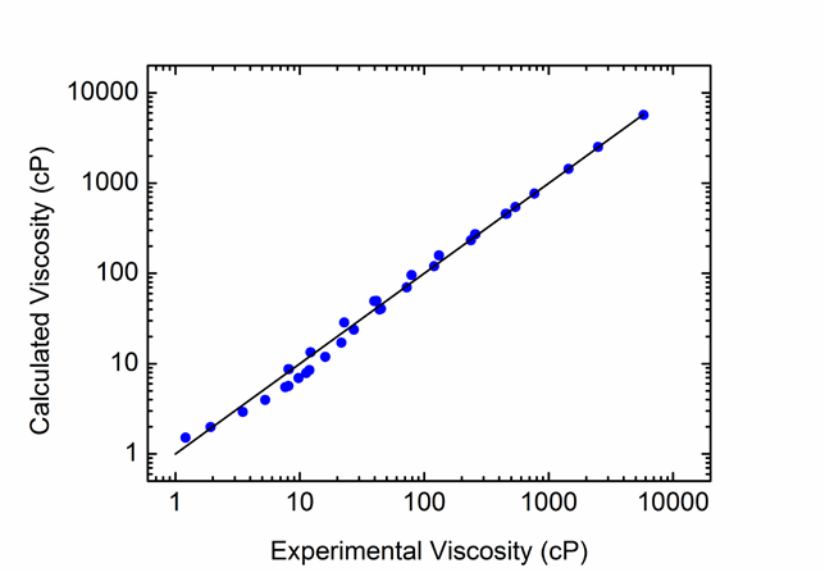

Figure 47: Experimental viscosity versus calculated viscosity with the scaling function

The viscosity data were also modeled with the surface fitting,

$$\ln\eta = \frac{a_0 + a_1T + b_1P + b_2P^2 + b_3P^3}{1 + a_2T + a_3T^2 + a_4T^3 + b_4P + b_5P^2} \tag{45}$$

where the viscosity, η, is in cP, temperature, T, is in K, and pressure, P, is in MPa. The coefficients of the surface fitting are given in Table 18.

Table 18: Coefficients of Equation 45 for Krytox® GPL 102

a_0	8.3982E+02
a_1	-1.5260E+00
b_1	5.7479E+00
b_2	-1.0080E-02
b_3	-7.4456E-06
a_2	-7.9547E-01
a_3	5.5200E-03
a_4	-6.0507E-06
b_4	3.6848E-01
b_5	-1.7100E-03

The mean absolute percentage deviation obtained with the surface fitting of Krytox® GPL 102 is 3.90 % which is within the experimental uncertainty range. The results are presented in the semi-log plot of viscosity vs. pressure Figure 48. Figure 49 shows the curve corresponding to the experimental viscosity versus calculated viscosity with Equation 45.

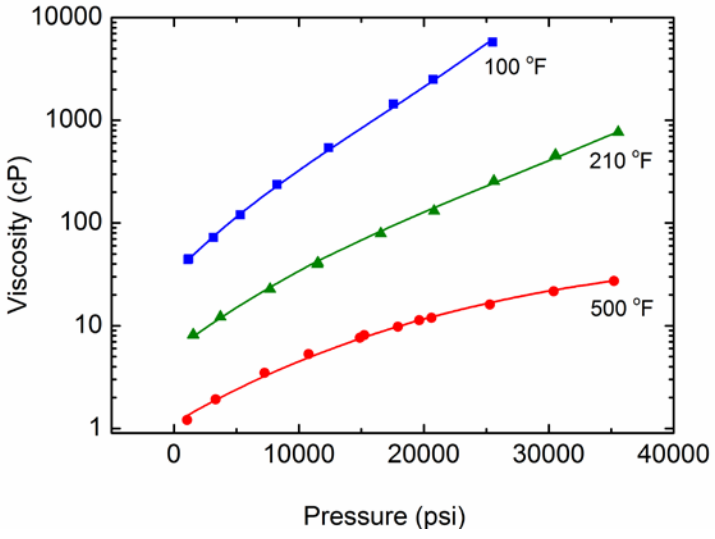

Figure 48: Semi-log plot of viscosity vs. pressure. Lines represent viscosity results obtained with the surface fitting

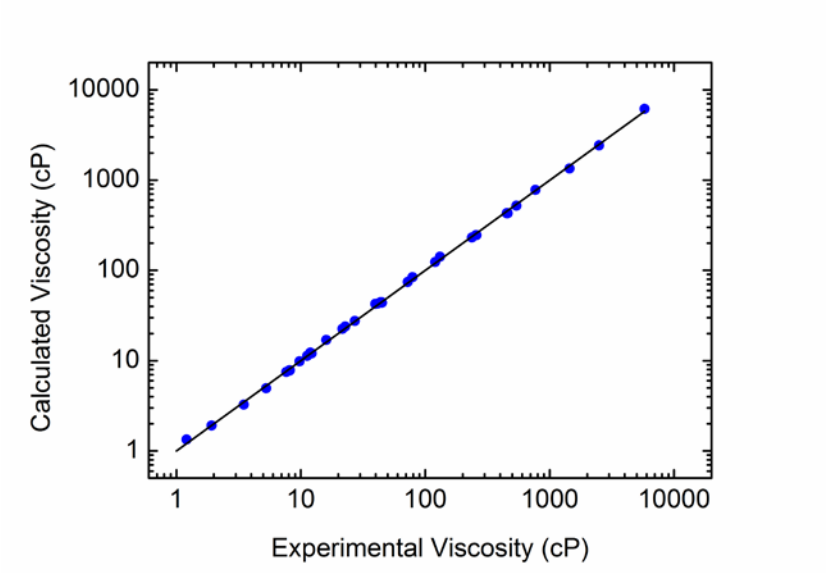

Figure 49: Experimental viscosity versus calculated viscosity with Equation 45

5.5 CONCLUSIONS

DuPont's Krytox® perfluoropolyether oils are colorless, odorless, thermally stable, low volatility, hydrophobic fluids that are promising candidates for a high temperature, high pressure (HTHP) Deepwater viscosity standard (DVS); a liquid that would exhibit of viscosity of roughly 20 cP at 260°C and 35000 psi. A novel windowed rolling ball viscometer (calibrated with dioctyl phthalate) were used to measure the viscosity of Krytox® GPL 102 at temperatures up to 260°C and pressures up to 40000 psi. The results were correlated with scaling theory and surface fitting.

6.0 CONCLUSIONS AND RECOMMENDATIOS

RPSEA (Research Partnership for Securing Energy for America), a non-profit corporation formed by a consortium of premier U.S. energy research universities, industry and independent research organizations with a stated mission “to provide a stewardship role in ensuring the focused research, development and deployment of safe, environmentally sensitive technology that can effectively deliver hydrocarbons from domestic resources to the citizens of the United States” [18], affirmed the need for accurate models for hydrocarbon fluid density and viscosity at extreme conditions associated with ultra-deep reservoirs.

6.1 PROJECT SUMMARY

Despite the significance of density and viscosity in the petroleum industry there is still a lack of experimental data particularly at extremely high temperature, high pressure (HTHP) conditions associated with ultra-deep petroleum formations found at depths of approximately 20000 ft or more, where the pressure and temperature can reach as high as 35000 psia and 500oF, respectively. In many applications, such as the simulation of oil reservoirs and the design of transport equipment, it is more convenient to use models to obtain such properties because experimental data might not be available at specific conditions and carrying out viscosity measurements at all temperatures, pressures, and compositions is time and cost prohibitive.

However, development of reliable models requires sufficient experimental data that cover the entire temperature and pressure ranges of interest.

A HTHP density prediction model has been developed by utilizing the concept of volume- translation (VT) in the SRK and PR equations of state. Rather than correlating the volume-correction to saturated liquid densities, as is done in most prior volume translation methods, the volume-translation term in the HTHP VT-SRK EoS and HTHP VT-PR EoS is correlated to pure component, single-phase density literature data at HTHP conditions. The new proposed model provides very accurate density predictions over a wide range of temperature and pressure. The overall mean absolute percentage deviation (MAPD) of 1-2% obtained with the new model is substantially lower than those calculated with other models considered in this study.

A novel windowed, high temperature, high pressure rolling ball viscometer was designed and constructed specifically for this project. The viscometer has been calibrated with n-decane and used to measure the viscosity of n-octane for temperatures to 500oF and pressures to 35000 psia. A literature review of different viscosity models has shown that the friction theory (F-theory) and free volume theory (FV-theory) models are superior to many other viscosity models. A correction term added to the F-theory model has been proposed to get more accurate viscosity predictions.

In the oil industry, there is a need to identify a viscosity standard that is representative of light oils produced from ultra-deep formations found beneath the deep waters of the Gulf of Mexico. Deepwater viscosity standard (DVS) is a liquid that would exhibit a viscosity of roughly 20 cP at 500oF and 35000 psia. This work suggests Krytox® GPL 102 as a promising candidate for a HTHP DVS. The windowed rolling ball viscometer (calibrated with dioctyl phthalate) were

used to determine the viscosity of Krytox® GPL 102 at temperatures up to 500oF and pressures up to 36,000 psia, and all of the results were modeled with scaling theory.

6.2 SUGGESTIONS AND RECOMMENDATIONS

- By adding a linear variable differential transformer (LVDT) to the existing viscometer, the cell can be extended to allow simultaneous viscosity and density measurements. The internal floating piston, as shown in Figure 50, will be connected to a rod that has a magnetic end piece (LVDT core), and as the piston moves the magnetic core travels through the LVDT and the location of the piston can be tracked by a position sensor.

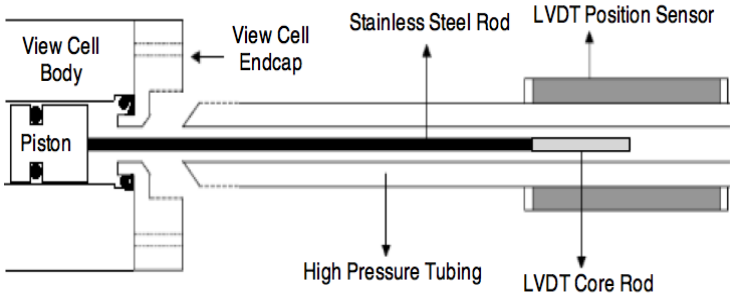

Figure 50: LVDT allows density measurements [16]

- By replacing the o-ring seals with gold seals and the floating piston with a metal bellows, the cell can be operated at a higher temperature of at least 600^{o}F.
- In case of an opaque fluid such as crude oil, fiber optic cables that consist of both light source fibers and light receiving fibers, can be used to detect the position of a ball with

d/D> 0.99. A “point” of the shiny surface of the ball can be seen as it rolls past the window, it will reflect the light back to the cable for a brief moment.

- The extension of the free volume theory model to mixtures should be studied.

APPENDIX A

PRESSURE AND TEMPERATURE EFFECTS ON DIAMETER RATIO

Change in radius of ball due to pressure

Isothermal compressibility: $\beta_T = -\frac{1}{V}\left(\frac{\partial V}{\partial P}\right)_T$; $\beta_T = \frac{3(1-2\nu)}{E}$

Volume of ball: $V = \frac{4}{3}\pi \cdot r^3$

Change in radius of ball: $\Delta r = r_2 - r_1 = r_1\left(\exp(-\frac{\beta_T (P_2 - P_1)}{3}) - 1\right)$

where ν is the Poisson's ratio and E is the Young's Modulus which can be read from this table [123].

INCONEL® alloy 718

Modulus of Elasticity[a]

Temperature, °F	Modulus of Elasticity, ksi x 10^3		Poisson's Ratio[b]	Temperature, °F	Modulus of Elasticity, ksi x 10^3		Poisson's Ratio[b]
	Young's Modulus	Torsional Modulus			Young's Modulus	Torsional Modulus	
70	29.0	11.2	0.294	1300	23.0	8.9	0.292
100	28.8	11.2	0.291	1400	22.3	8.5	0.306
200	28.4	11.0	0.288	1500	21.3	8.1	0.321
300	28.0	10.9	0.280	1600	20.2	7.6	0.331
400	27.6	10.8	0.280	1700	18.8	7.1	0.334
500	27.1	10.6	0.275	1800	17.4	6.5	0.341
600	26.7	10.5	0.272	1900	15.9	5.8	0.366
700	26.2	10.3	0.273	2000	14.3	5.1	0.402
800	25.8	10.1	0.271				
900	25.3	9.9	0.272				
1000	24.8	9.7	0.271				
1100	24.2	9.5	0.276				
1200	23.7	9.2	0.283				

[a]Hot-rolled flat heat-treated 1800°F/1 hr, A.C. + 1325°F/8 hr, F.C. 20°F/hr to 1150°F, held for total aging time of 18 hr. Dynamic testing involved frequencies of from 813 to 571 cps in bending and from 3110 to 2097 cps in torsion.

[b]Computed from (E-2G)/2G, where E is Young's Modulus and G is torsional modulus.

Radial expansion of the cell [124]

$$\delta_r = \frac{Pr^2}{bE}\left(1-\frac{\nu}{2}\right)$$

where b is the wall thickness.

APPENDIX B

DRAWINGS OF THE VISCOMETER CELL

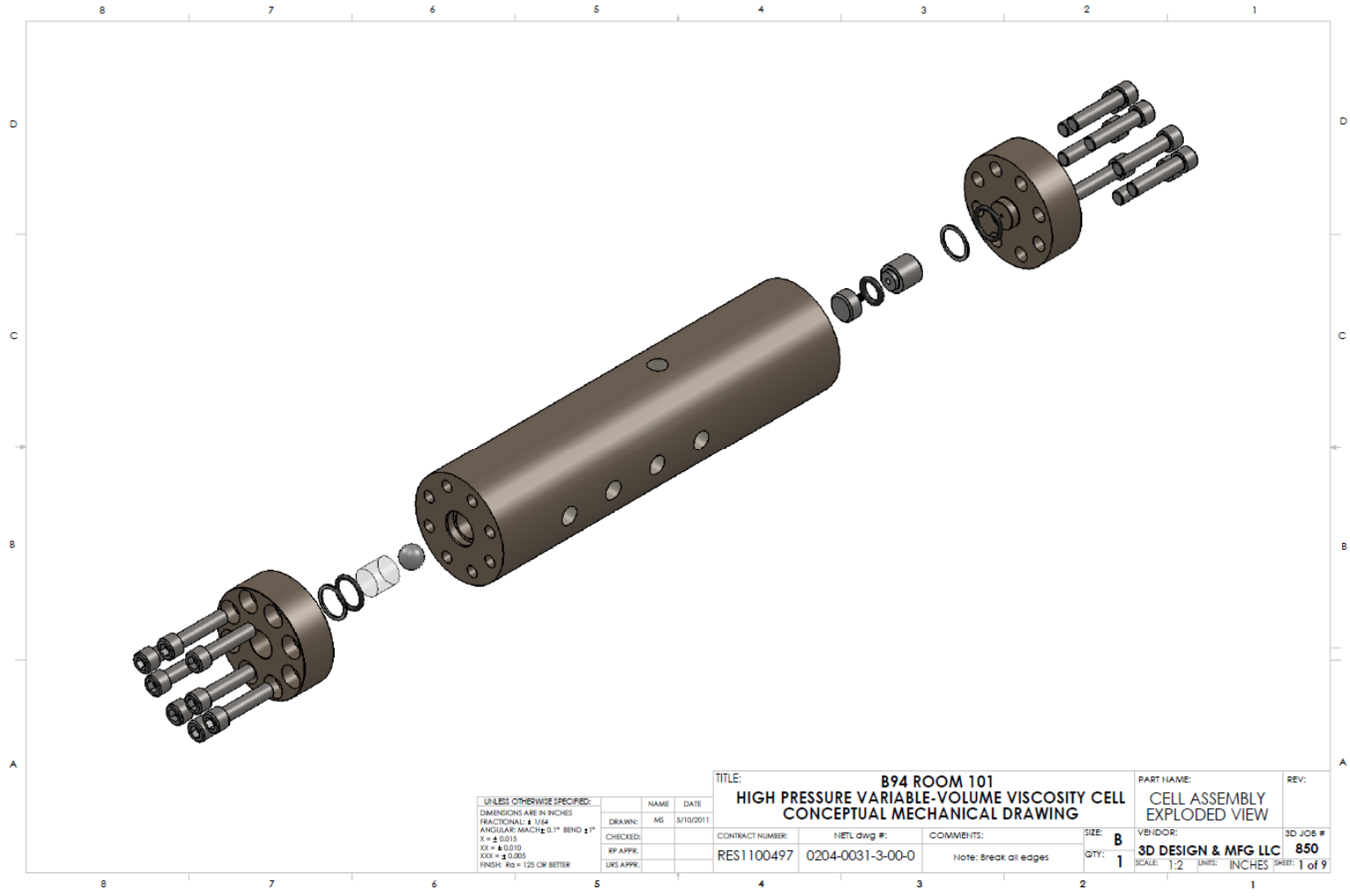

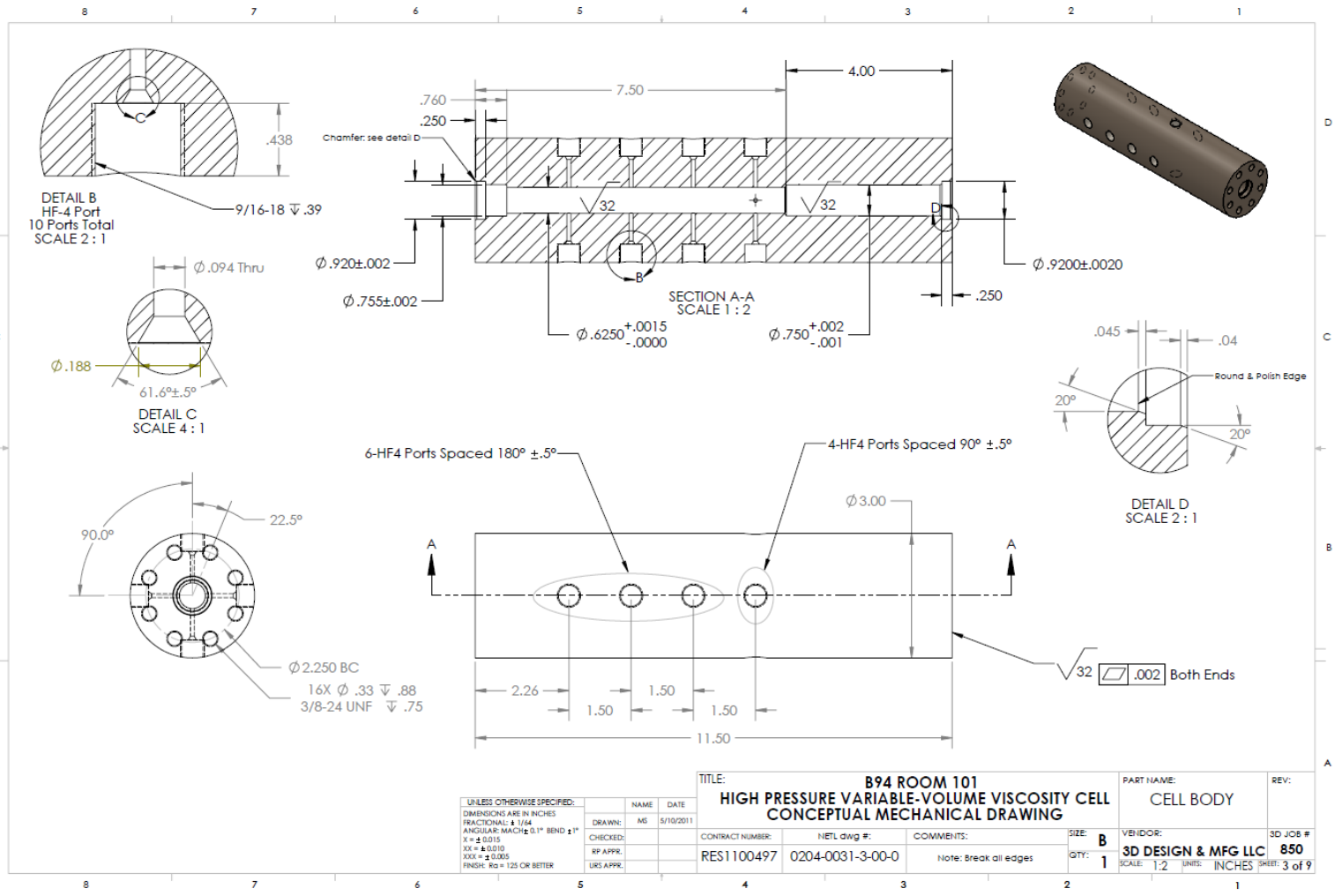

UNLESS OTHERWISE SPECIFIED:		NAME	DATE
DIMENSIONS ARE IN INCHES FRACTIONAL: ± 1/64 ANGULAR: MACH± 0.1° BEND ± 1° X = ± 0.015 XX = ± 0.010 XXX = ± 0.005 FINISH: Ra = 125 OR BETTER	DRAWN:	MS	5/10/2011
	CHECKED:		
	RP APPR.		
	URS APPR.		

TITLE:			PART NAME:	REV:
B94 ROOM 101 HIGH PRESSURE VARIABLE-VOLUME VISCOSITY CELL CONCEPTUAL MECHANICAL DRAWING			CELL BODY	
CONTRACT NUMBER:	NETL dwg #:	COMMENTS:	SIZE: B QTY: 1	VENDOR: 3D DESIGN & MFG LLC SCALE: 1:2 UNITS: INCHES
RES1100497	0204-0031-3-00-0	Note: Break all edges		3D JOB # 850 SHEET: 3 of 9

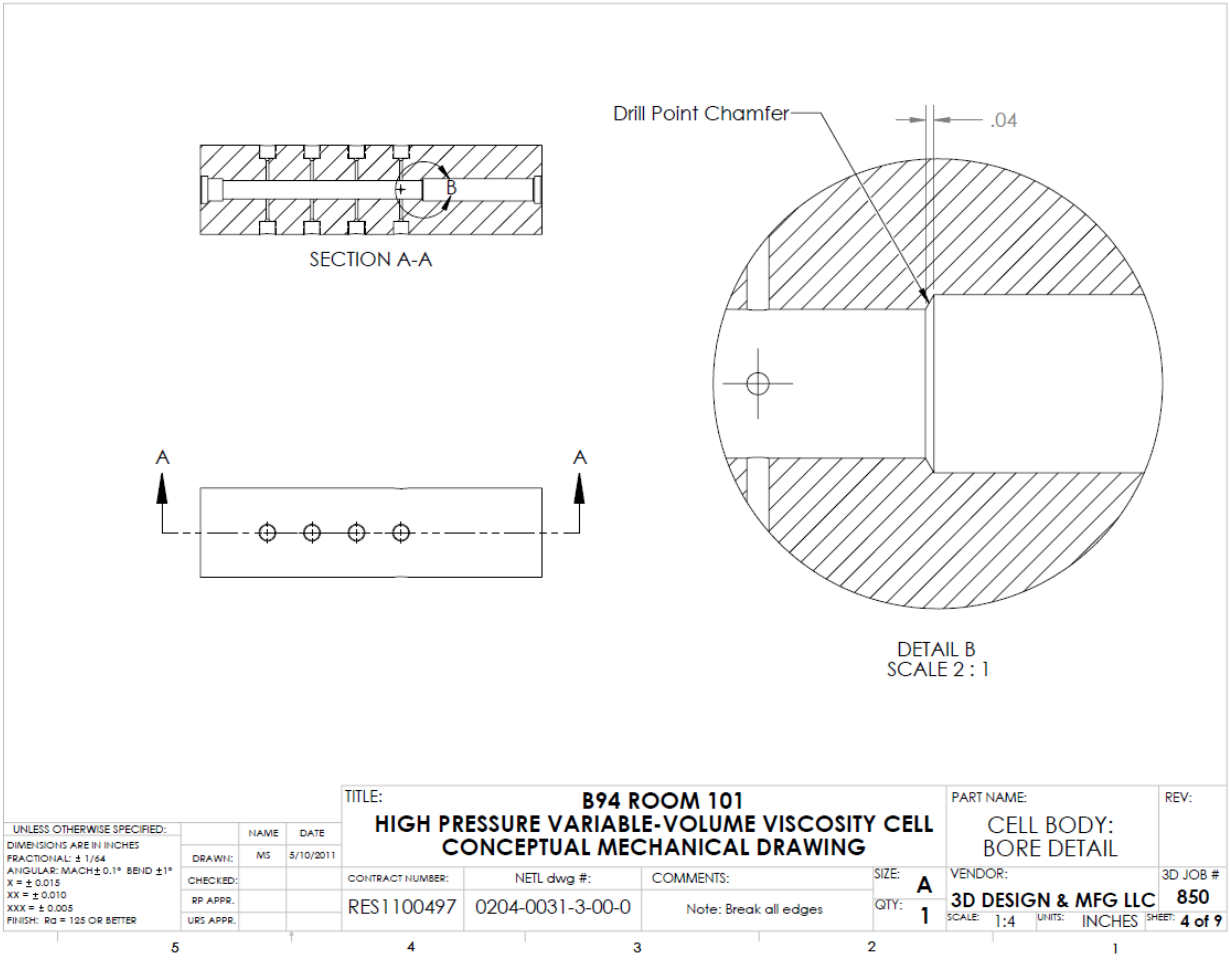

UNLESS OTHERWISE SPECIFIED: DIMENSIONS ARE IN INCHES FRACTIONAL: ± 1/64 ANGULAR: MACH ± 0.1° BEND ± 1° X = ± 0.015 XX = ± 0.010 XXX = ± 0.005 FINISH: Ra = 125 OR BETTER		NAME	DATE	TITLE: **B94 ROOM 101 HIGH PRESSURE VARIABLE-VOLUME VISCOSITY CELL CONCEPTUAL MECHANICAL DRAWING**				PART NAME: CELL BODY: BORE DETAIL	REV:
	DRAWN:	MS	5/10/2011						
	CHECKED:			CONTRACT NUMBER:	NETL dwg #:	COMMENTS:	SIZE: A	VENDOR:	3D JOB #
	RP APPR.			RES1100497	0204-0031-3-00-0	Note: Break all edges	QTY: 1	**3D DESIGN & MFG LLC**	**850**
	URS APPR.							SCALE: 1:4 UNITS: INCHES	SHEET: **4 of 9**

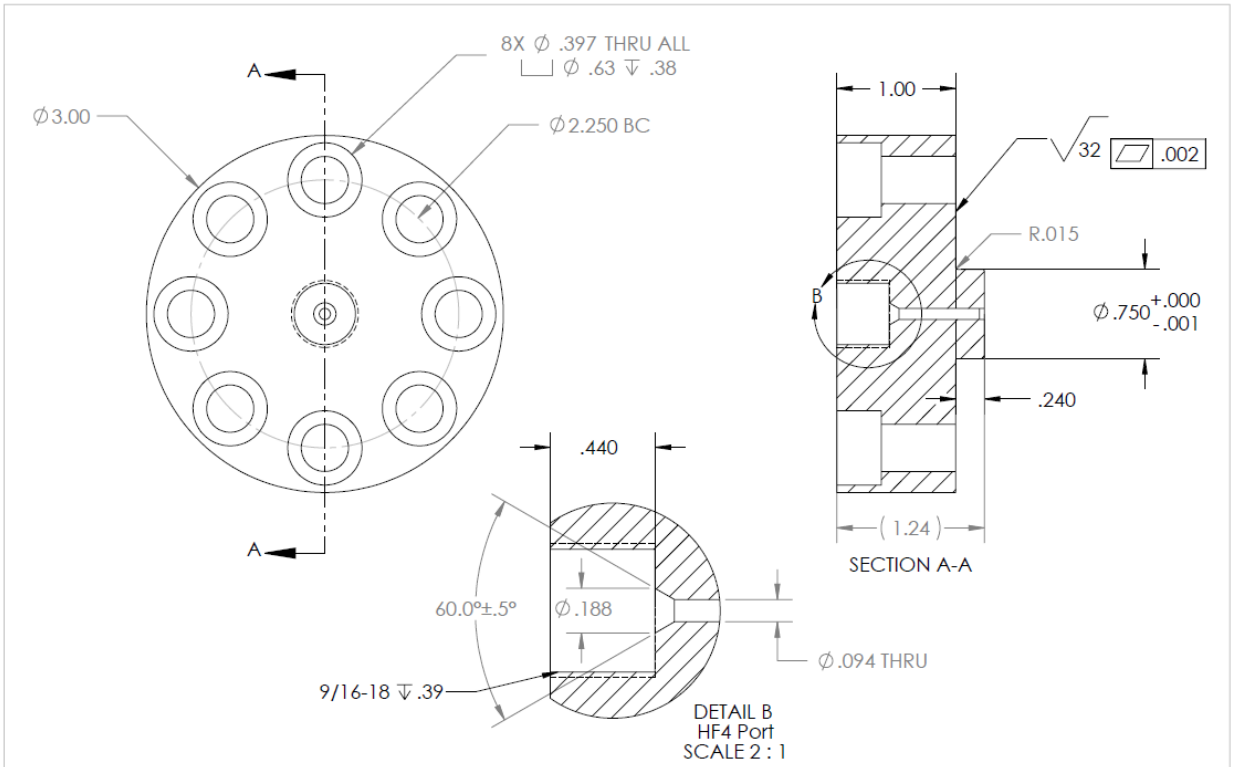

UNLESS OTHERWISE SPECIFIED:		NAME	DATE
DIMENSIONS ARE IN INCHES FRACTIONAL: ± 1/64 ANGULAR: MACH± 0.1° BEND ±1° X = ± 0.015 XX = ± 0.010 XXX = ± 0.005 FINISH: Ra = 125 OR BETTER	DRAWN:	MS	5/10/2011
	CHECKED:		
	RP APPR.		
	URS APPR.		

TITLE: **B94 ROOM 101**
HIGH PRESSURE VARIABLE-VOLUME VISCOSITY CELL
CONCEPTUAL MECHANICAL DRAWING

PART NAME: END CAP- INPUT

REV:

CONTRACT NUMBER:	NETL dwg #:	COMMENTS:	SIZE:	VENDOR:	3D JOB #
RES1100497	0204-0031-3-00-0	Note: Break all edges	A	3D DESIGN & MFG LLC	850
			QTY: 1	SCALE: Full UNITS: INCHES	SHEET: 5 of 9

5 4 3 2 1

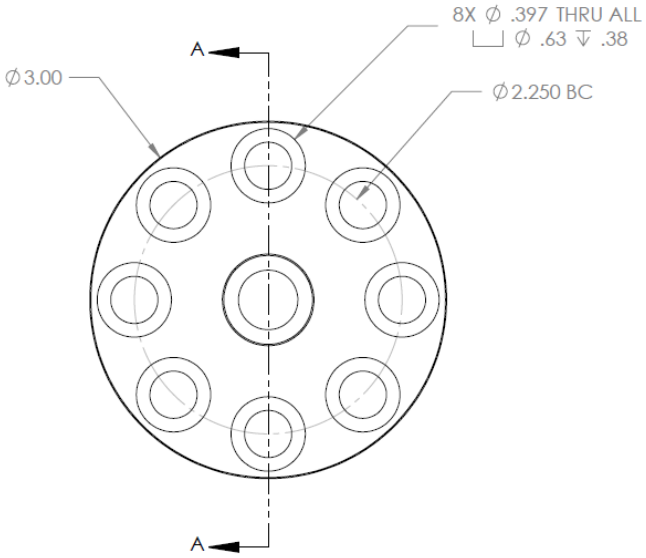

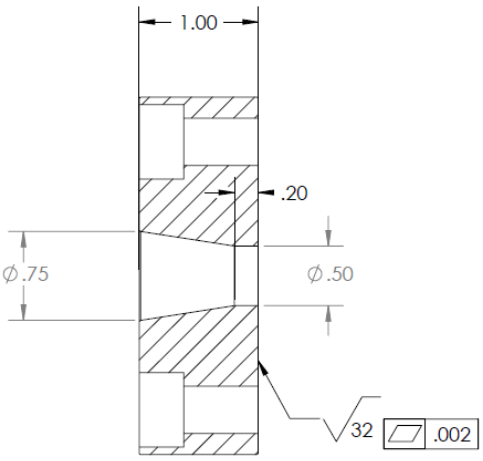

SECTION A-A

UNLESS OTHERWISE SPECIFIED: DIMENSIONS ARE IN INCHES FRACTIONAL: ± 1/64 ANGULAR: MACH ± 0.1° BEND ±1° X = ± 0.015 XX = ± 0.010 XXX = ± 0.005 FINISH: Ra = 125 OR BETTER		NAME	DATE	TITLE: **B94 ROOM 101 HIGH PRESSURE VARIABLE-VOLUME VISCOSITY CELL CONCEPTUAL MECHANICAL DRAWING**				PART NAME: END CAP- VIEWPORT	REV:
	DRAWN:	MS	5/10/2011						
	CHECKED:			CONTRACT NUMBER:	NETL dwg #:	COMMENTS:	SIZE: A	VENDOR:	3D JOB #
	RP APPR.			RES1100497	0204-0031-3-00-0	Note: Break all edges	QTY: 1	**3D DESIGN & MFG LLC**	**850**
	URS APPR.							SCALE: Full UNITS: INCHES	SHEET: 6 of 9

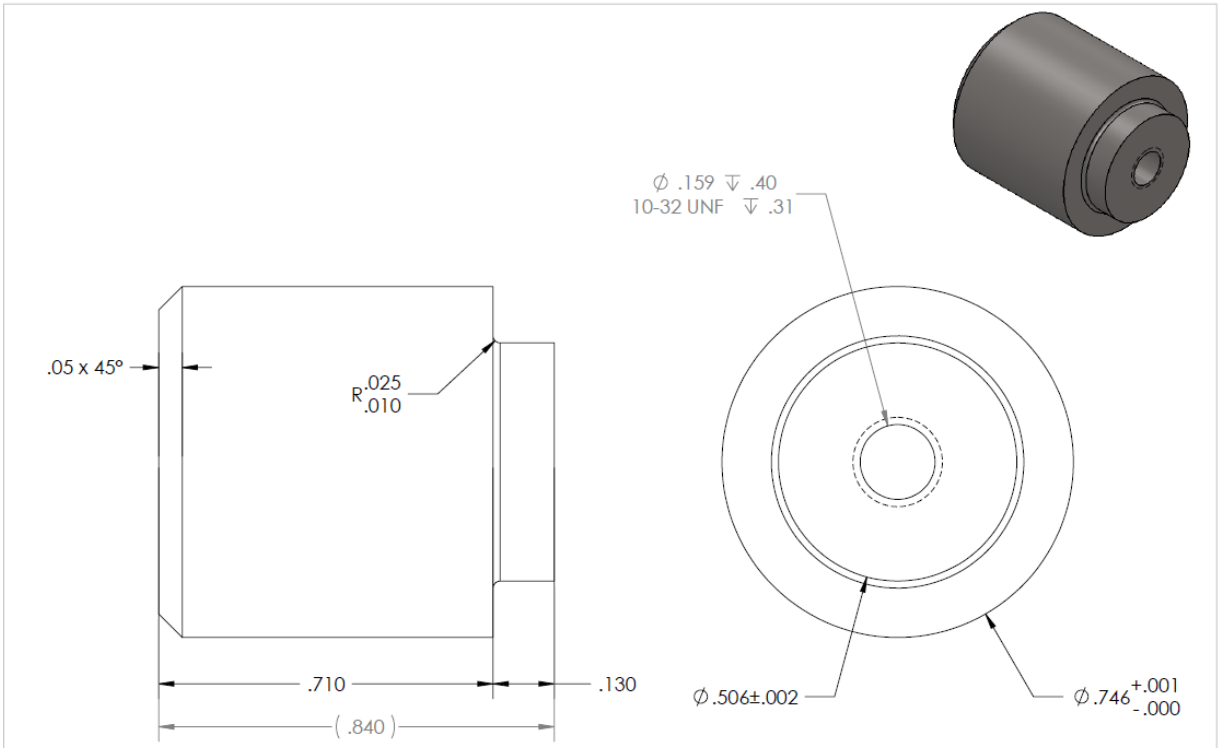

UNLESS OTHERWISE SPECIFIED: DIMENSIONS ARE IN INCHES; FRACTIONAL: ± 1/64; ANGULAR: MACH ± 0.1° BEND ±1°; X = ± 0.015; XX = ± 0.010; XXX = ± 0.005; FINISH: Ra = 125 OR BETTER			
	NAME	DATE	
DRAWN:	MS	5/10/2011	
CHECKED:			
RP APPR.			
URS APPR.			

TITLE: **B94 ROOM 101**
HIGH PRESSURE VARIABLE-VOLUME VISCOSITY CELL
CONCEPTUAL MECHANICAL DRAWING

PART NAME: PISTON - PART 1

REV:

CONTRACT NUMBER:	NETL dwg #:	COMMENTS:	SIZE:	VENDOR:	3D JOB #
RES1100497	0204-0031-3-00-0	Note: Break all edges	A	3D DESIGN & MFG LLC	850
			QTY: 1	SCALE: 4:1 UNITS: INCHES	SHEET: 7 of 9

5 4 3 2 1

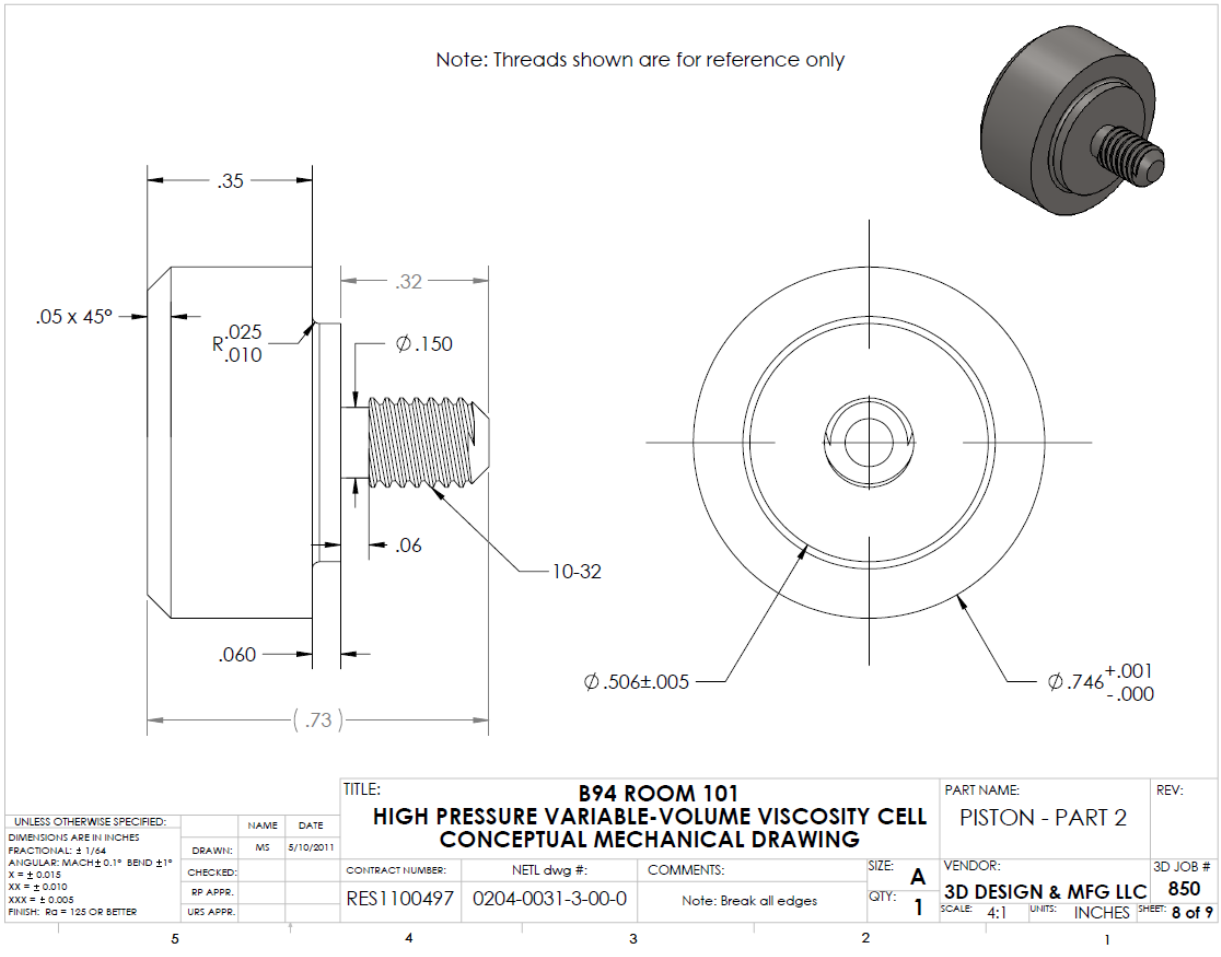

UNLESS OTHERWISE SPECIFIED: DIMENSIONS ARE IN INCHES FRACTIONAL: ± 1/64 ANGULAR: MACH ± 0.1° BEND ± 1° X = ± 0.015 XX = ± 0.010 XXX = ± 0.005 FINISH: Ra = 125 OR BETTER		NAME	DATE
	DRAWN:	MS	5/10/2011
	CHECKED:		
	RP APPR.		
	URS APPR.		

TITLE: **B94 ROOM 101**
HIGH PRESSURE VARIABLE-VOLUME VISCOSITY CELL
CONCEPTUAL MECHANICAL DRAWING

PART NAME: PISTON - PART 2

REV:

CONTRACT NUMBER:	NETL dwg #:	COMMENTS:	SIZE:	VENDOR:	3D JOB #
RES1100497	0204-0031-3-00-0	Note: Break all edges	A	3D DESIGN & MFG LLC	850
			QTY: 1	SCALE: 4:1 UNITS: INCHES	SHEET: 8 of 9

5 4 3 2 1

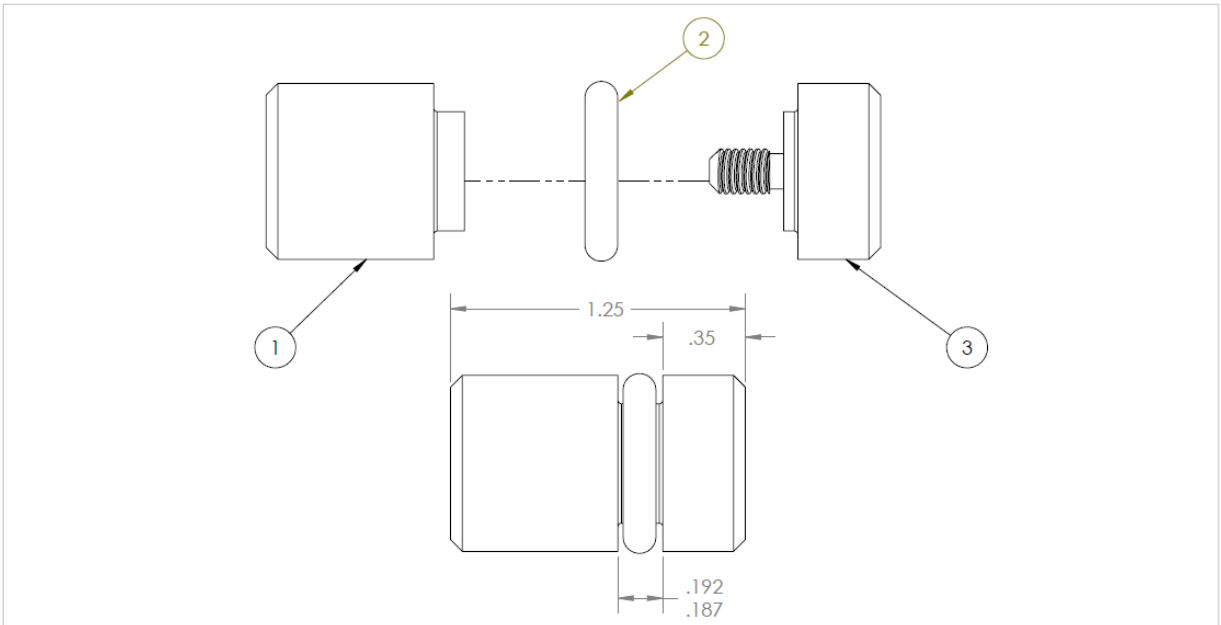

ITEM NO.	SHEET NO.	PART DESCRIPTION	QTY.
1	7	Piston-Part 1	1
2		-206 Oring	1
3	8	Piston-Part 2	1

UNLESS OTHERWISE SPECIFIED:
DIMENSIONS ARE IN INCHES
FRACTIONAL: ± 1/64
ANGULAR: MACH ± 0.1° BEND ±1°
X = ± 0.015
XX = ± 0.010
XXX = ± 0.005
FINISH: Ra = 125 OR BETTER

	NAME	DATE
DRAWN:	MS	5/10/2011
CHECKED:		
RP APPR.		
URS APPR.		

TITLE:
B94 ROOM 101
HIGH PRESSURE VARIABLE-VOLUME VISCOSITY CELL
CONCEPTUAL MECHANICAL DRAWING

PART NAME: PISTON ASSEMBLY

REV:

CONTRACT NUMBER:	NETL dwg #:	COMMENTS:	SIZE:	QTY:
RES1100497	0204-0031-3-00-0	Note: Break all edges	A	1

VENDOR: **3D DESIGN & MFG LLC**

3D JOB # **850**

SCALE: 2:1 UNITS: INCHES SHEET: **9 of 9**

5 4 3 2 1

APPENDIX C

BLOCK DIAGRAM OF THE LABVIEW PROGRAM

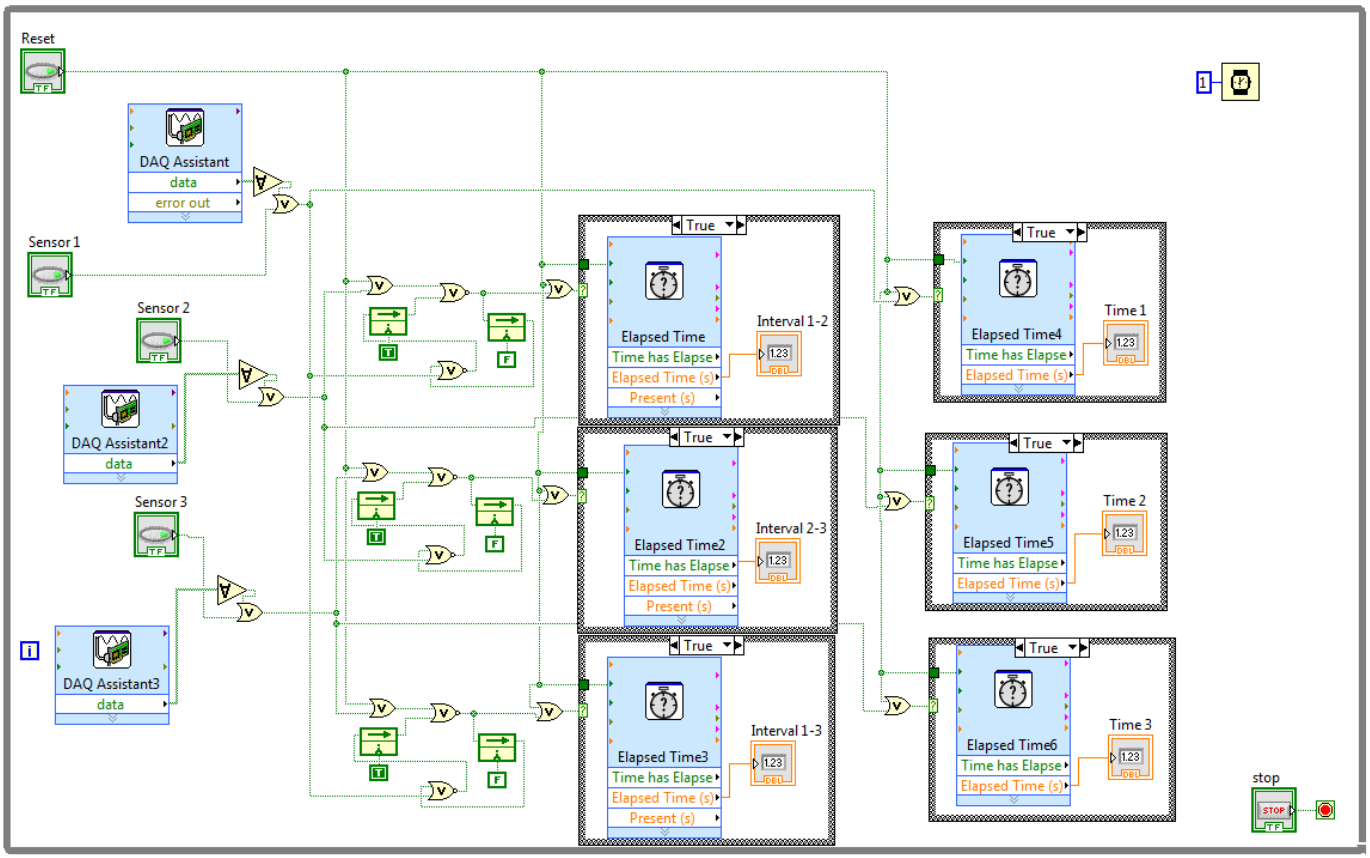

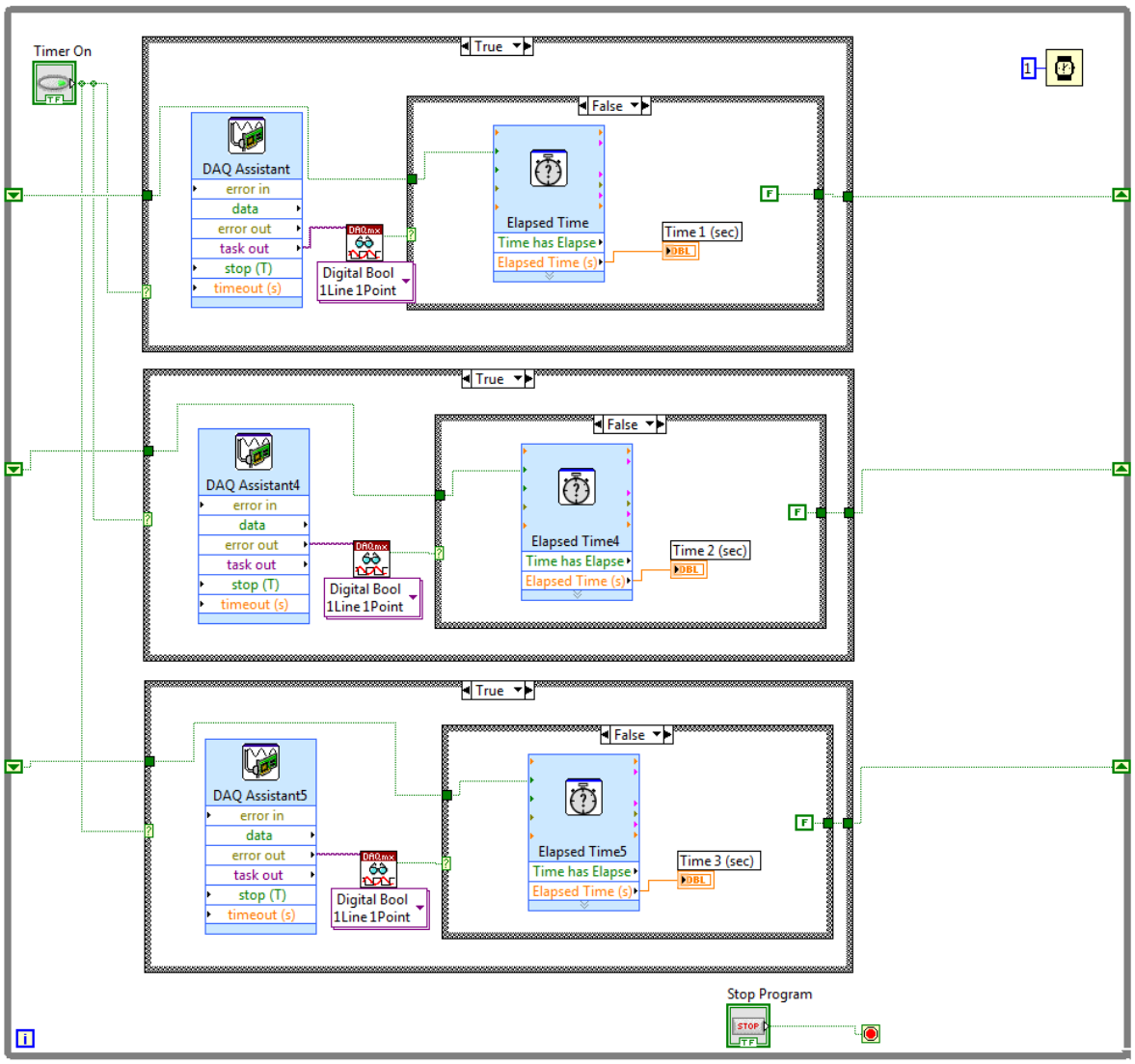
Timer On
True
False
DAQ Assistant
error in
data
error out
task out
stop (T)
timeout (s)
Digital Bool
1Line 1Point
Elapsed Time
Time has Elapse
Elapsed Time (s)
Time 1 (sec)
DBL
DAQ Assistant4
Elapsed Time4
Time 2 (sec)
DAQ Assistant5
Elapsed Time5
Time 3 (sec)
Stop Program
STOP

APPENDIX D

EXPANDED UNCERTAINTY IN VISCOSITY MEASUREMENTS

$$\eta = \frac{k\left(\rho_b - \rho_{fl}\right)\sin\theta}{\left(d/t\right)}$$

$$U_\eta = Ku_\eta = K\sqrt{\left(\frac{\partial\eta}{\partial k}\right)^2\delta_k^2 + \left(\frac{\partial\eta}{\partial\rho_b}\right)^2\delta_{\rho_b}^2 + \left(\frac{\partial\eta}{\partial\rho_{fl}}\right)^2\delta_{\rho_{fl}}^2 + \left(\frac{\partial\eta}{\partial\theta}\right)^2\delta_\theta^2 + \left(\frac{\partial\eta}{\partial d}\right)^2\delta_d^2 + \left(\frac{\partial\eta}{\partial t}\right)^2\delta_t^2}$$

$$\frac{\partial\eta}{\partial k} = \frac{\left(\rho_b - \rho_{fl}\right)\sin\theta}{\left(d/t\right)}$$

$$\frac{\partial\eta}{\partial\rho_b} = \frac{k\sin\theta}{\left(d/t\right)}$$

$$\frac{\partial\eta}{\partial\rho_{fl}} = \frac{-k\sin\theta}{\left(d/t\right)}$$

$$\frac{\partial\eta}{\partial\theta} = \frac{k\left(\rho_b - \rho_{fl}\right)\cos\theta}{\left(d/t\right)}$$

$$\frac{\partial\eta}{\partial d} = \frac{-k\left(\rho_b - \rho_{fl}\right)\sin\theta}{\left(d^2/t\right)}$$

$$\frac{\partial\eta}{\partial t} = \frac{k\left(\rho_b - \rho_{fl}\right)\sin\theta}{d}$$

K (coverage factor)=2 for confidence of 95%

BIBLIOGRAPHY

[1] G. Soave, Equilibrium Constants from a Modified Redlich-Kwong Equation of State, Chemical Engineering Science, 27 (1972) 1197-1203.

[2] D.Y. Peng, D.B. Robinson, A new two-constant equation of state, Industrial & Engineering Chemistry Fundamentals, 15 (1976) 59-64.

[3] G. Schmidt, H. Wenzel, A Modified van der Waals Type Equation of State, Chemical Engineering Science, 35 (1980) 1503-1512.

[4] W.G. Chapman, G. Jackson, K.E. Gubbins, Phase equilibria of associating fluids. Chain molecules with multiple bonding sites, Molecular Physics, 65 (1988) 1057-1079.

[5] W.G. Chapman, K.E. Gubbins, G. Jackson, M. Radosz, New reference equation of state for associating liquids., Ind. Eng. Chem. Res., 29 (1990) 1709-1721.

[6] J. Gross, G. Sadowski, Perturbed-chain SAFT: An equation of state based on a perturbation theory for chain molecules, Ind Eng Chem Res, 40 (2001) 1244-1260.

[7] I. Polishuk, Hybridizing SAFT and cubic EOS: What can be achieved?, Industrial & Engineering Chemistry Research, 50 (2011) 4183-4198.

[8] G.M. Kontogeorgis, E.C. Voutsas, I.V. Yakoumis, D.P. Tassios, An equation of state for associating fluids, Ind. Eng. Chem. Res., 35 (1996) 4310-4318.

[9] G.M. Kontogeorgis, I.V. Yakoumis, H. Meijer, E. Hendriks, T. Moorwood, Multicomponent phase equilibrium calculations for water–methanol–alkane mixtures, Fluid Phase Equilibria, 158–160 (1999) 201–209.

[10] G.M. Kontogeorgis, M.L. Michelsen, G.K. Folas, S. Derawi, N.V. Solms, E.H. Stenby, Ten years with the CPA (Cubic-Plus-Association) equation of state. Part 1. Pure compounds and self-associating systems, Ind. Eng. Chem. Res., 45 (2006) 4855-4868.

[11] M.J. Pratas, M.B. Oliveira, M.J. Pastoriza-Gallego, A.J. Queimada, M.M. Piñeiro, J.A.P. Coutinho, High-pressure biodiesel density: Experimental measurements, correlation, and Cubic-Plus-Association Equation of State (CPA EoS) modeling, ACS, 25 (2011) 3806-3814.

[12] I. Polishuk, Till which pressures the fluid phase EOS models might stay reliable?, J. of Supercritical Fluids, 58 (2011) 204-215.

[13] R. Span, Multiparameter equations of state: An accurate source of thermodynamic property data, 1 edition ed., Springer, Berlin, 2000.

[14] G. Scalabrin, L. Bettio, P. Marchi, L. Piazza, D. Richon, An extended equation of state modeling method I. pure fluids, International Journal of Thermophysics, 27 (2006) 1281-1318.

[15] G. Scalabrin, L. Bettio, P. Marchi, P. Stringari, A fundamental equation of state for sulfur hexafluoride (SF6) in extended equation of state format, J. Phys. Chem. Ref. Data, 36 (2007) 617-662.

[16] K. Liu, Y. Wu, M.A. McHugh, H. Baled, R.M. Enick, B.D. Morreale, Equation of state modeling of high-pressure, high-temperature hydrocarbon density data, Journal of Supercritical Fluids, 55 (2010) 701-711.

[17] A.J. Queimada, C. Miqueu, I.M. Marrucho, G.M. Kontogeorgis, J.A.P. Coutinho, Modeling vapor–liquid interfaces with the gradient theory in combination with the CPA equation of state, Fluid Phase Equilibria, 228–229 (2005) 479–485.

[18] RAPSEA, http://www.rpsea.org.

[19] A. Peneloux, E. Rauzy, A consistent correction for Redlich-Kwong-Soave volumes, Fluid Phase Equilibria, 8 (1982) 7-23.

[20] W.R. Ji, D.A. Lempe, Density improvement of the SRK equation of state, Fluid Phase Equilibria, 130 (1997) 49-63.

[21] L.S. Wang, J. Gmehling, Improvement of the SRK equation of state for representing volumetric properties of petroleum fluids using Dortmund Data Bank, Chemical Engineering Science, 54 (1999) 3885-3892.

[22] K. Magoulas, D.P. Tassios, Thermophysical properties of n-alkanes from C1 to C20 and their prediction for higher ones, Fluid Phase Equilibria 56 (1990) 119-140.

[23] P. Ungerer, C. Batut, Prédiction des propriétés volumétriques des hydrocarbures par une translation de volume améliorée, Revue de l'Institut Francais du Petrole 52 (1997) 609-623.

[24] P. Ungerer, C. Batut, G. Moracchini, J. Sanchez, H.B. de Sant'Ana, J. Carrier, D.M. Jensen, Measurement and prediction of volumetric and transport properties of reservoir fluids at high pressure, Revue de l'Institut Francais du Petrole 53 (1998) 265-281.

[25] P. Ungerer, H.B. De Sant'Ana, Reply to the letter to the editor by O. Pfohl about the paper "Evaluation of an improved volume translation for the prediction of hydrocarbon

volumetric properties" [FPE 154, 193-204 (1999)], Fluid Phase Equilibria, 163 (1999) 161-162.

[26] H.B. de Sant'Ana, P. Ungerer, J.C. de Hemptinne, Evaluation of an improved volume translation for the prediction of hydrocarbon volumetric properties, Fluid Phase Equilibria, 154 (1999) 193-204.

[27] J.C. de Hemptinne, P. Ungerer, Accuracy of the volumetric predictions of some important equations of state for hydrocarbons, including a modified version of the Lee-Kesler method, Fluid Phase Equilibria 106 (1995) 81-109.

[28] O. Pfohl, Letter to the editor ‘‘Evaluation of an improved volume translation for the prediction of hydrocarbon volumetric properties’’, Fluid Phase Equilibria 163 (1999) 157-159.

[29] K. Frey, Improving thermodynamic property estimation through volume translation, in, Massachusetts Institute of Technology, 2010.

[30] P.M. Mathias, T. Naheiri, E.M. Oh, A Density Correction for the Peng-Robinson Equation of State, Fluid Phase Equilibria, 47 (1989) 77-87.

[31] J. Tester, K. Frey, C. Augustine, R.P. Ciccolini, S. Paap, M. Modell, Volume translation in equations of state as a means of accurate property estimation, Fluid Phase Equilibria, 260 (2007) 316-325.

[32] J. Tester, K. Frey, M. Modell, Density-and-temperature-dependent volume translation for the SRK EOS: 1. Pure fluids, Fluid Phase Equilibria, 279 (2009) 56-63.

[33] H.H. Reamer, B.H. Sage, Volumetric behavior of cyclohexane, Industrial & Engineering Chemistry, 2 (1957) 9-12.

[34] A.K. Doolittle, Specific volumes of n-alkanes, Journal of Chemical and Engineering Data 9(1964) 275-279.

[35] NIST Thermophysical Properties of Fluid Systems, http://webbook.nist.gov/chemistry/fluid/.

[36] U. Setzmann, W. Wagner, A New Equation of State and Tables of Thermodynamic Properties for Methane Covering the Range from the Melting Line to 625-K at Pressures up to 1000-Mpa, Journal of Physical and Chemical Reference Data, 20 (1991) 1061-1155.

[37] H. Miyamoto, M. Uematsu, Measurements of vapor pressures from 280 to 369 K and (p, rho, T) properties from 340 to 400 K at pressures to 200 MPa for propane, International Journal of Thermophysics, 27 (2006) 1052-1060.

[38] Y. Wu, B. Bamgbade, K. Liu, M.A. McHugh, H. Baled, R.M. Enick, W. Burgess, D. Tapriyal, B.D. Morreale, Experimental measurements and equation of state modeling of

liquid densities for longchain n-alkanes at pressures to 265 MPa and temperatures to 523 K, Fluid Phase Equilibria, 311 (2011) 17-24.

[39] S.R.R. Deul, E.U. Franck, The dielectric constant and density of benzene to 400°C and 3000 bar, Berichte der Bunsengesellschaft für Physikalische Chemie, 95 (1991) 515-519.

[40] F.J. Vieira dos Santos, C.A. Nieyo de Castro, Viscosity of toluene and benzene under high pressure, International Journal of Thermopgysics, 18 (1997) 367-378.

[41] G. Sadowski, J. Gross, Modeling polymer systems using the perturbed-chain statistical associating fluid theory equation of state, Ind Eng Chem Res, 41 (2002) 1084-1093.

[42] G. Sadowski, J. Gross, Application of the perturbed-chain SAFT equation of state to associating systems, Ind Eng Chem Res, 41 (2002) 5510-5515.

[43] E.C. Voutsas, G.D. Pappa, K. Magoulas, D.P. Tassios, Vapor liquid equilibrium modeling of alkane systems with equations of state: "Simplicity versus complexity", Fluid Phase Equilibria, 240 (2006) 127-139.

[44] E.A. Brignole, M. Cismondi, J. Mollerup, Rescaling of three-parameter equations of state: PC-SAFT and SPHCT, Fluid Phase Equilibria, 234 (2005) 108-121.

[45] S. Stamataki, D. tassios, Performance of cubic EoS at high pressures, Revue de l'Institut Francais du Petrole, 53 (1998) 367-377.

[46] G. Soave, S. Gamba, L.A. Pellegrini, SRK equation of state: Predicting binary interaction parameters of hydrocarbons and related compounds, Fluid Phase Equilibria 299 (2010) 285-293.

[47] J.M. Beaudon, J.P. Kohn, Multiphase and volumetric equilibria of the methane-+decane binary system at temperatures between -36o and 15OoC, Journal of Chemical and Engineering Data, 12 (1967) 189-191.

[48] P.C. Joyce, M.C. Thies, Vapor-liquid equilibria for the hexane + hexadecane and hexane + 1-hexadecanol systems at elevated temperatures and pressures, Journal of Chemical and Engineering Data, 43 (1998) 819-822.

[49] P. Dauge´, A. Baylaucq, L. Marlin, C. Boned, Development of an isobaric transfer viscometer operating up to 140 MPa. Application to a methane + decane system, Journal of Chemical and Engineering Data, 46 (2001) 823-830.

[50] J.H. Dymond, K.J. Young, P, ρ, T behaviour for n-hexane + n-hexadecane in the range 298 to 373 K and 0.1 to 500 MPa, Journal of Chemical Thermodynamics 11 (1979) 887-895.

[51] N.B. Vargaftik, Tables on the Thermophysical Properties of Liquids and Gases, Hemisphere, Washington, D.C., 1975.

[52] F. Audonnet, A.A.H. Pádua, Simultaneous measurement of density and viscosity of n-pentane from 298 to 383 K and up to 100 MPa using a vibrating-wire instrument, Fluid Phase Equilibria, 181 (2001) 147-161.

[53] A.L. Lee, R.T. Ellington, Viscosity of n-pentane, Journal of Chemical and Engineering Data 10 (1965) 101-104.

[54] T.R. Das, C.O. Reed Jr, P.T. Eubank, PVT surface and thermodynamic properties of n-pentane, Journal of Chemical and Engineering Data 22 (1977) 3-8.

[55] M.S. Zabaloy, E.A. Brignole, On volume translations in equations of state, Fluid Phase Equilibria, 140 (1997) 87-95.

[56] J.V. Sengers, R.F. Kayser, C.J. Peters, H.J. White Jr., Equations of State for Fluids and Fluid Mixtures, First ed., Elsevier, Amsterdam, 2000.

[57] J.L. Daridon, H. Carrier, B. Lagourette, Pressure dependence of the thermophysical properties of n-pentadecane and n-heptadecane, International Journal of Thermophysics, 33 (2002) 697-708.

[58] J.L. Daridon, B. Lagourette, J.-P.E. Grolier, Experimental measurements of the speed of sound in n-hexane from 293 to 373 K and up to 150 MPa, International Journal of Thermophysics, 19 (1998) 145-160.

[59] D.R. Caudwell, J.P.M. Trusler, V. Vesovic, W.A. Wakeham, Viscosity and density of five hydrocarbon liquids at pressures up to 200 MPa and temperatures up to 473 K, J. Chem. Eng. Data, 54 (2009) 359-366.

[60] Y. Wu, B. Bamgbade, M.A. McHugh, in preparation.

[61] B. A. Bamgbade, Y. Wu, H. O. Baled, R. M. Enick, M. A. McHugh, Experimental density measurements of bis(2-Ethylhexyl) phthalate at elevated temperatures and pressures, to be submitted to the Journal of Chemical Thermodynamics.

[62] J. Marrero. R. Gani, Group-contribution based estimation of pure component properties, Fluid Phase Equilibria, 183-184 (2001) 183-208.

[63] C.M.B.P. Oliveira, W.A. Wakeham, The viscosity of five liquid hydrocarbons at pressures up to 250 MPa, Int. J. Thermophys., 13 (1992) 773-790.

[64] E. Kiran, Y.L. Sen, High-pressure viscosity and density of n-alkanes, International Journal of Thermophysics, 13 (1992) 411-442.

[65] Y. Tanaka, H. Hosokawa, H. Kubota, T. Makita, Viscosity and density of binary mixtures of cyclohexane with n-octane, n-dodecane, and n-hexadecane under high pressures, International Journal of Thermophysics, 12 (1991) 245-264.

[66] K. Rajagopal, L.L.P.R. Andrade, M.L.L. Paredes, High-pressure viscosity measurements for the binary system cyclohexane + n-hexadecane in the temperature range of (318.15 to 413.15) K, J. Chem. Eng. Data, 54 (2009) 2967–2970.

[67] M.A. Hern´andez-Galv´an, F. Garc´ıa-S´anchez a, R. Mac´ıas-Salinas, Liquid viscosities of benzene, n-tetradecane, and benzene + n-tetradecane from 313 to 393K and pressures up to 60MPa: Experiment and modeling, Fluid Phase Equilibria, 262 (2007) 51-60.

[68] A.E. Flowers, Viscosity measurement and a new viscometer, Proc. Am. Soc. Testing Materials, 14II (1914) 565-616.

[69] M.D. Hersey, The theory of the torsion and rolling-ball viscometers, and their use in measuring the effect of pressure on viscosity, J. Wash. Acad. Sci., 6 (1916) 525-530.

[70] B.H. Sage, Measurement of viscosities of liquids saturated with gases at high pressures, Ind. Eng. Chem. Anal. Ed., 5 (1933) 261-263.

[71] F. Hoeppler, The eccentric fall of spheres through liquids or gases in cylinders, Z. Tech. Physik, 14 (1933) 165-169.

[72] R.M. Hubbard, G.G. Brown, The rolling ball viscometer, Industrial and Engineering Chemistry, Anal. Ed., 15 (1943) 212-218.

[73] B.H. Sage, W.N. Lacey, Effect of pressure upon viscosity of methane and two natural gases, in: Los Angeles and Oklahoma City meetings, october 1937.

[74] L.T. Carmichael, B.H. Sage, Viscosity of liquid ammonia at high pressures, Industrial and Engineering Chemistry, 44 (1952) 2728-2732.

[75] E.M. Stanley, R.C. Batten, Rolling-ball viscometer for measuring viscosity of fluids at high pressures and moderate temperatures, Analytical Chemistry, 40 (1968) 1751-1753.

[76] C.V. Voorst, C.V. Duijn Jr, An improved and simplified design for a Hoeppler-type (rolling ball) microviscometer, Journal of Physics E: Scientific instruments 9(1976) 613-615.

[77] R.H. Geils, R.C. Keezer, Small-volume, inclined, falling-ball viscometer, Rev. Sci. Instrum., 48 (1977) 783-785.

[78] K. Nishibata, M. Izuchi, A rolling ball viscometer for high pressure use, Physica, 139 & 140B (1986) 903-906.

[79] S. Sawamura, T. Yamashita, Rolling-ball viscometer for studying water and aqueous solutions under high pressure, in: 14th International Conference on the Properties of Water and Steam, Kyoto, 2004, pp. 429-434.

[80] D. Tomida, A. Kumagai, K. Qiao, C. Yokoyama, Viscosity of [bmim][PF6] and [bmim][BF4] at high pressure, International Journal of Thermophysics, 27 (2007) 39-47.

[81] Y. Sato, H. Yoshioka, S. Aikawa, R.L. Smith Jr, A Digital variable-angle rolling-ball viscometer for measurement of viscosity, density, and bubble-point pressure of CO2 and organic liquid mixtures, Int. J. Thermophys, 31 (2008) 1896-1903.

[82] B.H. Sage, Measurement of viscosities of liquids saturated with gases at high pressures, Industrial and Engineering Chemistry, Analytical Edition, 5 (1933) 261-263.

[83] A.F. Benning, W.H. Markwood, The viscosities of liquid freon compounds, Refrig. Eng., 37 (1939) 243-247.

[84] V. Spée, in: Trans. Chem. Engr. Congr., World Power Conf., Percy Lund, Humphries and Co, London, 1937, pp. 1-29.

[85] B.H. Sage, W.N. Lacey, Effect of pressure upon viscosity of methane and two natural gases, Trans. Am. Inst. Mining Met. Engrs., 127 (1938) 118-134.

[86] H.W. Lewis, Calibration of the rolling ball viscometer, Analytical Chemistry, 25 (1953) 507-508.

[87] S.M. Corporation, http://www.specialmetals.com/products/inconelalloy718.php

[88] M. Izuchi, K. Nishibata, A high pressure rolling ball-viscometer up to 1 GPa, Jap. J. Appl. Phys., 25 (1986) 1091-1096.

[89] J. Šesták, F. Ambros, On the use of the rolling-ball viscometer for the measurement of rheological parameters of power law fluids, Rheol. Acta, 12 (1973) 70-76.

[90] R.A. Horne, D.S. Johnson, The viscosity of water under pressure, The Journal of Physical Chemistry, 70 (1966) 2182-2190.

[91] L.D. Naake, G. Wiegand, E.U. Franck, The viscosity of n-decane to high temperatures of 573 K and high pressures of 300 MPa, Z. Phys. Chem., 216 (2002) 1295-1310.

[92] S.E. Quinones-Cisneros, C.K. Zeberg-Mikkelsen, E.H. Stenby, The friction theory (f-theory) for viscosity modeling, Fluid Phase Equilibria, 169 (2000) 249-276.

[93] S.E. Quinones-Cisneros, C.K. Zeberg-Mikkelsen, E.H. Stenby, One parameter friction theory models for viscosity, Fluid Phase Equilibria, 178 (2001) 1-16.

[94] A. Allal, C. Boned, Q. Baylaucq, Free-volume viscosity model for fluids in the dense and gaseous states, Phys. Rev. E, 64 (2001), 011203.

[95] S.P. Tan, H. Adidharma, B. F. Towler, M. Radosz, Friction theory and free-volume theory coupled with statistical associating fluid theory for estimating the viscosity of pure n-alkanes, Ind. Eng. Chem. Res., 44 (2005) 8409-8418.

[96] S. Chapman, T.G. Cowling, D. Burnett, The mathematical theory of non-uniform gases, in, Cambridge University Press, Cambridge, 1970.

[97] T.H. Chung, M. Ajlan, L.L. Lee, K.E. Starling, Generalized multiparameter correlation for nonpolar and polar fluid transport properties, Ind. Eng. Chem. Res., 27 (1988) 671-679.

[98] J.H. Dymond, J. Robertson, J.D. Isdale, Transport properties of nonelectrolyte liquid mixtures. Viscosity coefficients for n-octane, n-dodecane, and equimolar mixtures of n-octane + n-dodecane and n-hexane + n-dodecane from 25 to 100~ at pressures up to the freezing pressure or 500 MPa, International Journal of Thermophysics, 2 (1981) 133-154.

[99] D. R. Caudwell, J. P. M. Trusler, V. Vesovic, W. A. Wakeham, The viscosity and density of n-dodecane and n-octadecane at pressures up to 200MPa and temperatures up to 473K, International Journal of Thermophysics,25, No. 5 (2004) 1339-1352.

[100] D. L. Hogenboom, W. Webb, J. A. Dixon, Viscosity of several liquid hydrocarbons as a function of temperature, pressure, and free volume, J. Chem. Phys., 46 (1967) 2586-2598.

[101] http://transp.eng.auth.gr/iatp/e_iatp9.html

[102] http://www.slb.com/services/testing/reservoir_sampling/fluid_lab/hpht_pvt_studies/hpht_viscosity_standards.aspx

[103] http://www.slb.com/~/media/Files/testing/other/viscosity_standards_for_hpht_and_high_viscosity_conditions.ashx

[104] http://www.slb.com/~/media/Files/testing/other/hpht_viscosity_standards_workshop_2010_summary.ashx

[105] http://www.slb.com/~/media/Files/testing/other/high_pressure_viscometers.ashx

[106] http://www.slb.com/~/media/Files/testing/other/industrial_reference_fluids_viscosity.ashx

[107] R.M. Enick, E. Beckman, A. Yazdi, V. Krukonis, H. Schonemann, J. Howell, Phase behavior of CO_2-perfluorpolyether oil mixtures and CO_2-perfluoropolyether chelating agent mixtures, Journal of Supercritical Fluids, 13 (1988) 121-126.

[108] M.E. Paulitis, V.J. Krukonis, R. Kurnik, R. Reid, Supercritical fluid extraction, Reviews in Chemical Engineering, 1(2) (1983) 179-211.

[109] W. Gussler, M. Pless, J. Maxey, P. Grover, J. Perez, J. Moon, T. Boaz, A New extreme HP/HT viscometer for new drilling-fluid challenges, paper SPE 99009 presented at the 2006 IADC/SPE Drilling Conference, Miami, Florida, Feb 21-23, 2006; SPE Drilling and Completion, June 2007, 81- 89.

[110] B. A. Bamgbade, Y. Wu, W. A. Burgess, M. A. McHugh, Experimental density and PC-SAFT modeling of Krytox® (Perfluoropolyether) at pressures to 275 MPa and temperatures to 533 K, Fluid Phase Equilibria, 332 (2012) 159-164.

[111] W.T. Ashurst, W.G. Hoover, Dense fluid shear viscosity and thermal conductivity-the excess, AIChE J., 22 (2) (1975) 410-411.

[112] S. Bair, R. Casalini, A scaling parameter and function for the accurate correlation of viscosity with temperature and pressure across eight orders-of-magnitude of viscosity, ASME J. Tribology, 130 (2008) 041802.

[113] S. Bair, A. Laesecke, Normalized Ashurst-Hoover scaling and a comprehensive viscosity correlation for compressed liquids, ASME Journal of Tribology, 134 (2012) 021801.

[114] S. Bair, Estimating the viscosity of Krytox 143AD at 172 MPa and 200 °C, private communication.

[115] Selby, Kim, DuPont performance lubricants, private communication, April 4, 2010

[116] Klein schmidt, Bradbury and Mark, Viscosity and density of Over 40 lubricating fluids of known composition at pressures to 150,000 psi and temperatures to 425^{o}F , A report of the ASME research committee on lubrication prepared with the assistance of the advisory board on pressure viscosity of ASME, ASME, New York, 1953

[117] B. A. Bamgbade, Y. Wu, H. O. Baled, R. M. Enick, M. A. McHugh, Experimental density measurements of bis(2-Ethylhexyl) phthalate at elevated temperatures and pressures, to be submitted to the Journal of Chemical Thermodynamics.

[118] H. Baled, R. M. Enick, Y. Wu, B. Bamgbade, M. A. McHugh, W. A. Burgess , D. Tapriyal, B. D. Morreale, Y. Soong, Volume translated SRK and PR equations of state for the prediction of high-temperature, high-pressure hydrocarbon density, 2012 AIChE Annual Meeting, Pittsburgh, PA, USA, October 28-November 02, 2011.

[119] J. H. Dymond, R. Malhotra, The Tait equation: 100 Years on, International Journal of Thermodynamics, 9 (1988) 941-951.

[120] H. Baled, R. M. Enick, W. Burgess, D. Tapriyal, B. D. Morreale, Y. Wu, B. A. Bamgbade, M. McHugh, S. Bair, V. Krukonis, Perfluoropolyether oils as candidates for the deepwater viscosity standard of 20 cP at 500^{o}F and 35000 psia, 12th IATP Conference, Boulder, CO, USA, June 24, 2012.

[121] H. Baled, R. Enick, W. Burgess, J. Jain, B. Morreale, Y. Soong, D. Tapriyal, Y. Wu, B. Bamgbade and M. A. McHugh, A Windowed, variable-volume, rolling ball viscometer rated to 260^{o}C and 275 MPa, 18th Symposium on Thermophysical Properties, Boulder, CO, USA, June 24 – 29, 2012.

[122] DuPont Krytox performance lubricants product overview, 2002, pp. 1–12.

[123] Special Metals: Inconel Alloy 718, www.specialmetals.com.

[124] D. Roylance, Pressure Vessels. 2001. Pages 1-10.